UNIVERSIDADE TECNOLÓGICA FEDERAL DO PARANÁ

PROGRAMA DE PÓS-GRADUAÇÃO EM ENGENHARIA MECÂNICA E DE MATERIAIS

JOSÉ CARLOS CORDEIRO JUNIOR

EXPERIMENTAL CHARACTERIZATION OF INHIBITED CARBON DIOXIDE HYDRATES ABOVE THE UPPER QUADRUPLE POINT

DISSERTAÇÃO DE MESTRADO

CURITIBA

2019

JOSÉ CARLOS CORDEIRO JUNIOR

EXPERIMENTAL CHARACTERIZATION OF INHIBITED CARBON DIOXIDE HYDRATES ABOVE THE UPPER QUADRUPLE POINT

Dissertação apresentada como requisito parcial à obtenção de título de Mestre em Engenharia Mecânica e de Materiais, Área de Concentração em Engenharia Térmica, do Departamento de Pesquisa e Pós-Graduação, do Campus Curitiba, da UTFPR.

Orientador: Prof. Moisés A. Marcelino Neto, Dr.
Coorientador: Prof. Rigoberto E. M. Morales, Dr.

CURITIBA

2019

Dados Internacionais de Catalogação na Publicação

Cordeiro Junior, José Carlos
Experimental characterization of inhibited carbon dioxide hydrates above the upper quadruple point [recurso eletrônico] / José Carlos Cordeiro Junior.-- 2019.
1 arquivo de texto (116 f.) : PDF ; 2,74 MB.

Modo de acesso: World Wide Web.
Texto em inglês com resumo em português.
Dissertação (Mestrado) - Universidade Tecnológica Federal do Paraná. Programa de Pós-graduação em Engenharia Mecânica e de Materiais. Área de Concentração: Engenharia Térmica, Curitiba, 2019.
Bibliografia: f. 96-100.

1. Engenharia mecânica - Dissertações. 2. Hidratos. 3. Dióxido de carbono. 4. Regra de fase e equilíbrio. 5. Equilíbrio químico. 6. Inibidores químicos. 7. Glicol de etileno. 8. Sal. 9. Termodinâmica. 10. Métodos de simulação. I. Marcelino Neto, Moisés Alves, orient. II. Melgarejo Morales, Rigoberto Eleazar, coorient. III. Universidade Tecnológica Federal do Paraná. Programa de Pós-graduação em Engenharia Mecânica e de Materiais. IV. Título.

CDD: Ed. 23 -- 620.1

Biblioteca Central do Câmpus Curitiba - UTFPR
Bibliotecária: Luiza Aquemi Matsumoto CRB-9/794

Ministério da Educação
Universidade Tecnológica Federal do Paraná
Diretoria de Pesquisa e Pós-Graduação

UNIVERSIDADE TECNOLÓGICA FEDERAL DO PARANÁ
CAMPUS CURITIBA

TERMO DE APROVAÇÃO DE DISSERTAÇÃO Nº 358

A Dissertação de Mestrado intitulada**: EXPERIMENTAL CHARACTERIZATION OF INHIBITED CARBON DIOXIDE HYDRATES ABOVE THE UPPER QUADRUPLE POINT**, defendida em sessão pública pelo Candidato **José Carlos Cordeiro Junior**, no dia 12 de julho de 2019, foi julgada para a obtenção do título de Mestre em Engenharia, área de concentração: Engenharia Térmica, e aprovada em sua forma final, pelo Programa de Pós-Graduação em Engenharia Mecânica e de Materiais – PPGEM.

BANCA EXAMINADORA:
Prof. Dr. Moisés Alves Marcelino Neto - Presidente - UTFPR
Prof. Dr. Paulo Henrique Dias dos Santos - UTFPR
Prof. Dr. Marcos Lucio Corazza - UFPR

A via original deste documento encontra-se arquivada na Secretaria do Programa, contendo a assinatura da Coordenação após a entrega da versão corrigida do trabalho.

Curitiba, _____de _____de 20___.

Carimbo e assinatura do Coordenador do Programa

_____

ACKNOWLEDGEMENTS

I am thankful for all those who supported me on the completion of this work, which would not be possible without the help of the following individuals and organizations.

I want to deeply thank my mother Isaura de Oliveira and my uncles Fernando de Oliveira and Keith Lewis. Without their friendship, support and advice, none of this would have been possible.

I would like to express my sincere gratitude to my master's advisor Prof. Moisés A. Marcelino Neto, who has been amazing in giving me scientific directions to the development of this work.

I greatly thank Prof. Rigoberto E. M. Morales for giving me the amazing opportunity to for my master's study. His belief in my potential was of great importance to the conclusion of this work.

I thank Prof. Amadeu Sum from the Colorado School of Mines (USA) for his help and guidance to the consistency evaluation developed by his research group and applied here.

I express my sincere gratitude to the following fellow students at NUEM: Carina Stahnke, whose friendship and support was essential; Celina Kakitani, who has greatly helped with the development of the experimental work and evaluation of results. And the support and friendship of the following fellow students and faculty members at NUEM: Amanda Guembaroski, Ana Beltrão Santana, Gabriel Torelli, Reinaldo Justiniano, Hedilberto Barros and Afonso Miguel Junior.

The author acknowledges the financial support from ANP and FINEP through the Human Resources Program to Oil and Gas segment PRH-ANP (PRH 10-UTFPR) and from TE/CENPES/PETROBRAS.

“Success is born from will, determination and persistence to reach an objective. Even if the main goal is missed, those who seek and overcome obstacles will, to the very least, do admirable things.”

José de Alencar.

ABSTRACT

CORDEIRO JUNIOR, José Carlos. **EXPERIMENTAL CHARACTERIZATION OF INHIBITED CARBON DIOXIDE HYDRATES ABOVE THE UPPER QUADRUPLE POINT**. 2019. 116p. Master's Dissertation – Postgraduate Program in Mechanical and Materials Engineering, Federal University of Technology – Paraná. Curitiba, Brazil. 2019.

Under specific conditions, water molecules can combine with gas molecules forming a solid crystalline structure called hydrates. The formation of this ice-like phase can block pipelines and is a major flow assurance concern in oil and gas industries. Carbon dioxide is a natural contaminant present in petroleum. As oilfields are being explored in regions with more severe conditions, it can condensate and thus an upper quadruple point appears in the hydrate phase equilibrium. Above this point, hydrate forms from liquid carbon dioxide and water. Thermodynamic inhibitors, such as MEG, are commonly used in petroleum industry and act by changing the conditions at which hydrates can form, essentially preventing their appearance. In offshore oil and gas production, water that can potentially form hydrates is naturally inhibited with salts. This way, the use of thermodynamic inhibitors can be optimized with the presence of salts. With this in mind, the influence of NaCl and MEG in the phase equilibrium of carbon dioxide hydrates was evaluated. An equilibrium cell connected to a syringe pump was used to determine experimental phase equilibrium points of inhibited carbon dioxide hydrates. In order to achieve high pressures to ensure the condensation of the gas phase, an isobaric procedure was used. By changing the temperature of the cell, hydrates form, consuming CO_2, which is replaced by the syringe pump in order to keep a constant pressure. New equilibrium experimental data for pressures varying from 8.5 to 25 MPa were determined. The consistency of the data collected was evaluated with good results, confirming its reliability. Lastly, the experimental data collected were compared with prediction software products and models in order to evaluate their accuracy. Commercial software Multiflash and PVTSim offered good results for systems inhibited with MEG and NaCl, while the open source CSMGem software was able to give decent results in pure water system and with mixture of inhibitors, except in high concentrations, where it greatly super-estimated the inhibition effect. Sirino et al. (2018) and the Hu-Lee-Sum correlation were conservative on its results, generally sub-estimating the inhibition effect of inhibitors.

Keywords: Hydrates. Carbon dioxide. Upper quadruple point. MEG. NaCl.

RESUMO

CORDEIRO JUNIOR, José Carlos. **CARACTERIZAÇÃO EXPERIMENTAL DE HIDRATOS DE DIÓXIDO DE CARBONO INIBIDOS ACIMA DO PONTO QUÁDRUPLO SUPERIOR**. 2019. 116p. Dissertação de Mestrado – Programa de Pós-Graduação em Engenharia Mecânica e de Materiais, Universidade Tecnológica Federal do Paraná – Paraná, Curitiba, Brasil. 2019.

Sob condições específicas, moléculas de água podem se combinar com moléculas de gás, formando uma estrutura cristalina sólida chamada de hidratos. A formação dessa fase similar ao gelo pode bloquear tubulações, sendo uma grande preocupação da indústria de petróleo e gás. Dióxido de carbono é um contaminante natural presente no petróleo. Como campos de petróleo estão sendo explorados em regiões com condições mais severas (altas pressões e baixas temperaturas), dióxido de carbono presente pode condensar, causando o aparecimento de um ponto quádruplo superior no equilíbrio de fases de hidratos. Acima deste ponto, dióxido de carbono líquido se combina com água para formar hidratos. Inibidores termodinâmicos, como o MEG, são comumente utilizados pela indústria e agem alterando as condições de formação de hidratos, essencialmente prevenindo-os. Na exploração de petróleo em alto mar, a água que pode potencialmente formar hidratos é naturalmente inibida pela presença de sais. Dessa forma, o uso de inibidores termodinâmicos pode ser otimizado levando-se em conta a presença de sais. Com isso em mente, a influência de MEG e NaCl no equilíbrio de fases de hidratos foi avaliada. Uma célula de equilíbrio conectada diretamente à uma bomba seringa foi utilizada para determinar experimentalmente condições de equilíbrio de hidratos de dióxido de carbono. Visando atingir altas pressões para garantir a condensação do CO_2, uma metodologia isobárica foi utilizada. Controlando-se a temperatura da célula, hidratos foram formados. Com isso, CO_2 é consumido, o qual é reposto com o uso da bomba seringa afim de se manter a pressão da célula constante. Novos dados experimentais de equilíbrio de hidratos foram obtidos para pressões entre 8.5 e 25 MPa. A consistência termodinâmica dos dados coletados foi avaliada, confirmando sua confiabilidade. Por último, os dados experimentais obtidos neste trabalho foram comparados com predições de programas e de modelos afim de se avaliar a confiabilidade dos mesmos. Os programas comerciais Multiflash e PVTSim deram bons resultados para sistemas inibidos com MEG e NaCl. O programa de código aberto CSMGem foi capaz de prever sistemas com água pura e com misturas de inibidores com bons resultados, exceto em altas concentrações, onde houve uma superestimação da capacidade de inibição. O modelo de Sirino et al. (2018) e a correlação e Hu-Lee-Sum deram resultados conservadores, subestimando o poder de inibição dos componentes analisados.

Palavras-chave: Hidratos. Dióxido de carbono. Ponto quádruplo superior. MEG. NaCl.

LIST OF FIGURES

LIST OF TABLES

LIST OF SYMBOLS

SYMBOL	DESCRIPTION	UNIT
CO_2	Carbon Dioxide	-
C_p	Heat capacity	[J/mol.K]
f_i^P	Fugacity of component *i* in phase *P*	-
G	Gibbs free energy	[J/mol.K]
H	Hydrate Phase	-
$\overline{H}$	Molar enthalpy	[J/mol.K]
I	Ice	-
L_{H2O}	Liquid Aqueous Phase	-
L_{CO2}	Liquid Phase Rich in Carbon Dioxide	-
n	Hydration number	-
P	Pressure	[MPa] Mega Pascal
Q_1	Lower Quadruple Point	-
Q_2	Upper Quadruple Point	-
R	Ideal gas constant	[J/mol.K]
S	Entropy	[J/mol.K]
sI	Structure of Type I	-
sII	Structure of Type II	-
sH	Structure of Type H	-
T	Temperature	[K] Kelvin
t	Time	[h] hours
V	Volume	[ml] milliliters

V_{CO2}	Vapor Phase Rich in Carbon Dioxide	-
x_i	Molar fraction of component *i*	-
z	Compressibility coefficient	-
γ_i	Activity coefficient of component *i*	-
μ_i	Chemical potential of component *i*	-
σ	Standard deviation	-

LIST OF ABBREVIATIONS

AAD	Average Absolute Deviation
CPA	Cubic Plus Association
EoS	Equation of State
FALAB	Flow Assurance Laboratory
mass%	Mass Fraction Percentage
MEG	Monoethylene Glycol
NaCl	Sodium Chloride
NUEM	Multiphase Flow Center
RSD	Relative Standard Deviation
SRK	Soave-Redlich-Kwong
UTFPR	Federal University of Technology - Paraná
vol%	Volume Fraction Percentage

TABLE OF CONTENTS

1 INTRODUCTION

Through hydrogen bonding, water molecules link together to form a cavity that encapsulates gas molecules of a second type, forming a solid phase. This newly formed structure is technically called “clathrate hydrates”. For a more usual designation, they are also known as “natural gas hydrates” or simply “hydrates” (HAMMERSCHMIDT, 1934).

Such hydrate compounds can also be found naturally in the permafrost of arctic regions, where natural gas is trapped inside the solid hydrate phase. This brings a potential asset to be explored in industry, as some conservative estimates say that such reserves can be twice as big when compared to conventional fossil fuel reserves. Although the technology to explore such deposits does exist, there is still a need for studies on the environmental impact of this activity (KOH et al., 2011).

Other potential applications include the possibility of storing natural gas in form of hydrates, which may facilitate transport, as it would be in a solid state. Similarly, studies have been done to evaluate the feasibility to store and transport hydrogen as a hydrate solid state (KOH et al., 2011). In addition, hydrates can be used in separation processes, such as in the treatment of effluent gases, where the formation of hydrates capture gases, and in the desalinization of seawater (PARK et al., 2014).

As hydrates form, a new non-flowing solid phase is created. In gas and oil industries, the formation of natural gas hydrates can trigger blockages in pipelines (Figure 1.1), causing damages and preventing normal operations. The characterization of the hydrate equilibrium is then of significant importance in order to predict if and when such solid-state structures form (SLOAN et al., 2011).

The focus of this work is on evaluating the formation of hydrates in the oil and gas industries as a flow assurance problem, where their occurrences can have high economic costs.

Figure 1.1 - Hydrate plug being removed from a pipeline in a Petrobras installation.

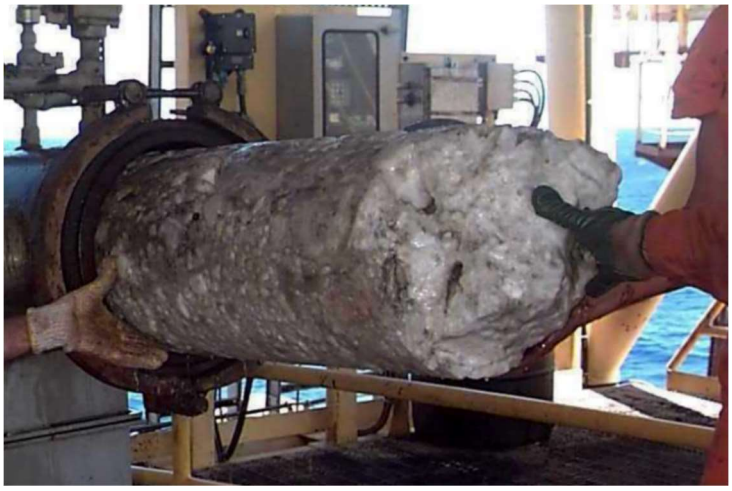

Source: Koh et al. (2011).

Hydrates usually form at high pressures and low temperatures, conditions those that exist at the bottom of the ocean. Figure 1.2 shows how the pressure and temperature change in pipelines in offshore oil extraction, from the wellbore to the offshore platform. The regions to the left of each curve are characterized for the formation of hydrates; consequently, to the right is where hydrates do not form.

A commonly used method for preventing the formation of hydrates is the addition of thermodynamic inhibitors. These compounds act by changing the equilibrium conditions at which hydrates form. By adding a sufficient amount of inhibitor for a given system, the hydrate formation region can be shifted to a safe operation condition, where hydrate formation does not occur.

In Figure 1.2, each dashed line (10, 20 and 30%) corresponds to a change in the equilibrium curve due to the presence of methanol, which acts as a thermodynamic inhibitor, lowering the equilibrium temperature of hydrates and thus preventing their formation. The circles on the graph indicate the distance along the pipeline, from the wellbore to the offshore platform.

After oil leaves the wellbore (10 km in Figure 1.2), although the pressure is high, the high temperature means that the system stays outside the hydrate formation region. However, through contact with the cold water at the bottom of the ocean (from 15 km to 70 km in Figure 1.2), the pipeline cools down, changing the system to hydrate formation conditions. By adding

enough inhibitor (for instance, 30% of methanol in the case shown in Figure 1.2), the hydrate formation region gets dislocated far from the operating conditions of the pipeline. The amount of inhibitor necessary can be optimized with the assistance of prediction software and, most importantly, reliable experimental equilibrium data (SLOAN and KOH, 2008).

Figure 1.2. Equilibrium curve for the formation of hydrates in offshore oil extraction.

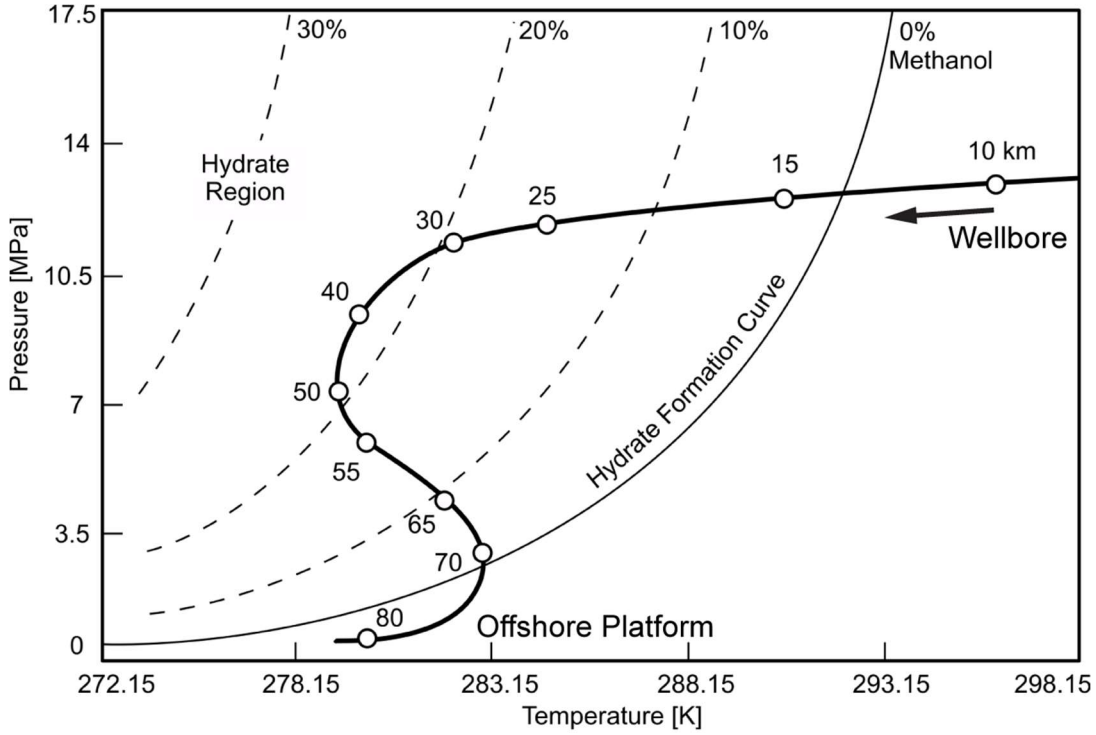

Source: Adapted from Sloan and Koh (2008).

Figure 1.3 shows an example of a hydrate cage, which is formed by water molecules and, in this case, encapsulates a methane molecule. This structure is stabilized by the Van der Waals forces between the molecules of the cavity and the molecule trapped inside it (guest molecule) (WEBER, 1987). Van der Waals forces are interactions between atoms that depend on the distance between them, which are far weaker than chemical bonding, despite that, it is still strong enough to enable the formation of hydrate cages when a gas molecule is present (ATKINS and JONES, 2008).

For hydrates to form, partially created cavities made of water molecules must encounter a gas molecule. For that reason, hydrate formation is mainly an interface

phenomenon. In the case of condensate, then hydrates form with the combination of water and condensate molecules. As an example, carbon dioxide (CO_2) liquefies at pressures above 60 bar at ambient temperature, so that when in contact with water at high pressures and low temperatures, hydrates can be formed from the diffusion of CO_2 molecules to the hydrate phase (CARROLL, 2014).

Figure 1.3. Hydrogen bonding (dashed lines) that forms the cavity in which the gas molecule gets trapped.

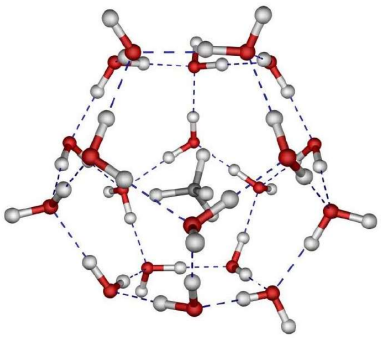

Source: Headrick et al. (2005).

Carbon dioxide is a natural contaminant present in petroleum. Table 1.1 shows the molar composition of selected oil fields around the world. For oilfields such as Kapuni in New Zealand and Uch in Pakistan shows almost half of CO_2 concentration. Although natural gas is usually mainly comprised of methane, the high concentrations of CO_2 can change the phase equilibrium for the formation of hydrates (OBANIJESU et al., 2010).

Table 1.1. Molar composition of selected oil fields.

	Molar composition (%)				
Chemical Composition	**Kirkuk Iraq**	**Uthmaniyah S. Arabia**	**Lacq France**	**Kapuni N. Zealand**	**Uch Pakistan**
Methane	56.9	55.5	69.0	45.6	27.3
Ethane	21.2	18.0	3.0	5.8	0.7
Propane	6	9.8	0.9	2.9	0.3
Butane	3.7	4.5	1	1.1	0.3
C_{5+}	1.6	1.6	-	0.8	-
Nitrogen	-	0.2	1.5	-	25.2
H_2S	3.5	1.5	15.3	-	-
CO_2	**7.1**	**8.9**	**9.3**	**43.8**	**46.2**

Source: Adapted from Obanijesu et al. (2010).

The pre-salt region in Brazil has significantly higher concentrations of carbon dioxide than other Brazilian oilfields. Some oilfields have concentrations between 8% and 12% while other can have concentrations above 50%. The presence of CO_2 in such high concentrations changes the phase equilibrium for the formation of hydrates (MELO et al., 2011).

Table 1.2 shows the properties of Methane (CH_4) and carbon dioxide (CO_2) hydrates. As both form hydrates of type sI, the tendency is that their mixture would also form sI hydrates. In addition, the hydrate pressure for CO_2 is lower than hydrates of CH_4, which could indicate that the presence of CO_2 in natural gas facilitates the formation of hydrates (CARROLL, 2014).

Table 1.2. Properties of CH_4 and CO_2 hydrates.

	Hydrate Structure	**Molar Mass [g/mol]**	**Hydrate Pressure at 273.15 K [MPa]**	**Density [g/cm³]**
Methane	sI	16.043	2.603	19.62
CO_2	sI	44.010	1.208	25.56

Source: Carroll (2014).

The phase equilibrium of the H_2O - CO_2 system is shown in Figure 1.4. The equilibrium curve where vapor CO_2 forms hydrates (L_W-H-V) is widely studied with a higher quantity of experimental data available in literature. However, the curve where liquid CO_2 forms hydrates (L_W-H-L_{CO2}) is less studied with much fewer data points available, as it will be shown in the following chapter.

Figure 1.4. Phase diagram of carbon dioxide hydrates. (a) Region above Q_2.

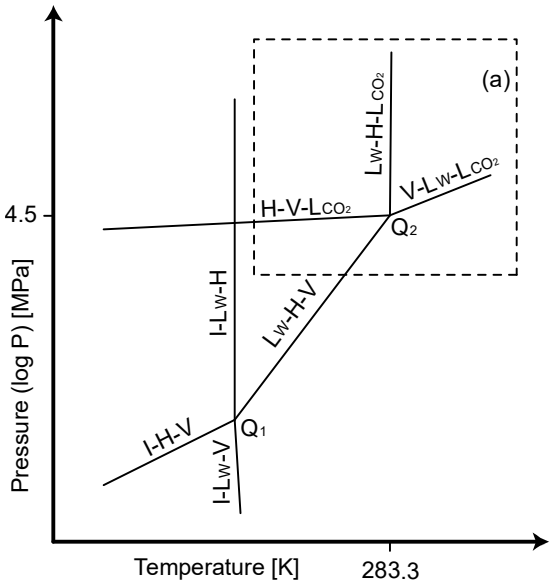

Source: Adapted from Sloan et al. (2008).

The phase diagram of CO_2 hydrates has an upper quadruple point that appears due to the condensation of the vapor phase (Q_2 in Figure 1.4). This point is characterized for the coexistence of four phases: liquid phase rich in CO_2 (L_{CO2}), vapor phase rich in CO_2 (V_{CO2}), liquid phase rich in water (L_{H2O}) and hydrate phase (H) (SLOAN and KOH, 2008).

In the region above the Q_2 point, CO_2 molecules from the liquid phase are trapped to form the hydrate solid phase, differently than the region bellow Q_2, where gas molecules diffuse from the gas phase to the solid hydrate phase.

Computer programs based on models that use thermodynamic statistics are able to give predictions of the hydrate equilibrium. Despite having a fundamental basis in thermodynamics, such models still rely on regression of experimental data for certain variables. Therefore, the accuracy of the software relies on the quality of the experimental data used for the regression.

By using thermodynamic correlations, Sa et al. (2018) suggested three criteria to evaluate the reliability of experimental data: consistency of Clausius-Clapeyron relation, consistency of the heat of dissociation and consistency of the water activity. By using this method, it is possible to affirm whether certain data is of good quality.

The experimental study for the equilibrium of carbon dioxide hydrates is a fundamental tool with which prediction models are adjusted. There is a lack of data for points above Q_2, especially with the presence of additives, such the thermodynamic inhibitors MEG and NaCl. This work focuses on obtaining experimental data for conditions of which condensed carbon dioxide combines with water to form hydrates with the presence of the aforementioned thermodynamic inhibitors. In addition, the comparison with prediction models is done and the consistency of the data obtained is evaluated.

1.1 OBJECTIVES

The purpose of this work is the experimental study of the phase equilibrium of carbon dioxide hydrates with the presence of thermodynamic inhibitors, specifically above the upper quadruple point (Q_2). In other words, it is the experimental determination of the H-L_W-L_{CO2} equilibrium curve. The analysis of the influence of thermodynamic inhibitors on the carbon dioxide (CO_2) hydrates phase equilibrium above Q_2 can help optimize the amount of inhibitor to use in a given situation in order to prevent the formation of hydrates. The thermodynamic inhibitors used were monoethylene glycol (MEG) and sodium chloride (NaCl). Although natural gas will have many other compounds present, the phase equilibrium of CO_2 hydrates can help understand the behavior of hydrates in natural gas with high concentrations of CO_2.

To evaluate the quality of the data collected, the consistency will be assessed. The criteria to be used was suggested by Sa et al. (2018), where three parameters are evaluated. First, it is the commonly used linearity of the Clausius-Clapeyron relation. The other two, not so commonly used, are the consistency of the heat of dissociation of hydrates and the activity of water.

All the experimental procedures were carried out at the Flow Assurance Laboratory (FALAB) at the Multiphase Flow Research Center (NUEM) of the Federal University of Technology - Parana (UTFPR). The laboratory has a phase equilibrium apparatus where a new procedure was developed in order to access the high-pressure regions where the vapor phase condensates.

Lastly, the experimental data collected will be compared with predictions done by the software products. Multiflash™ uses CPA equation of state (EoS), PVTSim™ uses a modified version of Soave-Redlich-Kwong (SRK) EoS and CSMGem uses the traditional SRK EoS. Data will also be compared to the prediction model developed by Sirino et al. (2018), which uses CPA EoS, and the Hu-Lee-Sum correlation for inhibited systems, which was proposed by Hu et al. (2017 a).

1.2 MOTIVATION

Hydrate formation brings a series of challenges in gas and oil industries. In offshore oil extraction, high pressures and low temperatures can be achieved, which may provide the necessary conditions for the formation of hydrates. This is a major flow assurance problem in the industry, not only for the economic loss that stopping the production causes, but also the for safety reasons, where the plugging of a pipeline by hydrates can cause major damages to equipment and injuries to working personnel (SLOAN et al., 2011).

A common prevention technique is the addition of thermodynamic inhibitors, where the equilibrium conditions of the system changes to one outside the hydrate formation region. Although it can prevent the formation of hydrates, the costs associated are very significant. For example, Canyon Express gas transport system spent around US$ 1million every eight days with the consumption of methanol and The Ormen-Lange Norwegian field uses a very large amount of the world's annual production of MEG in order to prevent the formation of hydrates. Other than the large costs with inhibitors, their recovery also significantly contributes to the overall expenses. That being said, the ability to correctly estimate the amount of inhibitor to be used in a given system is of great economic importance (SLOAN et al., 2011).

Carbon dioxide is a contaminant in oil. Depending on the oil field, its concentration can reach up to 50%. The study of the CO_2 influence on the flow in pipelines and on the thermodynamic phase equilibrium is then of great importance. As the flow in pipelines reaches high pressures, the condensation of the vapor phase becomes possible. The study of the phase equilibria of hydrates in condensate systems is then fundamental to ensure the safety and economic feasibility of oil and gas production.

As these high pressures in oil and gas production are common, it is necessary to study the action of thermodynamic inhibitors on the phase equilibrium above the upper quadruple point, characterized by the appearance of a condensate phase. The region above Q_2 for carbon dioxide hydrates is less studied with a lack of experimental data in literature, especially with the presence of thermodynamic inhibitors. This work focuses specifically in this region, in addition, the effect of MEG and NaCl as thermodynamic inhibitors is experimentally analyzed.

1.3 STRUCTURE OF THIS DISSERTATION

This dissertation is divided into 5 chapters. The first one introduces the subject of hydrate formation and their prevention in oil and gas industries as well as in other fields, and the concept of hydrate formation.

Chapter 2 presents a literature review on hydrate formation in oil and gas industries, followed by the types of hydrate crystalline structures. The experimental works available in literature for hydrates of carbon dioxide above Q_2 are also presented. Next, phase diagrams and the properties of the compounds used are presented. The different types of experimental procedures used in literature is also shown. Finally, the equations and concepts utilized in order to evaluate the consistency of data sets are presented.

In chapter 3, the reader will find the experimental procedure used. The experimental apparatus is described alongside its capabilities and limitations. The isobaric search method is explained in detail in this section.

The results are presented and discussed in chapter 4, where the experimental data collected is also evaluated for consistency. At the end, the data collected is compared with commercial software products and models predictions. The conclusions and suggestions for future work are presented in chapter 5.

2 LITERATURE REVIEW

In this chapter it is presented an introduction on hydrate structure and the particularities of carbon dioxide hydrates with and without thermodynamic inhibitors. The phase diagram and properties of the compounds used are shown. A review on experimental methods for determining equilibrium points of hydrates above Q_2 and previous works from available literature are also presented.

2.1 HYDRATE FORMATION IN OIL AND GAS INDUSTRY

The first reported work on the formation of gas hydrates in oil and gas industry was done by Hammerschmidt (1934). He noted that a structure similar to ice snow formed in pipelines in the presence of water and natural gas molecules, such as methane, ethane, propane and isobutane, consequently blocking the flow. Differently from snow, he noted that in high pressures (from 0.75 MPa to 5.5 MPa), those structures formed at significantly higher temperatures than ice (from 1.1 °C to 4.5 °C). Since then, hydrate formation has been a major problem in oil and gas industries, motivating research on their prevention.

In oil and gas industries, a few procedures can be carried out in order to either prevent or remediate hydrate formation. The addition of thermodynamic inhibitors does not prevent per se the formation of hydrates, but they shift the phase equilibrium curve of hydrate formation, causing the conditions for the formation of hydrates to be more severe (i.e. lower temperature or increased pressure). The addition of alcohols, such as methanol and MEG, is a common practice in the industry to lower the equilibrium temperature of hydrates. Table 2.1 shows the properties of commonly used thermodynamic inhibitors. All of those cited here exhibit some sort of polar interaction with water molecules, lowering its activity through hydrogen bonding (CARROLL, 2014).

Although methanol is used in hydrate inhibition, it has several drawbacks. For instance, as it usually is for alcohols such as ethanol, it can be highly flammable. Glycols are significantly less flammable and thus safer than the alcohols from this point of view. Another

common problem with the usage of methanol is its corrosion effect on pipelines. The use of corrosion prevention chemicals, in those cases, is necessary. However, depending on the chemicals used, they can actually be dissolved in methanol, making the corrosion problem a complicated one to address. An alternative then is the use of glycols, such as Triethylene-glycol (TEG) and Monoethylene-glycol. Having a molar mass of 150.17 g/mol, TEG has less than half of the inhibition effect when compared to MEG. For those reasons, MEG can be an attractive alternative as a thermodynamic inhibitor (CARROLL, 2014).

Table 2.1. Properties of common thermodynamic inhibitors.

	Methanol	**Ethanol**	**TEG**	**MEG**
Empirical formula	CH_4O	C_2H_6O	$C_6H_{14}O_4$	$C_2H_6O_2$
Molar mass [g/mol]	32.042	46.07	150.17	62.07
Boiling point [K]	337.85	351.55	561.15	471.15
Vapor pressure (at 293.15 K) [MPa]	0.0125	0.0057	<0.00001	1.1 E-6
Melting point [K]	175.15	161.15	268.85	260.15
Density (at 293.15 K) [g/cm³]	0.792	0.789	1.126	1.116
Viscosity (at 293.15 K) [cp]	0.59	1.2	49	21

Source: Adapted from Carroll (2014).

Similarly, salts also act as thermodynamic inhibitors, interfering with the water hydrogen bonds. Although is very unlikely that salts would be added as a thermodynamic inhibitor, mainly due to corrosion effects, the water extracted with the oil in offshore production is naturally inhibited with salts. For this reason, it is important to take into account its salinity in order to better optimize the amount of thermodynamic inhibitor to be used (SLOAN et al., 2011).

Low dosage hydrate inhibitors (LDHIs) has gained a lot of attention in the last two decades as a good alternative to control hydrate formation. The most common thermodynamic inhibitors are usually applied with concentrations between 20 mass% and 50 mass%, while LDHIs can be used with much lower additions of between 0.1 mass% and 1 mass%. Consequently, their use can significantly lower separation costs due to the presence of the inhibitor in the production streams (KELLAND, 2006).

Figure 2.1 shows a schematic theory of how hydrates form in pipelines in oil dominated systems. As time and distance in the pipeline increases, hydrate nucleation occurs and, subsequently, the agglomeration of those nuclei previously formed. As the agglomeration process continues, eventually enough hydrates are formed so that pipe plugging occurs (SLOAN et al., 2011).

LDHIs are classified into two categories: kinetic inhibitors and anti-agglomerants. Kinetic inhibitors act by delaying the formation of crystals, essentially increasing the induction time and allowing for the flowing of the fluid in question for longer without the presence of hydrates.

Figure 2.1. Hydrate formation process in pipelines.

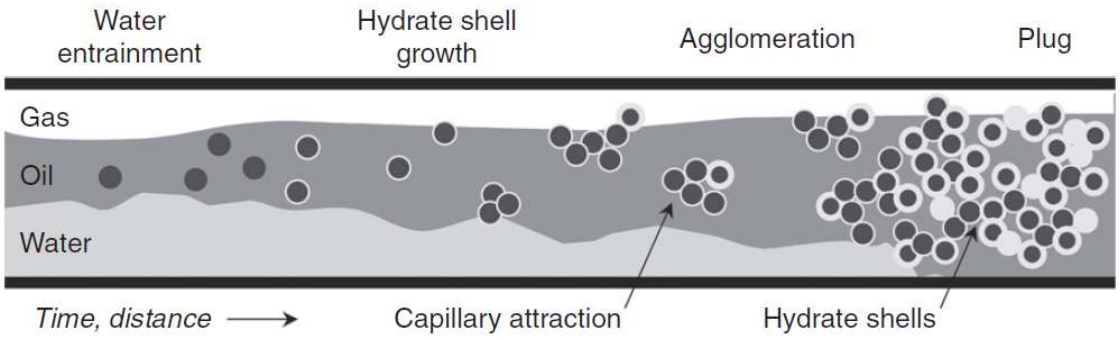

Source: Sloan et al. (2011).

Another technique used in industry is the dehydration of natural gas. With the removal of water, hydrate formation is not possible, thus it can be a good alternative depending on the circumstances. The dehydration of the gas also gives another benefit, which is the reduction of corrosion in pipelines. Some of the methods used for dehydration of gas are glycol dehydration (liquid absorbent), molecular sieves (solid absorbent), and refrigeration. Although it seems like a good alternative, dehydration is not feasible in many offshore oil production due to the equipment necessary and physical space availability (CARROLL, 2014).

To remediate the formation of hydrates plugs, heat and pressure can be used for their removal. The plugging of pipelines is very problematic in the industry. The formation of hydrates causes a loss of pressure, which can consequently cause a stop in production for maintenance with a high economic cost. Although the hydrate plug is often porous and

permeable, this not always the case, especially in condensate lines. The addition of MEG/water mixture is not always a good alternative, as the low temperatures increase the viscosity of the mixture, preventing it from reaching the whole of the plug. By heating the pipeline or the plug itself, the hydrate can be melted and thus the plug removed (AUSTVIK et al., 2000).

The depressurization of the pipeline can be performed in order to remove a hydrate plug. Differently from ice, the reduction of pressure causes the system to leave the hydrate formation region, essentially melting it. This process is not instantaneous and the hydrate plug melts radially. This can cause some dangerous situations, as the hydrate plug can turn into a projectile if it is not completely melted (PETERS et al., 2000).

The addition of thermodynamic inhibitors is the most commonly used method for the prevention of hydrates. However, for safety reasons, it is usually used in excess in order to guarantee normal operations. Methods such as pipeline heating have a very high initial cost, and kinetic and anti-agglomerants still need more studies in order to determine their mechanisms and effectiveness.

As every method has its advantages and drawbacks, the use of MEG as a thermodynamic inhibitor seems like a good approach for the prevention of hydrates. The knowledge of how much MEG is necessary to inhibit the formation of hydrates for a given system is of great economic value, as the overuse of MEG is common in the industry. As the water extracted with offshore oil and gas is naturally inhibited with salts, the study of the inhibition effect with mixtures of NaCl and MEG can help to optimize the amount of added thermodynamic inhibitors.

2.2 HYDRATE STRUCTURES

When hydrates form, they agglomerate as crystalline structures. The types of crystalline structures will depend on the type of gas molecule that is entrapped inside the hydrate cages. Figure 2.2 shows the classification of hydrate structures. These are formed by the combination of the following geometries: twelve pentagons (5^{12}); twelve pentagons and two hexagons ($5^{12}6^2$); twelve pentagons and four hexagons ($5^{12}6^4$); three squares, six pentagons and three hexagons ($4^3 5^6 6^3$); twelve pentagons and eight hexagons ($5^{12}6^8$). The combinations of

these cavities form the structure types sI, sII and sH, as shown in Figure 2.2 (SLOAN and KOH, 2008).

The type of hydrate structure that will be formed is highly dependent on the size of the guest molecules. The cavities 5^{12} and $4^3 5^6 6^3$ are smaller so that only small molecules can occupy them. The other cavities are larger, so either small or large molecules can occupy them. In the case of carbon dioxide hydrates, both small of large cavities are occupied by the same type of molecule, forming the structure of type I (SLOAN and KOH, 2008).

Figure 2.2. Types of hydrate Structures.

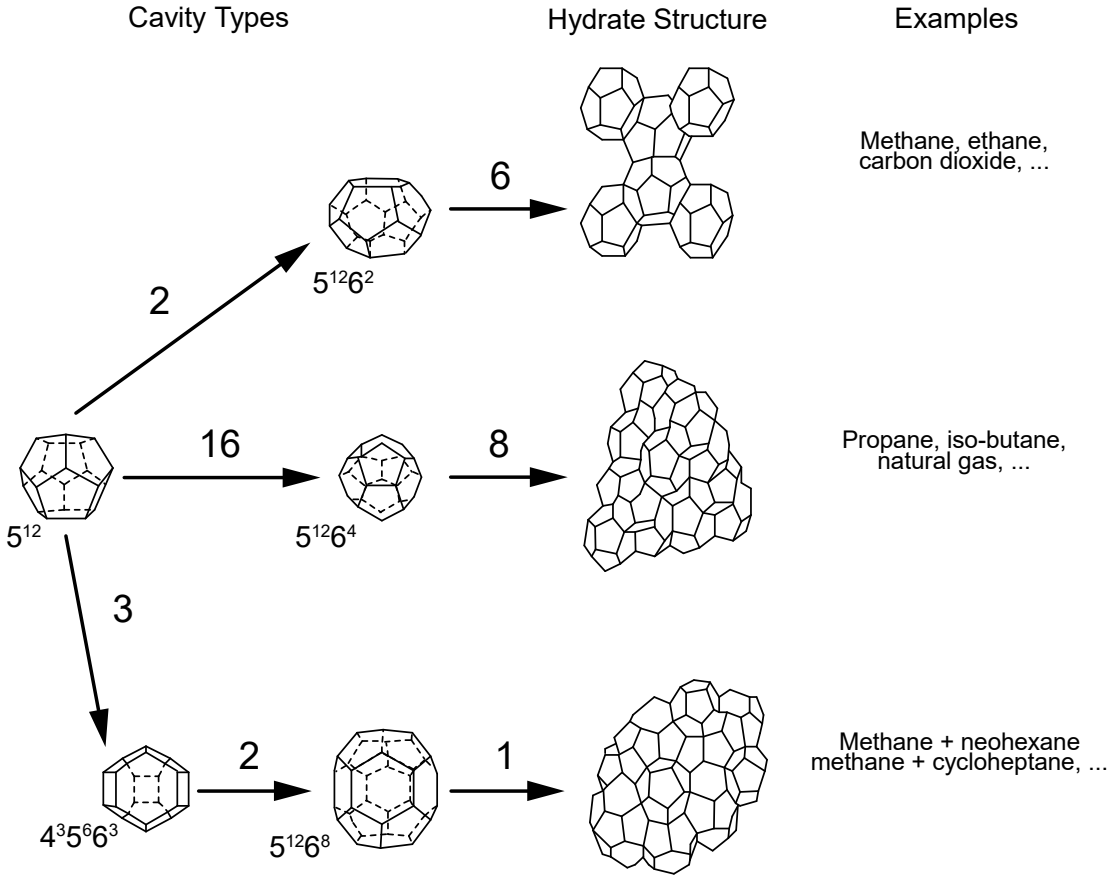

Source: Adapted from Sloan (2003).

For methane hydrates, the structure type I is formed. However, when it is mixed with a large molecule, even at small concentrations, the structure type II is formed. That can happen with natural gas, which is composed mainly of methane, where the larger molecules are able occupy the large cavities of structure II (SLOAN, 1991).

Figure 2.3 shows equilibrium curves for hydrates at different concentrations of methane and propane, plotted as the natural logarithm of pressure by temperature. The first curve on the top of the graph corresponds to the equilibrium of methane hydrates (indicated as 0), which forms structures of type I. As the concentration of propane is increased, the hydrates equilibrium curve stays lower and closer to the equilibrium curve for propane hydrates, which is the last curve bellow on the graph (indicated as 100). In that study, Sloan (1991) showed that even with small concentrations of propane added (starting with 1%), there is a significant change in the equilibrium pressure, indicating a change in the crystalline structure.

Figure 2.3. Methane hydrate phase equilibrium with small concentrations of propane.

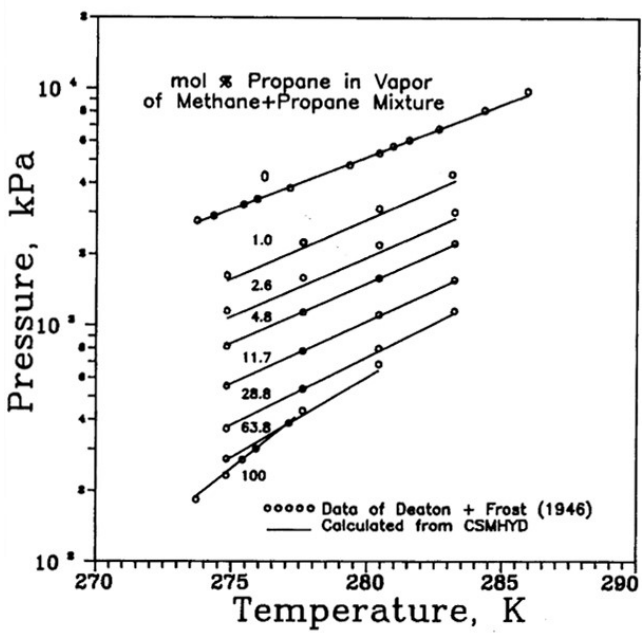

Source: Sloan (1991).

2.3 PHASE DIAGRAMS AND COMPONENTS PROPERTIES

The phase diagrams of the compounds used here are presented. They show the behavior of compounds with respect to solid-liquid-vapor phase changes. For each one, the

given particularities are shown and their diagrams can assist in developing a feasible experimental methodology and are essential for the prediction of formation of hydrates.

2.3.1 Water

The phase behavior of water is very well studied, which shown in Figure 2.4. Each curve represents an equilibrium of phases plotted as pressure versus temperature. Each region between phase change lines corresponds to a certain phase, except for the region to the right and above the critical point, where supercritical fluid exists. The triple point is characterized for the coexistence of the solid, liquid and vapor phases which, for water, it is at 0.0006 MPa / 649.90 K. The critical point is the condition that separates the vapor phase and the gas phase, which cannot condense. For water, the critical point is at 22.06 MPa / 649.90 K.

In case of compounds that suffer a decrease in volume when solidified (from (a) to (b) in Figure 2.4), in other words, the density of the solid phase is lower than the liquid phase, the inclination of the Solid-Liquid equilibrium line is similar as the one shown in Figure 2.4.

Figure 2.4. Water phase diagram (not to scale).

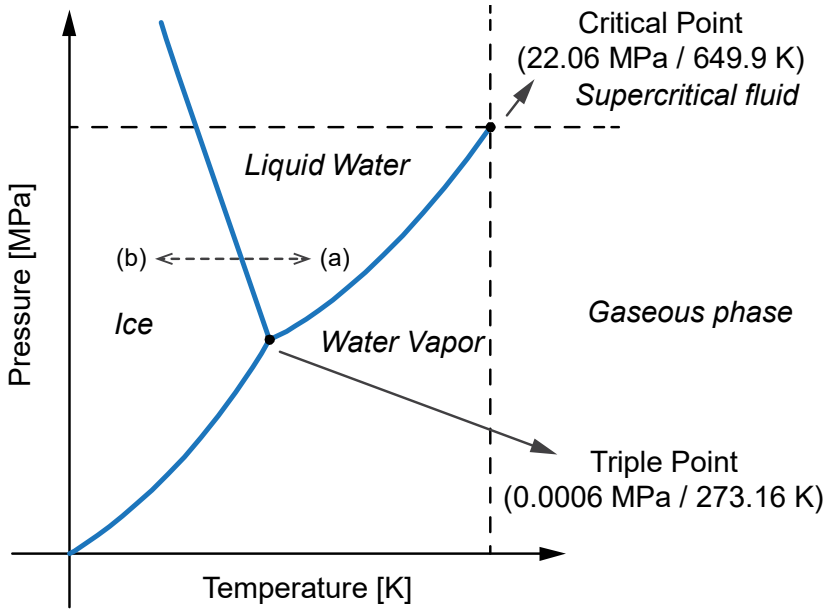

Source: critical and triple points from Moran et al. (2014).

The symmetry of the water molecule causes a permanent electric dipole momentum due to the distribution of charges. These type of molecules are called “polar molecules”. This local charge characteristic, despite being weaker than traditional chemical bonding, is responsible for the hydrogen bonding between water molecules (ATKINS and JONES, 2008).

Figure 2.5 shows the electron distribution for water molecules, where the two free electrons from the oxygen atom creates a local negative charge (δ^-). The hydrogen molecules have a positive local charge (δ^+) due to the displacement of its electrons towards the covalent bonds.

Figure 2.5. Electron distribution and hydrogen bonding in water molecules.

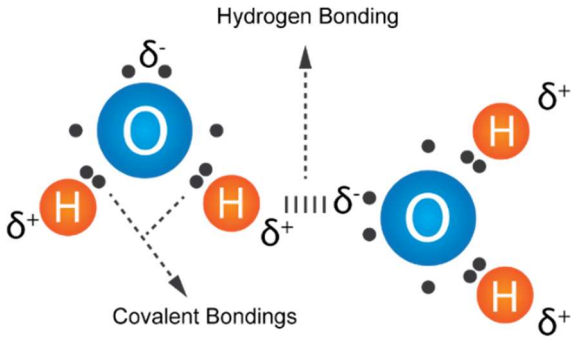

The density of water is shown in Figure 2.6 as predicted by the software Multiflash, plotted as density versus temperature. As it can be seen, the density of solid water is lower than liquid water. Although the difference is very small (around 0.08 g/cm³), this can still be used as a way to differentiate ice from hydrate through the comparison of volumes.

Figure 2.6. Density of water at 0.1 MPa as predicted by Multiflash 6.1 (2017).

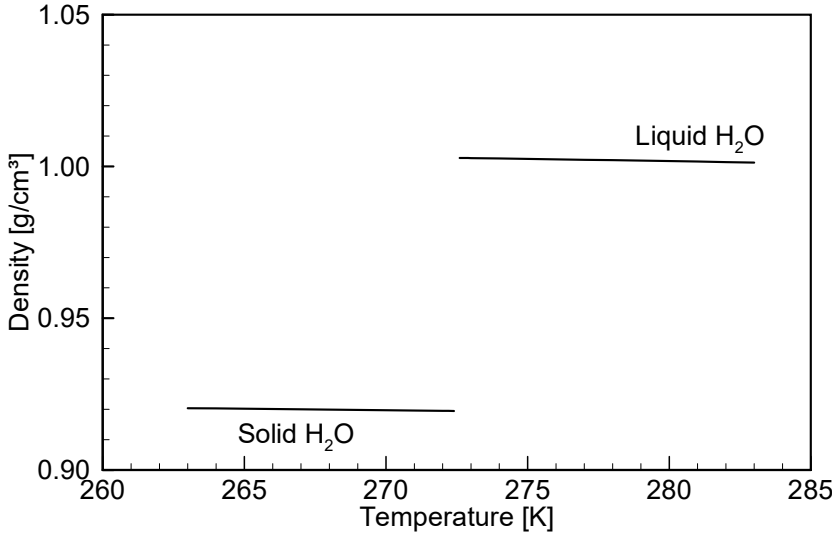

2.3.2 Carbon Dioxide

Figure 2.7 shows the phase diagram for carbon dioxide. The phase changes are plotted as pressure versus temperature. CO_2 has a critical point of 7.39 MPa / 304.0 K and a triple point of 0.519 MPa / 216.58 K. In offshore oil production, fluids generally flow at high pressures and low temperatures, falling inside a region where CO_2 liquefies.

In the case of carbon dioxide, the solid phase has a higher density that the liquid phase. For this reason, the inclination of the Solid-Liquid equilibrium line is tilted differently than that of the water, as shown in Figure 2.7 between (a) and (b).

Figure 2.7. Carbon dioxide phase diagram (not to scale).

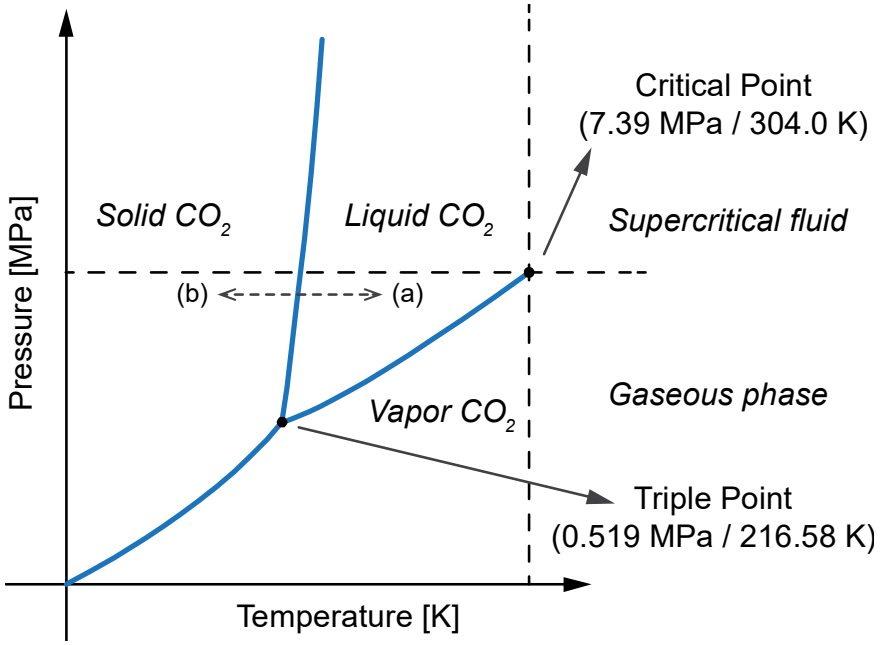

Source: critical and triple points from Angus et al. (1976).

Differently from water, carbon dioxide molecules are linear in geometry, meaning that they do not have an electric dipole momentum, making them non-polar molecules. For this reason, carbon dioxide has a low solubility in water, causing a second liquid phase to be formed when condensed (ATKINS and JONES, 2008).

2.3.3 Carbon Dioxide Hydrates

The phase diagram behavior of hydrates is highly dependent on the type of the guest molecule. In addition, the presence of thermodynamic inhibitors change the equilibrium conditions on the phase diagram.

The phase diagram of carbon dioxide hydrates has two quadruple points. The lower quadruple (Q_1) point appears due to the formation of ice. The upper quadruple point (Q_2) appears due to the condensation of the vapor phase.

Figure 2.8 shows the different regions in the phase diagram of carbon dioxide hydrates, plotted as the logarithm of pressure versus temperature. The Q_1 point (lower quadruple point) is characterized with the coexistence of four phases: ice, liquid water, hydrate and vapor CO_2. The Q_2 point indicates the coexistence of vapor CO_2, liquid CO_2, liquid water and hydrate phases. In the region above Q_2, carbon dioxide is in its liquid state. This means that when hydrates form in this region, liquid CO_2 will combine with liquid water to form hydrates, as illustrated by the blue arrow in Figure 2.8 (a). The region above Q_2 is the main focus of this work, as its displayed in the enlarged (a) area of Figure 2.8, through the determination of the H-L_W-L_{CO2} equilibrium line, shown as the orange line (SLOAN and KOH, 2008).

The region above Q_2 point is surrounded by two-phase regions. In order to determine the H-L_W-L_{CO2} equilibrium curves, an experimental procedure that starts at L_W-L_{CO2} region and goes to H-L_{CO2} region can be developed (SLOAN and KOH, 2008).

Above the Q_2 point, the equilibrium curve for hydrates changes and has a significantly higher inclination. This means that a small difference in temperature causes a big difference in equilibrium pressure. That being said, it is necessary that the experimental apparatus to be used is able reach high pressures to ensure the condensation of the gas phase.

Figure 2.8. Phase diagram for carbon dioxide hydrates. (a) Region above Q_2.

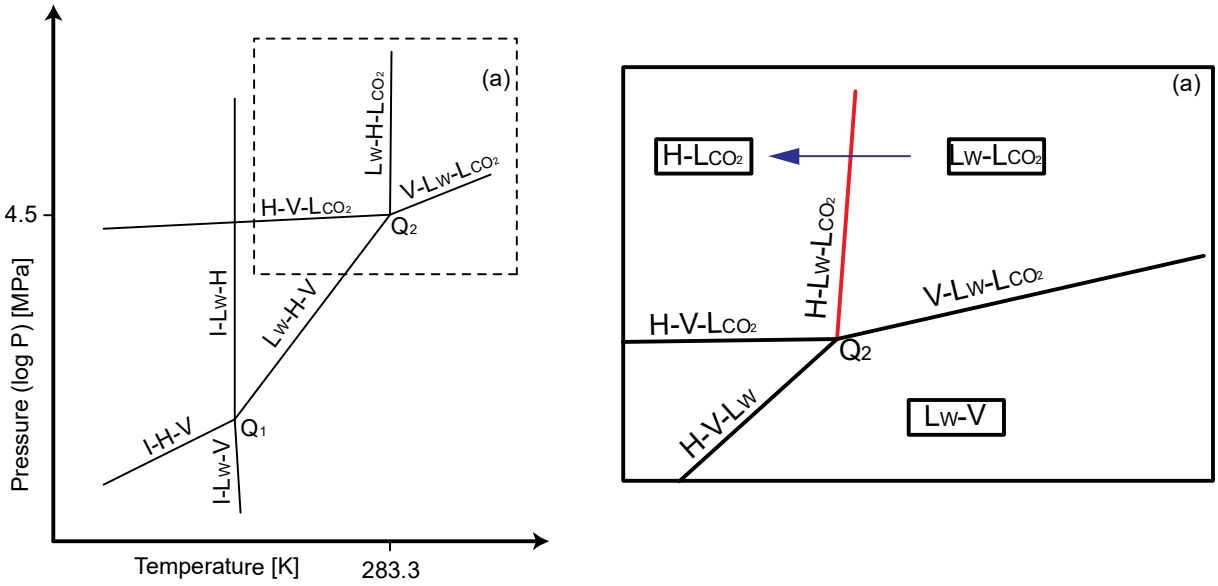

Source: Adapted from Sloan and Koh (2008).

2.3.4 Density Of The Phases

By using the Multiflash commercial software product, it is possible to get a glimpse into how the system behaves when kept at a constant pressure. At 10 MPa, carbon dioxide is condensed and has a density much closer to water than to gaseous CO_2. Figure 2.9 shows a comparison between the density versus temperature for water, CO_2 and hydrates of CO_2 as predicted by Multiflash. It is interesting to note that hydrates of CO_2 are actually denser than ice, meaning that this can be used to infer if the system has ice or hydrates present by measurements of temperature and volume at a constant pressure. Although these predictions can help understand how the system behaves, it is important to keep in mind that they may not be accurate, especially with CO_2 hydrates.

The work done by Aya et al. (1997) was able to find that the density of carbon dioxide hydrates is greater than of the two liquid phases. The relative density is between 1.09 and 1.11 for a pressure of 30 MPa, showing that Multiflash gives good agreement with the experimental data. This difference can then be used to identify the presence of hydrates by measurements of temperature, volume and pressure.

Figure 2.9 shows the density versus temperature for CO_2 hydrates, liquid CO_2, liquid H_2O and ice. As liquid water and liquid CO_2 combine to form hydrates, the density increases, as indicated by arrows in (a) in Figure 2.9. This ultimately means that in a system kept at a constant pressure, the formation of hydrates can be identified by a decrease in volume due to the higher density of the hydrate phase.

Figure 2.9. Density comparison for water, CO_2 and hydrates of CO_2 at 10 MPa as predicted by Multiflash. (a) Change in density with hydrate formation.

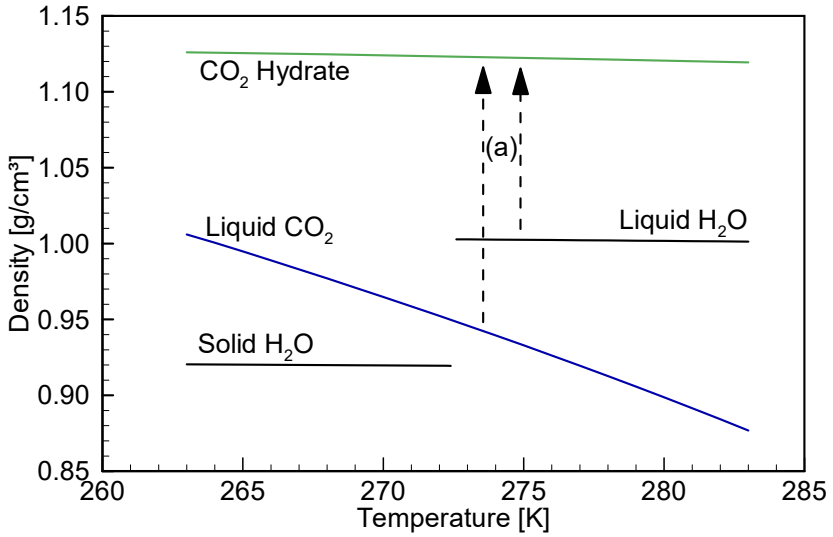

2.4 THERMODYNAMIC INHIBITORS

The presence of thermodynamic inhibitors changes the phase equilibrium for the formation of hydrates, allowing for prevention techniques that avoid hydrate formation. The thermodynamic inhibitors used are monoethylene glycol (MEG) and sodium chloride (NaCl).

In offshore oil extraction, the water obtained in the production is naturally inhibited by the presence of several types of salts. Even so, in order to operate outside of the hydrate zone, MEG can be used for this goal. The knowledge of how these compounds influence the formation of hydrates allows for the optimization of the amount of inhibitors to be used (SLOAN and KOH, 2008).

2.4.1 Sodium Chloride

Salts have a thermodynamic inhibition effect on the formation of hydrates through Columbic forces. These forces cause a competition between the ion molecules from the salt and the water molecules, meaning that less water molecules are available for the formation of hydrates, in other words, the activity of water is decreased.

Figure 2.10 shows the pressure versus temperature for the phase equilibrium of carbon dioxide hydrates, with and without the presence of NaCl. The region to the left of the curves is where hydrates can form and, to the right, where hydrates cannot exist. The continuous black lines are predictions done by Multiflash (2017). The V_{CO2}-L_{CO2}-L_{H2O} line indicates the boundary between liquid and vapor CO_2, which essentially delimitates the regions above and below the Q_2 point. The equilibrium curves bellow the Q_2 point indicate the phase equilibrium of hydrates formed with the presence of gaseous CO_2. Dashed lines and dashed-dotted lines represent the predictions done by the Hu-Lee-Sum correlation (HU et al., 2017 a) and CSMGem, respectively. The blue continuous lines are predictions done by the software product PVTSim. These same nomenclatures for software products and model predictions are used throughout this work.

Figure 2.10. Inhibition effect of NaCl on hydrate formation.

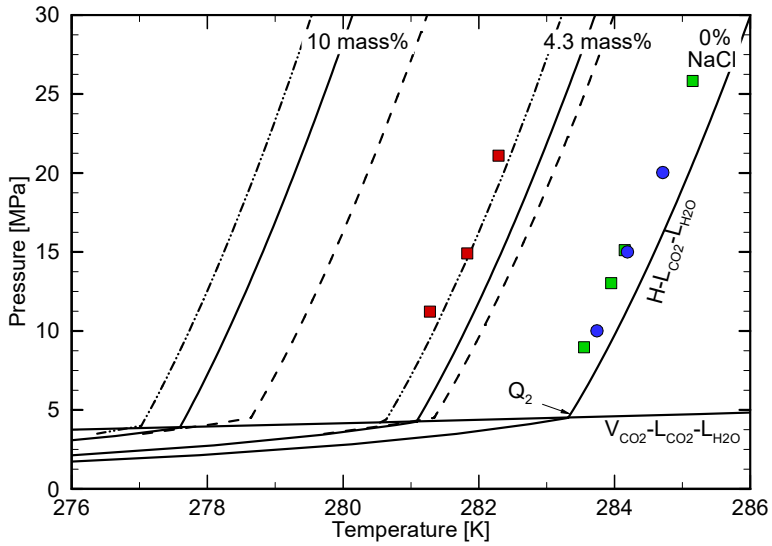

Ruffine and Trusler (2010);
Chapoy et al. (2011);
Shin et al. (2014);
Hu-Lee-Sum correlation;
CSMGem;
Multiflash;
PVTSim.

Figure 2.10 also shows the available data found in literature for the inhibition effect of NaCl dissolved in the water phase. In this case, only one work (Ruffine and Trusler, 2010) was found with experimental data for carbon dioxide hydrates above the Q_2 point with the presence of sodium chloride, highlighting the scarcity of data available in this region.

The presence of salts in the liquid aqueous phase causes a inhibition effect due to the interactions of the ions with the polar regions of the water molecules, acting as thermodynamic inhibitors (HU et al., 2017 b). Even with a small amount of salt added to the system, a significant shift in the equilibrium curve can be observed, as noted by Ruffine and Trusler (2010).

2.4.2 Monoethylene Glycol (MEG)

As mentioned before, Monoethylene glycol (MEG) is commonly used to inhibit the formation of hydrates. This thermodynamic inhibitor acts by interacting with other water molecules through hydrogen bonding, making water molecules less available to form the hydrate cage structure. Figure 2.11 illustrates how the hydroxyl group of the MEG molecule interacts with a water molecule due to the existence of a local electric dipole (indicated as δ^+ and δ^-) on both. Just like the hydrogen bonding between water molecules, the free electrons from the oxygen atom in water creates a local negative charge which interacts with the local positive charge of the hydroxyl (O-H) group in MEG. Since the MEG molecule has two hydroxyl groups, each molecule can interact with two water molecules, boosting their inhibition effect.

Figure 2.11. Interactions between MEG and water molecules (hydrogens bonded to carbon atoms are not shown).

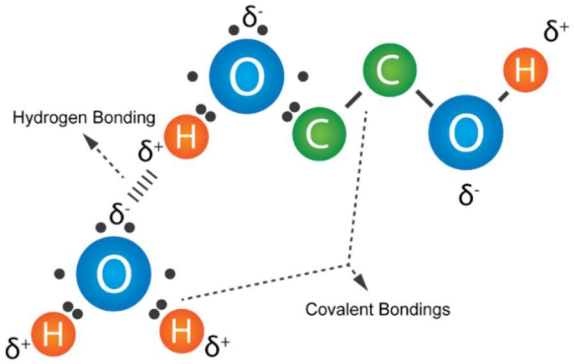

Figure 2.12 shows the inhibition effect of MEG in carbon dioxide hydrate formation. Above the upper quadruple point, there is a scarcity of data in literature, especially with the presence of additives such as MEG. One of the few data points found in literature are given by Ng and Robinson (1985) for 50 mass% of MEG.

In this same figure, it is shown the prediction of software for different concentrations of MEG. For the pure water system, the predictions are very similar between models. However, as inhibitor concentration gets higher, the discrepancies between models becomes more significant. This demonstrates the difficulties in predicting inhibited systems due to their complexity. Accuracy of models and software products can then be improved by new experimental data with different MEG concentrations.

Figure 2.12. Data available in literature for the inhibition effect of MEG.

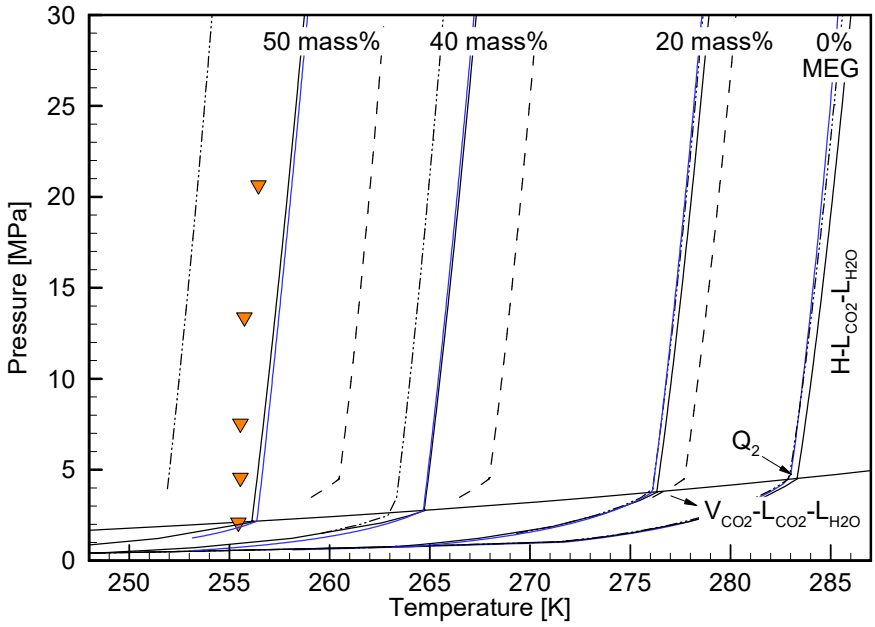

2.5 EXPERIMENTAL TECHNIQUES

In this section, it is presented the most commonly used experimental procedures for determining equilibrium points of hydrates available in literature: isochoric, isothermal and isobaric. Each of those have their own advantages and disadvantages, which are evaluated to define which method is best for the proposed work.

2.5.1 Overview

The first studies that were focused on the phase equilibrium of hydrates relied mainly on visual detection through windows or some sort of transparent apparatus. Initially, hydrates were formed at low pressures, facilitating the use of transparent materials. Hammerschmidt (1934) performed one of the first observations of natural gas hydrates using a Pyrex glass tube with pressures of up to 5.5 MPa. The experimental apparatus consisted of a closed flow loop cooled with a heat exchanger. For carbon dioxide hydrates above the Q_2 point, Takenouchi and Kennedy (1965) were the first to report experimental data, ranging from pressures of 4.5 to 186.2 MPa.

Deaton and Frost (1937) used a windowed equilibrium cell for observations of hydrates, noting their equilibrium conditions. Ng et al. (1985 b) gave experimental data on hydrates of CO_2 with the presence of methanol, noting its inhibition effect. They also obtained a few data points above Q_2. Their equilibrium cell was cooled with a chiller and the temperature at which hydrate crystals were no longer visible was taken as the equilibrium point.

Ohgaki et al. (1993) obtained CO_2 hydrates equilibrium data using seawater with an isochoric experimental procedure. By collecting data for temperature and pressure, they were able to determine graphically the equilibrium temperature, being more reliable than visual methods. Additionally, they noted that the use of seawater caused a lower shift in the equilibrium temperature when compared with pure water, indicating that the presence of salts have an inhibition effect.

Fan and Guo (1999) used an isothermal procedure to find equilibrium points of carbon dioxide hydrates. Using an equilibrium cell with a moving piston, the pressure was changed in order to form and dissociate hydrates. The equilibrium point was determined through analysis of pressure data. A few data points were collected near the upper quadruple point.

Mooijer-Van Den Heuvel et al. (2001) and (2002) used an isochoric procedure to find the equilibrium conditions for hydrates of CO_2. Their focus was on determining the H-V_{CO2}-L_{H2O} but with also a few data points above Q_2. The latter work also used organic additives. Despite having very accurate measurements of temperature and pressure, their determination of the equilibrium point still relies on the visual observation of hydrate crystals.

Kiyono et al. (2005) used an isochoric experimental procedure to determine Q_2 points for hydrates of HFC-134a. Due to the low pressures necessary to condense this compound, the procedure was done in a completely transparent apparatus, providing very good visualization, even above Q_2 where condensate exists. With measurements of temperature and pressure, the three-phase equilibrium line was determined by the visual confirmation of hydrates through the apparatus. Using this same approach, the Q_2 points were determined with the visualization of four phases: condensate-water-gas-hydrate.

Kim et al. (2011) and Shin et al. (2014) used a experimental apparatus that operates at a constant pressure with the use of a pressure generator. The more recent work focused on the inhibition effect of ionic liquids on the carbon dioxide hydrate equilibria above Q_2. The use of a sapphire window allowed for the visualization of hydrates at high pressures (up to 20 MPa). The equilibrium temperature was taken as the one where hydrate crystals were no longer visible in a heating process.

More recently, Nagashima et al. (2016) used a constant volume procedure with an mechanically agitated equilibrium cell. Their technique showed very satisfactory results for determining equilibrium points in the $H\text{-}V_{CO2}\text{-}L_{H2O}$ curve and data for the Q_1 point. Bi et al. (2013) also used an isochoric procedure, but the determination of the equilibrium point was done visually through a sapphire window with data above Q_2.

The visual observation of hydrate dissociation has several drawbacks. It is usually utilized with low pressures in order to allow for the use of transparent materials. The possible confusion with ice crystals means that equilibrium points should be preferably be taken above the ice formation temperature and, lastly, the determination of the dissociation temperature can take several hours or even days, which means that the constant care for the experiment is often not possible (SCHROETER et al., 1983).

As technology improved, the visual observation for the dissociation of hydrates became less used due to its reliability. Despite that, it is still significant when analyzing the influence of the hydrates on the flow in pipelines. As an example, Straume et al. (2016), from the same research group as the one in this work (NUEM), used a rocking cell with a visualization window, combined with temperature and pressure measurements, to study the formation and deposition of hydrates in non-emulsifying and condensate systems. The rocking

cell was kept immerse in a circulating bath connected to a chiller in order to control its temperature. Experiments were performed with pressures of up to 4.55 MPa.

The equilibrium points for the formation of hydrates can be more reliably determined through measurements of temperature, pressure and volume. By plotting data, the phase change can be determined graphically. Still, sapphire windows can be used simply to confirm the presence of hydrates. The next three sections shows the different types of methods that can be used to determine experimental points for the equilibrium of hydrates graphically.

2.5.2 Isochoric

In this type of procedure, volume is kept constant. Gas, water and inhibitors are added to the system at a predetermined pressure. The formation of hydrates is promoted by the decrease in temperature (SLOAN and KOH, 2008).

Figure 2.13 illustrates how an isochoric procedure can be performed by evaluating changes in temperature and pressure. Firstly, the system is cooled from A to B in order to promote the formation of hydrates. The point at which hydrates form is never certain, as it is a stochastic process. The formation of hydrates can be confirmed as it dramatically lowers the system pressure as gas molecules diffuse to the solid hydrate phase (SLOAN and KOH, 2008).

After hydrates are formed, the system is heated (from C to D) in order to promote the dissociation process. The point at which hydrates are done dissociating (D) is the equilibrium condition for the formation of hydrates. The dissociation point is chosen as the equilibrium condition because it is always the same, in contrast with the formation point B, which can easily change. In addition, after the system passes the point C, hydrate formation can occur as the system is in a region of a meta-stable state (SLOAN and KOH, 2008).

Following the steps of cooling and heating, the equilibrium point can then be determined graphically by the crossing of the cooling line (A-B) and the dissociation line in order to find D (MOOIJER-VAN DEN HEUVEL et al., 2001).

Figure 2.13. Isochoric experimental procedure.

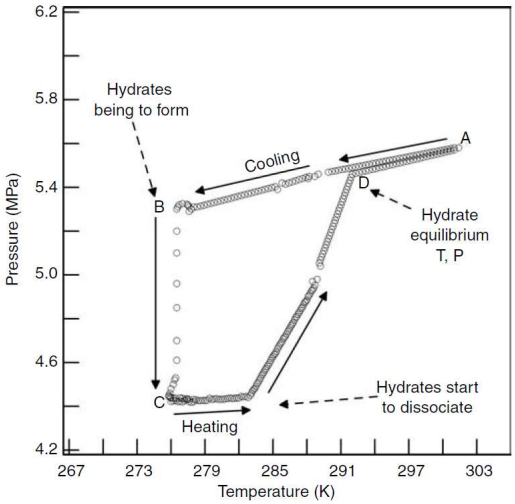

Source: Sloan and Koh (2008).

The isochoric procedure was also used by Kakitani (2014) MSc thesis, at the Multiphase Flow Center (NUEM), where this work was also developed. The procedure was performed in an equilibrium cell to determine the equilibrium point of hydrates of methane and mixtures of methane and carbon dioxide. Figure 2.14 shows the graph typically obtained by this type of experimental procedure. The red area in the graph indicates a decrease in pressure, which happens during the slow heating step due to a further formation of hydrates. All hydrates that are formed in this area are later dissociated, as the P-T curve goes back to the same inclination of the cooling step.

Figure 2.14. Isochoric experimental procedure performed by Kakitani (2014).

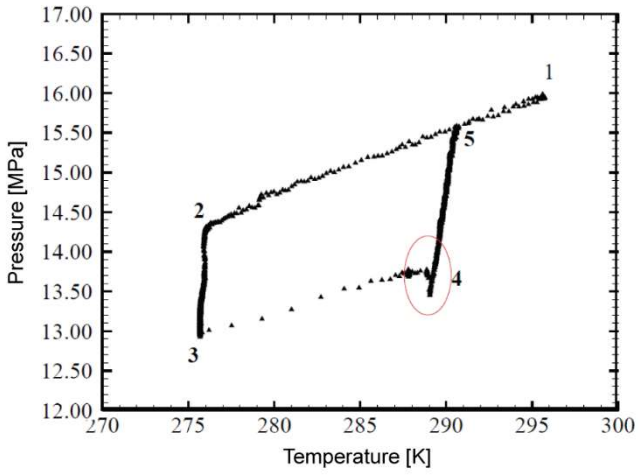

2.5.3 Isothermal

By maintaining a constant temperature, it is possible to identify the equilibrium conditions through the change of volume and pressure. Generally, the procedure is started at a pressure lower than the equilibrium one. Next, the pressure is gradually increased until all hydrates have been formed and, by lowering the pressure, hydrate dissociation is promoted. After all the hydrates have been dissociated, the measured pressure is at the equilibrium for the chosen temperature (SLOAN and KOH, 2008).

Another way to identify the dissociation point is to lower the pressure of the system in steps by the movement of a piston. As the piston moves, the volume increases and the system will respond by changing the pressure to match the new hydrate equilibrium condition. This step essentially finds points that are on the H-L-V equilibrium curve. When the pressure no longer decreases, it can be inferred that the equilibrium is no longer of hydrates but for two-phase L-V equilibrium curve. The last pressure recorded that had hydrates is the equilibrium pressure for the given temperature. This procedure was used by Guembaroski (2016) MSc thesis to determine equilibrium points for hydrates of carbon dioxide with the influence of selected thermodynamic inhibitors (Figure 2.15), which was also performed at NUEM.

Figure 2.15. Isothermal experimental procedure performed by Guembaroski (2016).

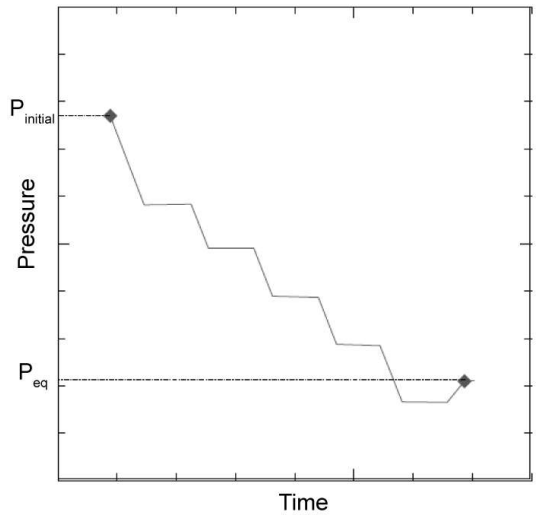

The isothermal experimental procedure has a considerable drawback when working with gas condensate, above Q_2. As is was shown in Figure 2.8 a), the inclination of the

equilibrium curve (L_w-H-L_{CO2}) is much higher in this region. This means that it is very difficult to find a constant temperature of which will give an equilibrium pressure above the Q_2 point.

2.5.4 Isobaric

For an isobaric procedure, the pressure of the system can be kept constant by the use of a moving piston, which changes the volume in order to control the pressure. The system can also be connected to an external source of gas, which is then used to add or remove the gas that is consumed by hydrate formation or dissociation (SLOAN and KOH, 2008).

For most cases, by lowering the temperature, initially the system will decrease in volume in order to keep a constant pressure. This initial decrease in density is due to the thermal contraction of the phases. This step is illustrated as 1 in Figure 2.16 (DAHM and VISCO, 2014).

After hydrates are formed (indicated as 2 in Figure 2.16), the system will change its volume due to the formation of a solid hydrate phase, which will typically have a different density than water. Another factor is the transfer of guest molecules to the hydrate phase, which commonly has a higher density as well.

The next step is the heating process, where the temperature is increased in order to promote the dissociation of hydrates. The temperature in which the hydrates finish dissociating is in the equilibrium temperature (T_{eq}) for the given pressure.

Figure 2.16. Isobaric experimental procedure.

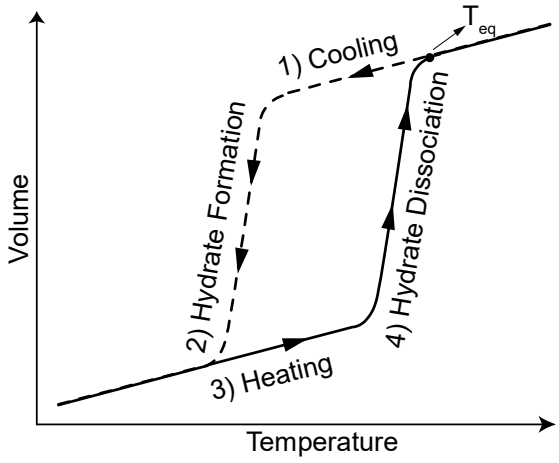

Besnard et al. (1991) was the first to use an isobaric experimental procedure using the amount of gas consumed in order to identify the formation of hydrates formed from gaseous carbon dioxide. A digital pump was used to add or remove gas as necessary to keep the pressure constant. The formation of hydrates was promoted by decreasing the temperature. As hydrates formed, gas was added to the cell (3-6 in Figure 2.17). After hydrates were formed, the temperature was slowly increased, causing a removal of gas from the system (7 in Figure 2.17) until all hydrates were dissociated. By plotting the volume of the gas added and the temperature, they were able to determine the equilibrium point for the chosen pressure (Final Decomp. Temp. in Figure 2.17).

Figure 2.17. Isobaric experimental procedure performed by Besnard et al. (1991).

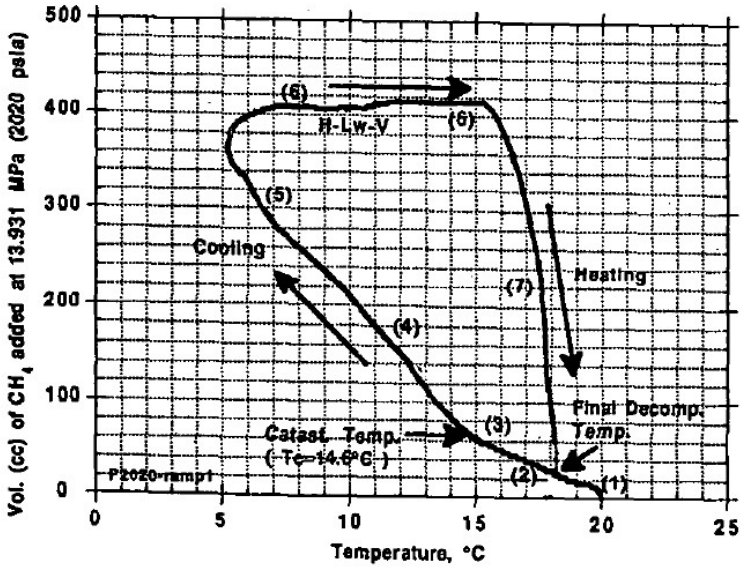

More recently, Chapoy et al. (2011) used an equilibrium cell with a moving piston that was used to keep a constant pressure. In this case, the amount of pressure fluid added to move the piston was measured and plotted with temperature. With a step heating process, the identification of the equilibrium point was determined with the change in inclination due to the dissociation of hydrates. This procedure is carried out similarly to the isochoric method, where a decrease in temperature causes the hydrates to form and the dissociation is promoted by a slow increase in temperature.

In the present work, the same isobaric method is used, but because of the high pressures necessary to condensate the gas phase, the differences in volume that allow for the identification of hydrates are considerably smaller. More details of this characteristic are discussed in Chapter 5 (Results).

2.6 CONSISTENCY OF THE DATA

For the experimental data, a consistency analysis can be performed in order to help determine if the data is reliable. The more traditional approach is the analysis of the Clausius-Clapeyron equation, which dictates that the phase change should follow its relation. The work done by Sa et al. (2018) proposes two more ways to analyze experimental data for hydrates: the consistency of the heat of dissociation and the water activity.

This way, three criteria can be analyzed to help determine the reliability of an experimental data set: 1. Consistency of the Clausius-Clapeyron relation; 2. Consistency of the heat of dissociation; and 3. Consistency of the water activity. In this section, the three criteria are presented and explained.

2.6.1 Clausius-Clapeyron Linearity Consistency Check

The determination of the heat of vaporization is a complicated and difficult procedure to be carried out experimentally. The Clausius-Clapeyron equation was initially proposed in order to calculate the heat of vaporization with the use of vapor pressure experimental data, which is much more viable in most cases (SLOAN and KOH, 2008).

$$\frac{dP}{dT} = \frac{\Delta H}{T\Delta V} \tag{1}$$

Equation (1) is a more general form of the Clausius-Clapeyron relation, where P is pressure, T is temperature, ΔH is the variation in energy associated with the phase change and ΔV is the change in volume. In the case of hydrates formed with gas, we have the following three-phase equilibrium.

aqueous liquid - hydrate - gas (2)

Because hydrates do not exist when the gas molecule is not present, the phase equilibria is characterized as univariant. This means that for a given system, pressure and temperature can be changed independently however, in order to maintain the state of the system, a corresponding change in the other variable must happen. This characteristic is not valid, for instance, in the case of the sorption equilibrium of a gas in a zeolite, being a di-variant equilibrium of which the Clausius-Clapeyron equation is not valid (VAN DER WALLS and PLATTEEUW, 1959).

The same will be valid for the equilibrium of hydrates formed with condensate, where the new solid phase is formed by the combination of water and condensate molecules. As shown by van der Walls et al. (1959), the Clausius-Clapeyron relation can be used to describe the phase equilibrium of hydrates, allowing for the calculation of the heat of dissociation with hydrate equilibrium experimental data. The Clausius-Clapeyron equation for hydrates is then given by Equation (3), where z is the compressibility coefficient and $\Delta H_{Dissociation}$ is the heat of dissociation of hydrates.

$$ln(P) = -\frac{\Delta H_{Dissociation}}{zR}\left(\frac{1}{T}\right) \quad (3)$$

Isolating the following term:

$$A = \frac{-\Delta H_{Dissociation}}{zR} \quad (4)$$

As R is the ideal gas constant and z can be assumed constant in a small temperature interval, A can thus be assumed constant (SA et al., 2018). This way, we obtain:

$$ln(P) = \frac{A}{T} + B \quad (5)$$

Figure 2.18 shows a representation of the plot from Equation (5), with the vertical axis being the natural logarithm of pressure ($ln(P)$) and, the horizontal axis, the inverse of temperature ($1/T$).

Figure 2.18. Plot of the Clausius-Clapeyron relation.

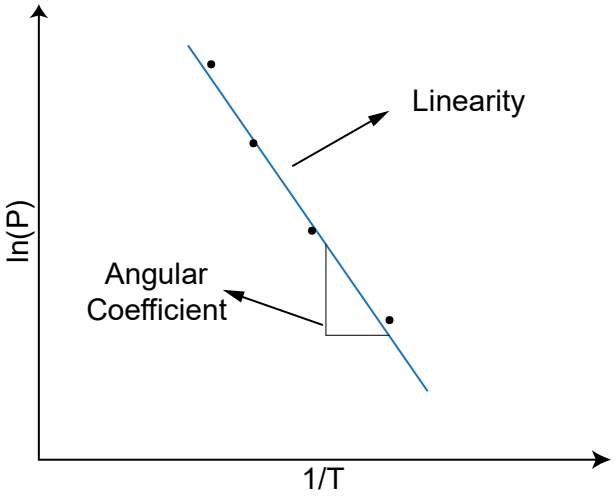

Thus, for a thermodynamically consistent set of data points, a linear relation between *ln(P)* and *1/T* must exist. Sa et al. (2018) suggested a range for pass, acceptable and failed consistency check for the linearity of the Clausius-Clapeyron relation. The deviation is calculated as shown in Equation (6), where R^2 is the coefficient of determination for the experimental data being evaluated.

$$\text{Deviation } (\%) = (1 - R^2) \times 100 \tag{6}$$

Table 2.2. Criteria for the linearity of the Clausius-Clapeyron relation.

Range	Verdict
≤ 2%	**Pass**
> 2% and < 5%	**Acceptable**
> 5%	**Fail**

2.6.2 Consistency Of The Heat Of Dissociation

A second consistency check also involves the Clausius-Clapeyron equation, but with regards to its slope, shown as the term *A* in Equation (4). For this case, it is assumed that the

coefficient of compressibility z and the heat of dissociation ΔH_d do not change significantly in a narrow temperature range (typically between 10 K – 20 K) (SA et al., 2018).

For simple thermodynamic inhibitors (such as MEG and NaCl), the interactions that cause a change in equilibrium conditions are between them and the water molecules, lowering the activity of the water, having no effect on the guest molecule. It is then reasonable to assume that the heat of dissociation will depend on the hydrate structure and guest molecules, not from the concentration of thermodynamic inhibitors (SA et al., 2018).

This way, the term A should stay constant regardless of thermodynamic inhibitor concentration. By comparing inhibited data with hydrates of pure water, it is expected that the term A stays unchanged. The data for hydrates of pure water is better studied in literature and can be used to help determine if the data for inhibited systems is adequate.

Equation (7) shows how the deviation from the pure water system is calculated, where the subscripts W and THI refers to the pure water and the thermodynamically inhibited systems, respectively. Table 2.3 shows the criteria proposed by Sa et al. (2018) for classifying the consistency check of experimental data as pass, acceptable and fail.

$$\text{Deviation (\%)} = \frac{A_{THI} - A_W}{A_{\text{W}}} \times 100 \tag{7}$$

Table 2.3. Criteria for the heat of dissociation consistency check.

Range	Verdict
≤ 5%	**Pass**
> 5% and < 10%	**Acceptable**
> 10%	**Fail**

2.6.3 Consistency Of The Water Activity

The third and last consistency check, as proposed by Sa et al. (2018), is not commonly used in the technical community. Based on the principles of freezing point depression, the suppression temperature due to the presence of thermodynamic inhibitors, is defined as the difference of equilibrium temperature between the system with pure water and the inhibited system, as expressed in Equation (8).

$$\Delta T = T_W - T_{THI} \tag{8}$$

From this point on, the following assumptions are made: the temperature does note vary significantly (from 10 to 20; hydrates form a pure phase, i.e. inhibitors do not form hydrates; the composition of the hydrate phase is constant; the composition of the hydrocarbon phase is constant; the enthalpy of dissociation of hydrates does not depend on thermodynamic inhibitor concentration. These assumptions alongside the deductions of equations are detailed in the Appendix A of this work. From those considerations, Equation (9) is obtained.

$$\frac{\Delta T}{T_0 T} = -\frac{nR}{\Delta H_d} ln\, a_W \tag{9}$$

The constant terms of Equation (9) can be arranged into a single constant (β).

$$\beta = \frac{nR}{\Delta H_d} \tag{10}$$

$$\frac{\Delta T}{T_0 T} = \beta\, ln\, a_W(x_i, T) \cong \beta\, ln\, a_W(x_i) \tag{11}$$

Using Equation (11), it is possible to conclude that the activity of water will change in relation to the suppression temperature, i.e. it can be related to the difference (ΔT) between the equilibrium temperature of the pure water (T_0) system and the inhibited system (T). That being said, the activity of water will be proportional to the left side of Equation (11).

To evaluate the consistency of the activity of water, the relative standard deviation (RSD), which is defined as the standard deviation divided by the average, of the $\Delta T/T_0T$ data for each concentration is calculated. The result is compared with the criteria in Table 2.4 to determine the verdict.

By using these assumptions and equations, Sa et al. (2018) proposed a criteria to evaluate the quality of hydrate equilibrium data, as shown in Table 2.4. This is a new way to evaluate the quality of experimental data, giving further credibility to experimental results.

Table 2.4. Criteria for the water activity consistency check.

Range	Verdict
≤ 5%	**Pass**
> 5% and < 10%	**Acceptable**
> 10%	**Fail**

2.7 OVERVIEW OF THE STATE OF THE ART

The formation of hydrates in oil and gas industries is a major flow assurance concern. Their prevention is often done with the use of thermodynamic inhibitors, which can be optimized by accounting for the presence of salts, lowering the amount of inhibitor used and subsequent purification costs. In oilfields with high concentrations of CO_2, the appearance of an upper quadruple point is possible, which changes the phase equilibrium of hydrates. Tree experimental methods are used in literature: isothermal, isochoric and isobaric. Each one has their own advantages and disadvantages and the one to be used takes into account the high pressures and the inclination of the equilibrium curve above the Q_2 point. Lastly, the evaluation of the consistency of the data provides an exceptional tool to ensure the reliability of the experimental data.

Table 2.5 shows the experimental data found in literature for CO_2 hydrates above the Q_2 point. Data for this region is very scarce with very few works with the addition of thermodynamic inhibitors. Most of the work available uses the isochoric method and very rarely used with the isothermal method.

Table 2.5. Data points found in literature for the region above Q_2 for CO_2 hydrates (L_w-H-L_{CO2}).

Author	Inhibitors (mass%)	Pressure Range [MPa]	Experimental Method
Takenouchi and Kennedy (1965)	-	4.5 186.2	Isochoric
Ng et al. (1985 b)	Methanol (10%, 20%), MEG (50%)	0.8 20	Isochoric Visual
Ohgaki et al. (1993)	Artificial Sea Water	4.386 8.930	Isochoric
Fan and Guo (1999)	-	0.5 5	Isothermal
Mooijer-Van Den H. et al. (2001)	-	5.97 7.35	Isothermal Isobaric Visual
Ruffine and Trusler (2010)	NaCl (4.3%)	5.9 47	Isochoric Visual
Chapoy et al. (2011)	-	8.97 35.43	Isobaric
Shin et al. (2014)	Ionic Liquids	5 20	Isobaric Visual

An experimental procedure was used that allowed for high pressures in order to guarantee that the CO_2 is present in its liquid state. Data for inhibited systems with NaCl, MEG and their mixtures not previously reported in literature was obtained for pressures between 8.5 and 25 MPa.

3 METHODOLOGY

In this section, the experimental procedure is presented. It was developed in order to allow for the experimental analysis of the formation of hydrates above the upper quadruple point, where pressures are high enough to allow for the presence of CO_2 condensate.

3.1 EXPERIMENTAL APPARATUS

The experimental apparatus used is located at the Laboratory of Flow Assurance, which is part of the Multiphase Flow Center (NUEM) at the Federal University of Technology - Parana (UTFPR). It was also previously used by Kakitani (2014), Ferrari et al. (2016) and Guembaroski (2016). Adaptations of the apparatus were made in order to enable the detection of hydrates formed with CO_2 condensate.

Figure 3.1 shows the schematics of the whole apparatus. It is composed by a gas cylinder (1) that can be connected to a syringe pump (7) for charging with the desired gas components. The syringe pump is directly connected to the equilibrium cell (3) through 1/8 in inner diameter piping (6). Whether the syringe pump is connect to the cell or to the gas cylinder (which is used to charge the syringe pump prior to the start of the experiment) is controlled by the set of valves (4). Two thermostatic baths (9) control the temperature of the syringe pump and the equilibrium cell, the latter circulates chiller fluid through its heat exchanger (5). The data for the volume of the pump, the temperature and the pressure of the cell are all collected and stored in a computer (8). A vacuum pump (2) is used to remove air from the piping and dissolved in the aqueous phase.

Figure 3.2 shows the actual experimental apparatus, where (2) is the syringe pump, which can be charged or connected to the equilibrium cell (1) through the adjustment of the valves (3). Two circulating baths (4) are used to control the temperature of the pump and the equilibrium cell.

Figure 3.1 Experimental apparatus. Main components: (1) gas cylinder; (2) vacuum pump; (3) equilibrium cell; (4) valves; (5) heat exchanger; (6) cell-syringe pump piping; (7) syringe pump; (8) computer; and (9) thermostatic baths.

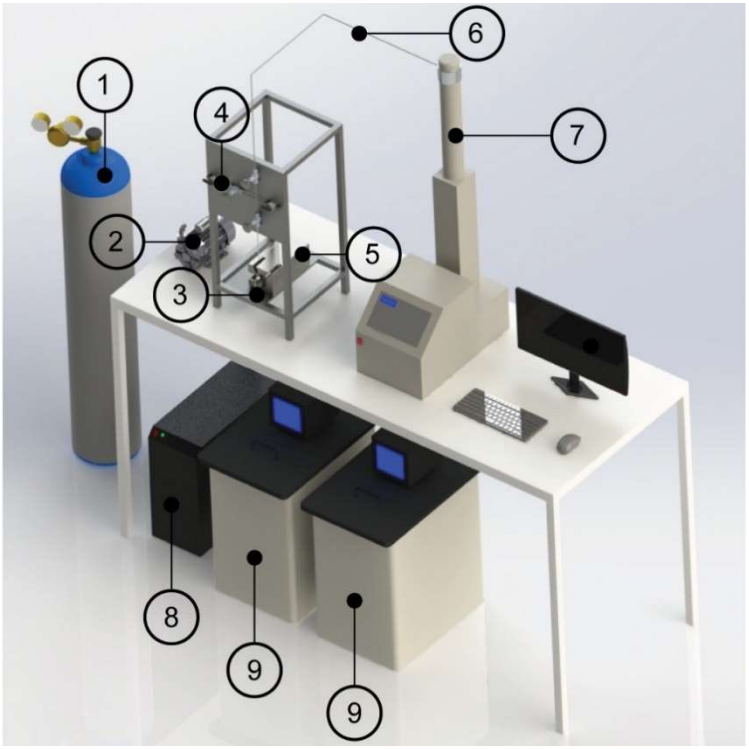

Figure 3.2 Experimental apparatus. Main components: (1) Equilibrium cell; (2) syringe pump; (3) valves; and (4) programmable circulating baths.

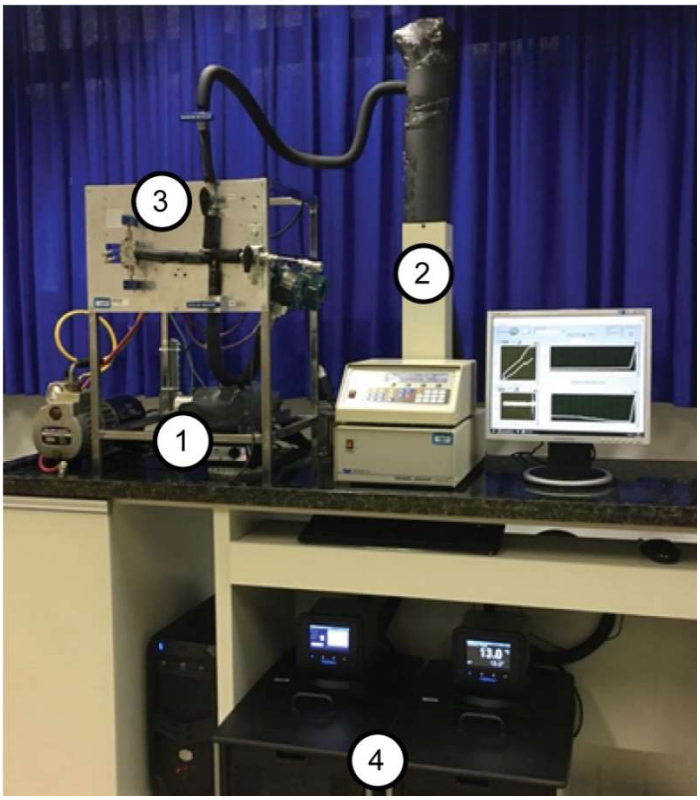

The equilibrium cell (Figure 3.3 and Figure 3.4) is made of stainless steel and can operate with pressures of up to 30 MPa. The temperature is controlled through a heat exchanger, where a mixture of MEG, ethanol and water is used with a programmable circulating bath. The bath has a temperature control ranging from 233 K to 473 K. The cell is directly connected to a syringe pump, which can add or remove CO_2 as necessary. The syringe pump is kept at a constant temperature with water running through its cooling jacket and a circulating bath.

A probe (PT-100) measures the temperature inside the cell, which has a range from 223.15 K to 623.15 K and an uncertainty of 0.21 K (95% confidence interval). A transducer (S-11 WIKA) also measures the pressure inside the cell, which has a range from 0 to 40 MPa and an uncertainty of 0.30% (95% confidence interval). The signals are received by a computer, which records the data over time. The complete uncertainty analysis is presented in the Appendix B of this work.

The equilibrium cell can be used in two configurations: visualization and high-pressure. For the visualization configuration (Figure 3.3), two sapphire windows allows for the lighting and direct visualization of the interior of the cell. This allows for the visual confirmation of the formation of hydrates or the condensate phase.

Figure 3.3 Equilibrium cell in visualization configuration. (1) Pressure and charging connections, (2) temperature measurement, (3) sapphire window, (4) front plug, (5) illumination window and (6) back plug.

To prevent problems with leakages at high pressures, the sapphire windows can be replaced with stainless steel blind plugs. The high-pressure configuration (Figure 3.4) allows for maximum tightening of the cell plugs, preventing leakages without the risk of breaking the sapphire window. The drawback is the impossibility of visual confirmation of the phases, which can be circumvented by the correct analysis of pressure, volume and temperature data for the identification of hydrates.

Figure 3.4. Equilibrium cell in high-pressure configuration. (1) Pressure and charging connections; (2) temperature measurement; (3) blind plugs.

A magnetic stirrer is used for agitation in order to provide better mixing of the compounds. The Teledyne® Isco® Syringe Pump (7 in Figure 3.1 and 2 in Figure 3.2) is directly connected to the equilibrium cell and has a capacity of 266.00 ml with an uncertainty of ±0.0001 ml. It has a function of constant pressure, which changes the volume of the pump in order to maintain the set point pressure. By keeping the temperature of the pump constant, any changes in volume will be a result of changes that occur inside the equilibrium cell.

3.2 MATERIALS

Carbon dioxide was provided by White Martins Industrial Gases. Monoethylene glycol was provided by Vetec Fine Chemicals. Table 3.1 shows the purities and chemical structures of these compounds. Distilled water was prepared in our own lab.

Table 3.1. Materials used in the hydrate equilibrium study.

N.	Chemical Name	Symbol	Purity	Chemical Structure
1	Carbon Dioxide	CO_2	99.99 mass%	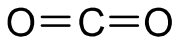
2	Monoethylene Glycol	MEG	99.5 mass%	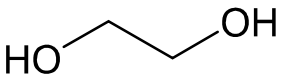
3	Sodium Chloride	NaCl	99 mass%	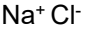
4	Distilled Water	H_2O	-	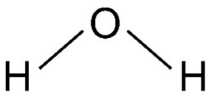

3.3 ISOBARIC EXPERIMENTAL PROCEDURE

The experimental procedure is performed at a high enough pressure in order to guarantee that the hydrates will be formed in the region above the upper quadruple point. The procedure consist of four main steps: 1. Preparation and charging of the cell; 2. Cooling; 3. Heating; and 4. Dissociation. During steps 2 onward, a syringe pump is used to add or remove CO_2 in order to keep a constant pressure.

As the equilibrium cell system is connected to an external source of CO_2, in this case it's the syringe pump, it is necessary to take into account the possibility of a component to be diffused to this external source. As the thermodynamic inhibitor used is MEG, it's solubility in the liquid phase rich in CO_2 is very low, the amount diffused from the aqueous phase is

negligible. The use of a more volatile compound could be different. The other thermodynamic inhibitor used is NaCl, which does not diffuse to the second liquid phase, but stays dissolved in the aqueous phase.

3.3.1 Preparation And Charging Of The Equilibrium Cell

Initially, a known amount of water is added to the equilibrium cell at ambient temperature and pressure. For experiments done with thermodynamic inhibitors, they are added to the water rich phase in this step.

Next, a vacuum pump is connected to the system. This way, the air that is inside the cell, piping and dissolved in the water is removed. This procedure allows for an increase in the carbon dioxide that is dissolved in water, favoring the formation of hydrates. Before applying vacuum to the cell, its temperature should be lowered in order to prevent water vapor to escape from the aqueous phase.

The syringe pump is then charged with CO_2, with its temperature maintained constant independently from the equilibrium cell. The valve that controls the connection between the syringe pump and the cell is then opened, allowing CO_2 to enter the equilibrium cell.

At this point, the equilibrium cell is charged with carbon dioxide, water and the intended thermodynamic inhibitor at the chosen pressure. After this, the cell is evaluated for the presence of any leaks. This is done by allowing the system to stay for a period of at least five hours at a constant temperature and pressure, so that the volume of the pump should remain unchanged when no leaks are present.

3.3.2 Cooling Step And Hydrate Formation

After the cell is properly prepared, the cooling process is initiated. This step must be performed at a rate that allows the system to achieve thermal equilibrium at each data point collected. To make sure that the equilibrium is maintained at each data point, this step is performed at a rate of 2 K per hour. When cooling, the volume initially decreases due to the thermal contraction of the liquid phases. With lower temperature, the density increases, causing a decrease in volume. When hydrates form, a sharper decrease in volume is expected. This is

due to the consumption of CO_2 molecules in the formation of hydrates. This step is illustrated as 1 in Figure 3.5.

Figure 3.5. Cooling and hydrate formation.

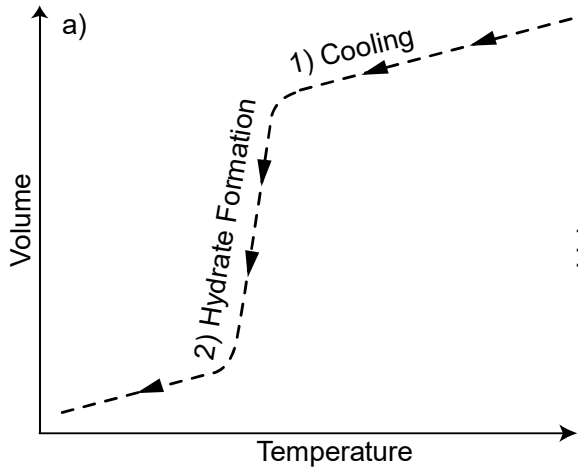

The confirmation of the formation of hydrates can be done in two ways: visually and graphically. As they form, carbon dioxide molecules are transferred from the liquid phase to the solid hydrate phase. As the syringe pump is set to keep a constant pressure, it lowers its volume, adding carbon dioxide to the cell as it is consumed. Thus, a decrease in volume for the same temperature is an indication that hydrates are being formed.

3.3.3 Heating Step And Equilibrium Point Determination

The heating process is illustrated as b in Figure 3.6. The system is initially heated at a fast rate until it is about 1 °C close to a preliminary dissociation point. This point is determined by preliminary tests performed with a faster heating step. The fast heating step is done in order to save time and it does not influence in the final dissociation temperature, as hydrates will still exists when the slow heating step is performed. After the fast heating step, the system is slowly heated to allow for the points at the dissociation line to be obtained always in equilibrium.

As the cell is heated, the volume of the syringe pump is expected to increase due to the thermal expansion of the phases, shown as 3) in Figure 3.6. When hydrates start to dissociate (4) in Figure 3.6), the inclination of the Volume versus Temperature line changes as carbon

dioxide molecules are transferred from the hydrate phase to the liquid phase rich in CO_2. After all hydrates have dissociated, the V-T line is expected to change inclination again and match the cooling line previously done.

Figure 3.6. Steps in the isobaric experimental procedure: (a) cooling and formation of hydrates; (b) heating and dissociation of hydrates.

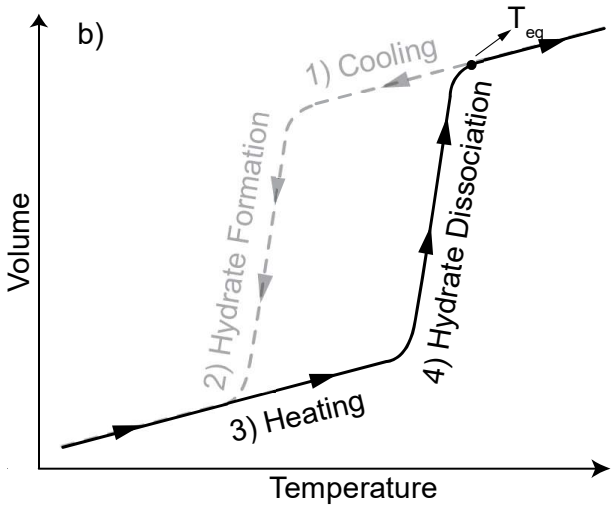

The graphical determination of the equilibrium point can be done either by crossing the cooling and dissociation lines or directly finding the change in inclination after the dissociation is completed (shown as T_{eq} in Figure 3.6). This experimental procedure is known as the isobaric search method (SLOAN and KOH, 2008).

After the temperature of system goes lower than the equilibrium temperature, hydrates may form. However, hydrate formation is a stochastic process, with a region where the system is in a metastable state, as shown in Figure 3.7. In other words, it is in thermodynamic conditions for hydrates to be formed but they may not for kinetic reasons. Therefore, the equilibrium temperature for the formation of hydrates can be defined as the temperature at which all hydrates are dissociated, which will always be the same for a given system (SLOAN and KOH, 2008).

Figure 3.7. Equilibrium temperature determination with the isobaric experimental procedure.

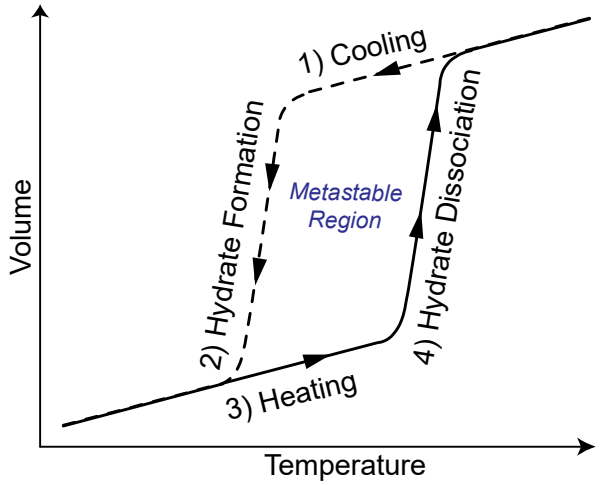

3.4 MEASUREMENTS

In this section, the measurements techniques used in order to find equilibrium points are presented. Temperature, volume and pressure data are collected and used to find equilibrium temperatures graphically.

3.4.1 Pressure, Temperature And Volume Control

As the syringe pump is set to constant pressure mode, any changes inside the equilibrium cell will reflect in its volume as it removes or adds carbon dioxide as necessary to keep a constant pressure. As the procedure is done, the data for volume of the pump is acquired and stored in a computer. Connected to the cell is also a pressure transducer, which has its measurements acquired and saved with a computer. This data is used to confirm that the pressure is indeed being kept constant by the syringe pump, which has a maximum pressure of 5.17 MPa with an uncertainty of 0.5% of the full span. The pressure is measure with an S-11 WIKA transducer, which has a range from 0 to 40 MPa with an uncertainty of 0.30% (95% confidence interval). The complete uncertainty analysis is presented in the Appendix B of this work.

The temperature of the equilibrium cell is controlled with a heat exchanger around the cell and it is connected to a programmable circulating bath. As exchanger fluid, a mixture of 60 vol% MEG, 20 vol% ethanol and 20 vol% water is used. With this mixture, the circulating bath can reach its lower limit of 248.15 K (-25 °C) without freezing. The volume is acquired from the syringe pump, which has a precision of 0.0001 ml.

Figure 3.8 shows a test that was done during approximately 8 hours where the pump was set to a constant pressure of 13 MPa and the cell was kept at a constant temperature of 287.26 K. As expected, the signal measured by the pressure transducer was also constant and at the same pressure that was set in the syringe pump, indicating that the pump is able to satisfactorily keep a constant pressure.

Figure 3.8. Pressure inside the equilibrium cell connected to the syringe pump on the constant pressure setting.

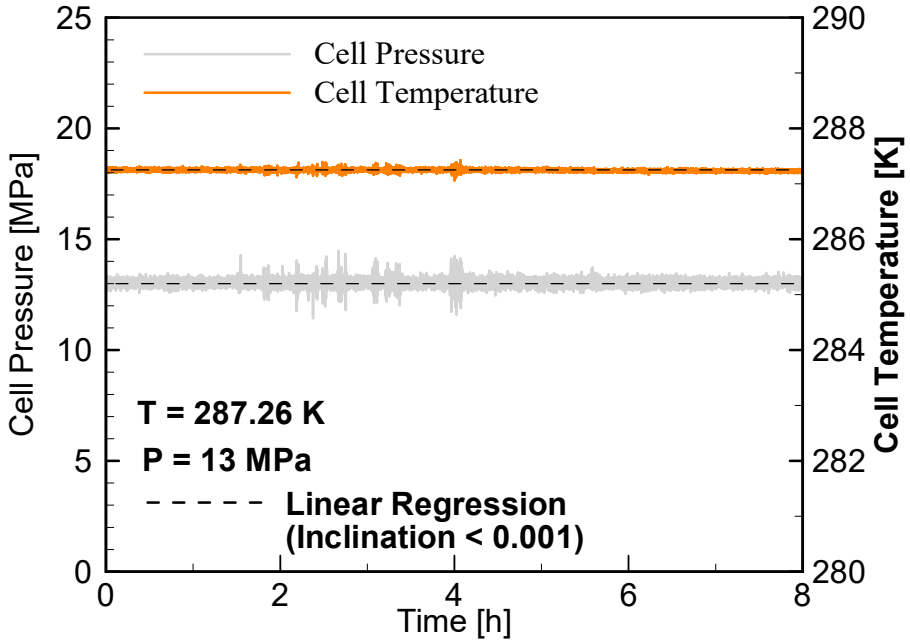

It was noted that room temperature changes could affect the experiments. In order to minimize this problem, some precautions were taken. These are explained in detail in the Appendix C.

3.4.2 Experimental Procedure Preliminary Tests

By controlling the temperature of the cell, a response in the volume is analyzed. For a preliminary evaluation purpose, a fast experiment was done in order to evaluate what is the behavior of the system when analyzing the changes in temperature and volume. Figure 3.9 shows the several steps in a usual isobaric procedure performed in this work. In the cooling step, is possible to see that the volume decreases or increases according to the temperature.

Figure 3.9. Temperature and volume in time for a typical isobaric procedure with a slow heating step. (a) Hydrate formation; (b) dissociation.

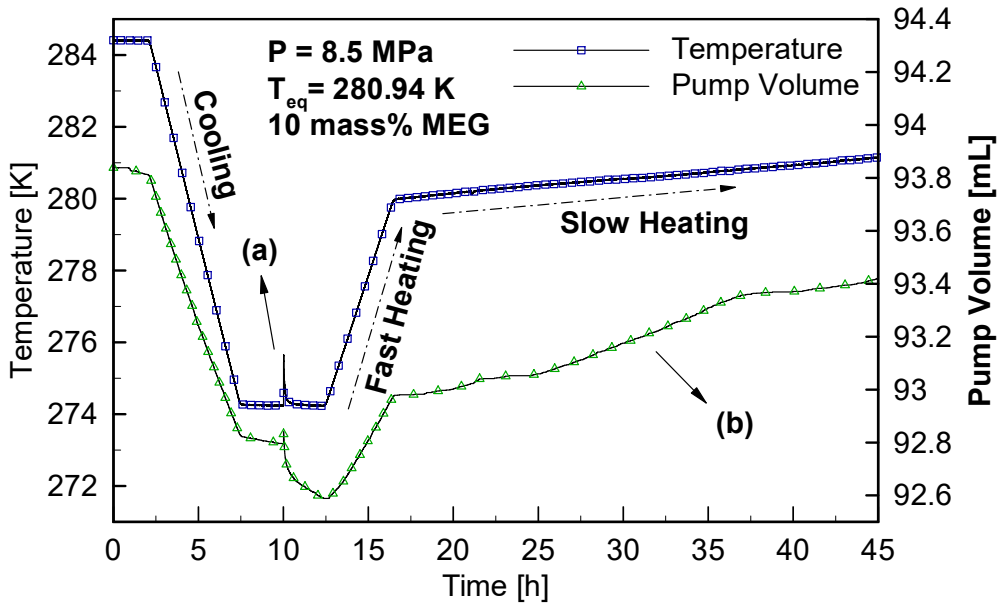

Figure 3.9 shows the temperature and volume with a dissociation promoted at a slower heating rate of 0.1 K/h. The procedure is initiated with the cooling of the cell, followed by a constant temperature period where, in this case, hydrates formed (a). Next, the fast heating step is initiated. At about 1 K before the dissociation temperature, the slow heating step is initiated and, consequently, hydrate dissociation occurs (b). As hydrates dissociate, molecules diffuse from the solid phase to the two liquid phases, increasing the volume measured in the pump. This causes a change in the inclination of the volume, as indicated in (b).

In region marked as (a), there is a decrease in volume during the slow heating step. This happens due to the increased formation of hydrates. This can be affirmed because all the decrease in volume at (a) is compensated in the increase in the dissociation of hydrates at (b).

Table 3.2 shows an example of how long each step takes for a typical experiment. It starts with the cooling step at a rate of 2 K/h, which takes about 6.5 hours depending on how much of a sub-cooling is necessary for the formation of hydrates. After hydrates are formed, the system is allowed to stay at a constant temperature for at least 4 hours.

Next, a fast heating is done until about 1 K before the predicted equilibrium point, which is taken from previous faster experiments. After that, the slow heating, which is performed at a rate varying between 0.02 and 0.06 K/h, which is done to guarantee that the equilibrium in each temperature is achieved. The exact rate is determined with the observation of the response of the volume due to the temperature change, making sure that the system is allowed to achieve equilibrium. This way, each inhibited experiment usually takes about 95 hours to fully complete, as shown in the example of Table 3.2.

Table 3.2. Example of cooling and heating rates.

	From [K]	To [K]	Rate [K/h]	Time [h]
Cooling	287	274	2	6.5
Formation	274	274	-	4
Fast Heating	274	283	2	4.5
Slow Heating	283	287	0.05	80
			Total Time:	**95**

3.5 TEST GRID

The tests were performed at pressures and concentrations shown in Table 3.3 for CO_2 hydrates with pure water and with the presence thermodynamic inhibitors. These pressures were chosen in order to achieve the condensation of the gas phase, allowing for measures above Q_2 and within a range that the experimental apparatus can work with. Concentrations of MEG were chosen within a range that covers the low and high concentrations that the industry uses. Finally, the concentrations of NaCl were chosen in a range that the experimental apparatus can work even when mixed with MEG.

Table 3.3. Test grid with pressures and concentrations of thermodynamic inhibitors and their mixtures.

Pressure	**8.5 MPa**	**13 MPa**	**18 MPa**	**25 MPa**
Pure system	Pure water			
x mass% MEG	10			
	20			
	30			
x mass% NaCL	5			
	10			
5 mass% NaCL + x mass% MEG	10			
	20			
	30			

All the concentrations in this work are in respect to the aqueous phase, meaning that the concentration of a given inhibitor will be its mass (m) divided by sum of inhibitor mass and water, as shown in Equation (12) for a given inhibitor 1.

$$\text{mass\% of inhibitor 1} = \frac{m_{\text{inhibitor 1}}}{m_{\text{inhibitor 1}} + m_{\text{inhibitor 2}} + m_{\text{water}}} \times 100\% \qquad (12)$$

4 RESULTS AND DISCUSSION

In this chapter, the results obtained are presented and discussed. In order to validate the experimental procedure, data points for CO_2 and pure water were done and compared with available data in literature. Next, the results with the presence of thermodynamic inhibitors are shown and the consistency check of the data is performed. Lastly, the data from this work is compared with predictions from software products and models.

4.1 HYDRATE FORMATION AND DISSOCIATION

After the cell is charged with water and the desired thermodynamic inhibitor, vacuum is applied, removing air that eventually is dissolved in the water, thus increasing the amount of CO_2 that can be dissolved in the aqueous phase, increasing the amount of hydrates that can be formed. In this step, the temperature of the cell is kept low (close to 273 K) in order to prevent water vapor from escaping the aqueous phase.

After the vacuum procedure is completed, the valve that connects the syringe pump to the equilibrium cell is slowly opened, allowing CO_2 to enter the cell. At first, it is possible to visualize two phases: vapor phase rich in CO_2 and aqueous phase. By increasing the pressure, vapor CO_2 condenses and three phases can be visualized: vapor phase rich in CO_2, liquid phase rich in CO_2 and aqueous phase (Figure 4.1 (a)). Finally, the desired pressure is set on the syringe pump. This way, all the CO_2 condenses and only two phases are visualized: liquid phase rich in CO_2 and aqueous phase (Figure 4.1 (b)). By visualizing the phase transitions, it can be inferred that the chosen pressure is in fact high enough to be above the upper quadruple point.

Figure 4.1. a) Charging of the cell with carbon dioxide (V-L-L equilibrium), b) pressurized system (L-L equilibrium).

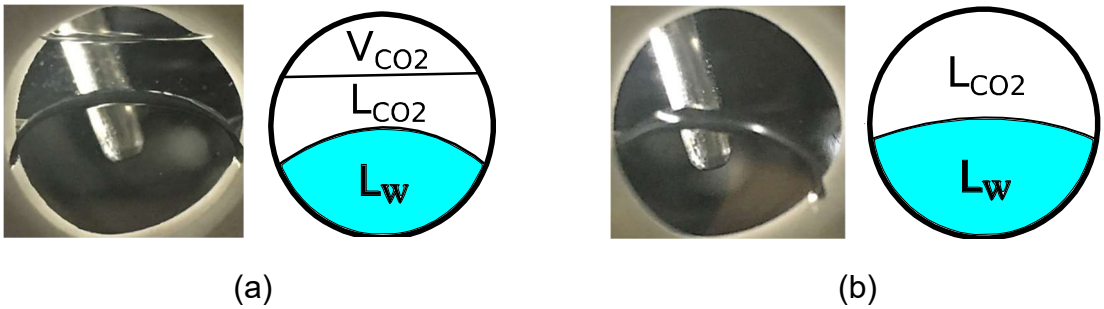

After the charging of the cell and the leak check is completed, the cooling of the cell is started in order to induce the formation of hydrates. When working with pressures bellow 15 MPa, the sapphire window can be used to visualize the interior of the cell in order to confirm that hydrates are present and to visualize the phases shown in Figure 4.1.

Hydrate formation is also an exothermic process and they initially form very quickly, which causes a sudden spike in temperature due to the release of heat from the reaction. Figure 4.2 shows the raise in temperature when hydrates are formed (2) during the constant temperature period. This behavior allows another way to confirm hydrate formation graphically without the need of visualization.

Figure 4.2. Temperature spike when hydrates are formed.

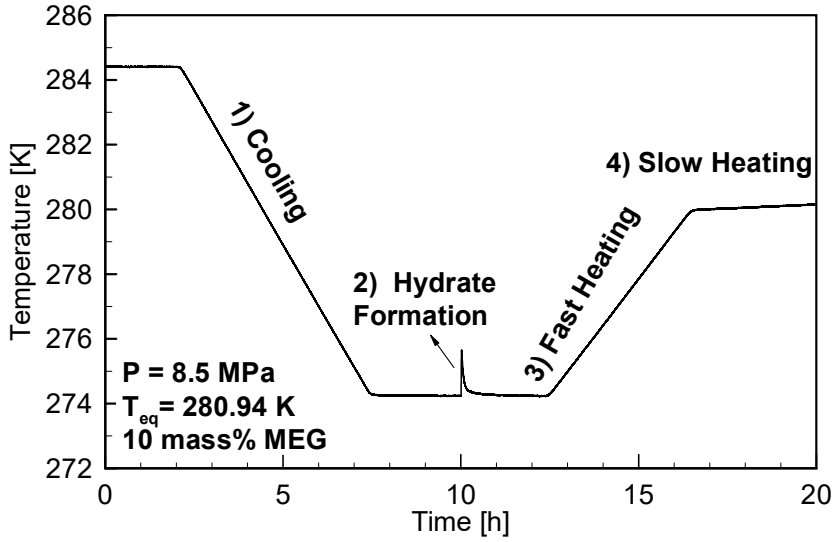

Figure 4.3 shows the moment right after hydrates have formed, as indicated as 2 in Figure 4.2. As it can the seen in Figure 4.3 (a), hydrates initially form at the L_{CO2}-L_{H2O} interface, leaving a non-converted amount of water below the hydrate layer, as it is also indicated in (b).

Figure 4.3. (a) Hydrates formed initially at the interface; (b) schematic of the hydrate layer formed at the interface.

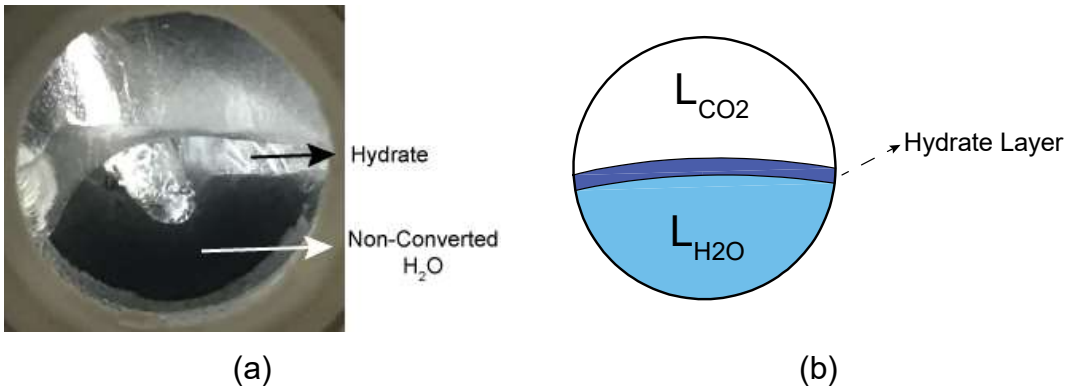

After hydrates form, the system is kept at a low temperature to allow for the highest conversion possible. Figure 4.4 shows three examples of hydrates that were formed at a pressure of 15 MPa. These pictures were taken during the constant low temperature step, after hydrate formation has stabilized.

Figure 4.4. Examples of hydrates formed at 15 MPa.

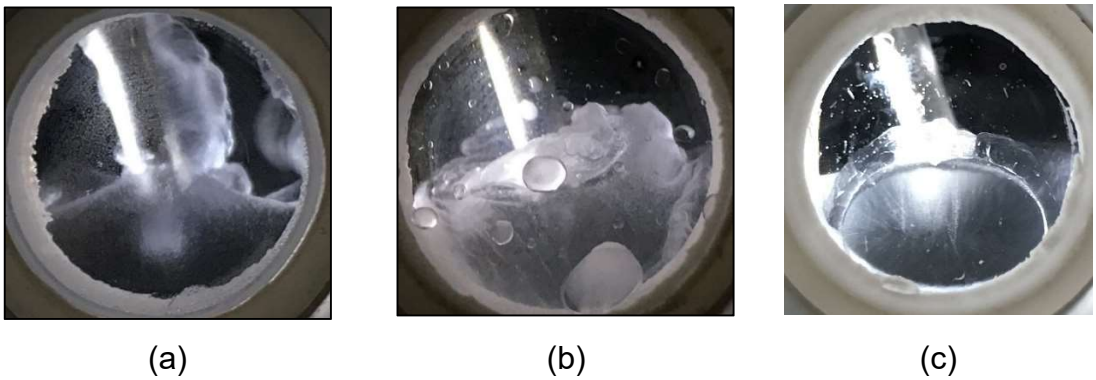

4.1.1 Equilibrium Temperature Determination

For determining the equilibrium temperature for a given pressure, data for volume and temperature are plotted. As shown in Figure 4.5, the equilibrium point is the crossing of the cooling lines and dissociation lines. Those can be identified by the change in inclination of the curves in the volume versus temperature graph and, through linear regression, the intersection of the lines can be determined. This procedure was performed for every data point obtained.

Figure 4.5. Example of determining the equilibrium temperature graphically in a pure water hydrate system.

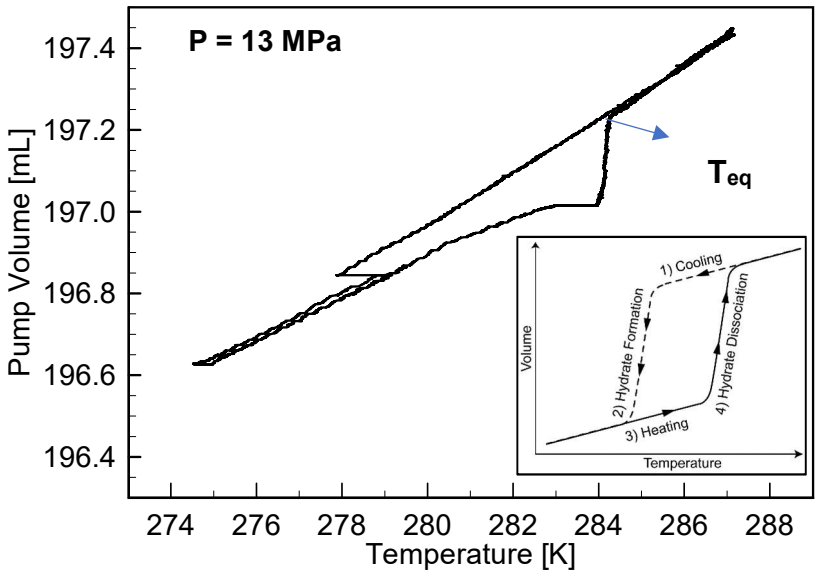

For the experiment done in Figure 4.6, throughout the cooling step, the volume decreases initially due to the thermal contraction of the liquid phases. Once hydrates form, the inclination changes, indicating the formation of hydrates. As the cooling process continues, more hydrates are formed and the volume changes accordingly. Because the agitation in the cell is not efficient, it cannot be guaranteed that all the water converts into hydrates. In addition, when the hydrate solid phase forms, the magnetic stir bar gets involved with hydrate and does not move. However, because the focus of this work is the dissociation point, as long as enough hydrates are formed, the equilibrium point can be determined by allowing enough time through temperature steps to ensure that each data point is collected at the equilibrium.

In the fast heating step, volume increases due to the thermal expansion of the phases. As the experiment starts the slow heating step, the volume decreases again. This happens because more hydrates are formed, as the system is still inside the hydrate region. When the equilibrium temperature is achieved, the volume measured by the pump goes back to that of the cooling line, indicating that all hydrates have been dissociated and the equilibrium temperature can be determined for the given pressure.

A linear regression is done with the data points that are consistent with the cooling and dissociation steps. For a good linear regression, the value for R^2 must be close to one. As seen in Figure 4.6, values of 0.99 for R^2 are obtained, indicating that the experiment was reliable, confirming that the dissociation process is indeed linear with respect to volume and temperature.

Figure 4.6. Equilibrium point determination. System with CO_2 and pure water.

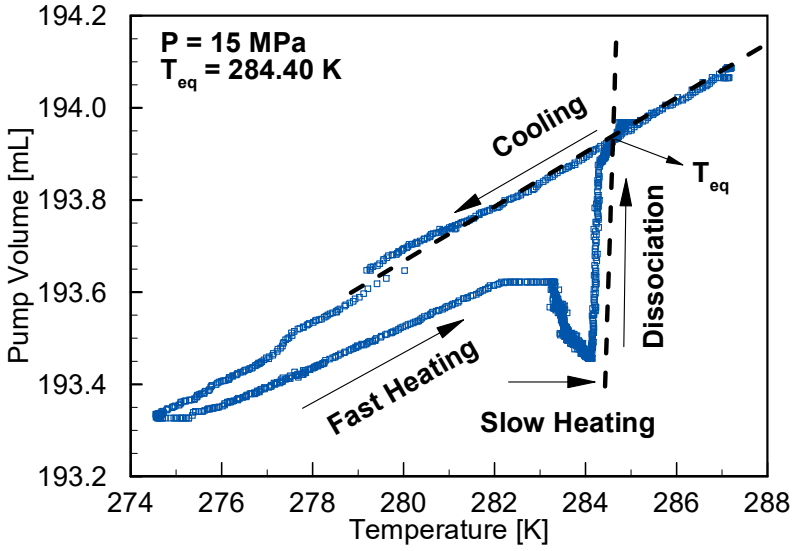

4.2 PURE WATER SYTEM

In order to validate the data points obtained with the developed experimental procedure, comparisons with data available in literature was done. The data available in the region above Q_2 is very limited, being mostly for systems of carbon dioxide and pure water, i.e. with no additives. Table 4.1 shows the results obtained for equilibrium points of the pure water system.

Table 4.1. Data for CO_2 and pure water obtained.

Pressure [MPa]	Temperature [K]
8.5	283.68
13	284.14
18	284.57
25	285.21

Figure 4.7 shows the data collected and the available data in literature for pressure and temperature equilibrium points in a pure water system. It also shows predictions done by the following: CSMGem, Multiflash, PVTSim and Sirino et al. (2018). In order to facilitate the identification of the Q_2 point, the equilibrium curve for the three-phase L_{CO2}-V_{CO2}-L_{H2O} was plotted according to Multiflash prediction.

Figure 4.7. Data from this work compared with data available in literature for hydrates of CO_2 and pure water.

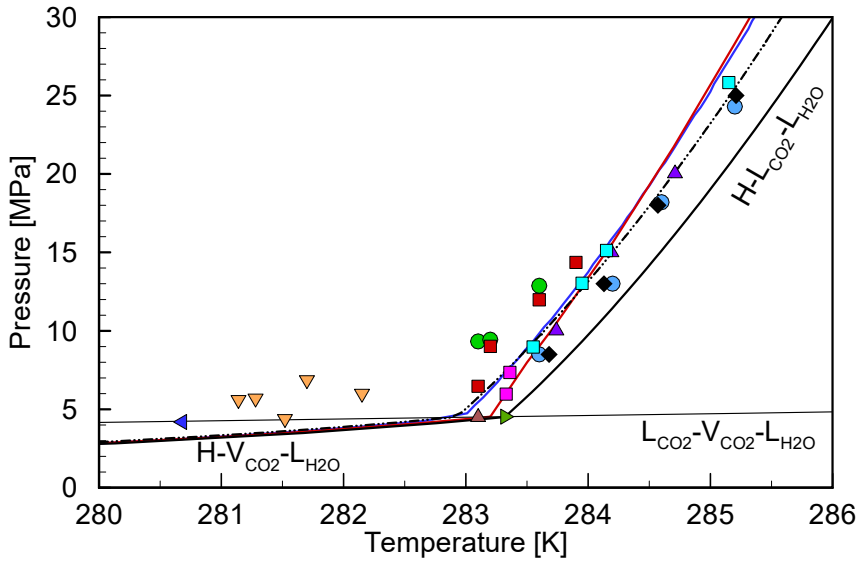

- This Work;
- Shin et al. (2014);
- Chapoy et al. (2011);
- Mooijer-Van Den Heuvel et al. (2001);
- Fan and Guo (1999);
- Ohgaki et al. (1993);
- Ng and Robinson (1985);
- Takenouchi and Kennedy (1965);
- Q_2 - Ruffine and Trusler (2010);
- Q_2 - Seo and Lee (2001);
- Q_2 - Unruh and Katz (1949);
- CSMGem;
- Multiflash;
- PVTSim;
- Sirino et al. (2018).

The consistency of the linearity of the Clausius-Clapeyron relation was evaluated for the data available in literature for carbon dioxide hydrates of pure water. All the sources cited in Figure 4.7 according to this criteria. The deviation was evaluated according to Equation (6).

Some data points available in literature for carbon dioxide hydrates with pure water failed this consistency check. Ng and Robinson (1985) data showed a deviation of 9.04%, Ohgaki et al. (1993) resulted in a deviation of 83.54%, Mooijer-Van Den Heuvel et al. (2001) only had two data points, so this criteria was not evaluated.

Table 4.2 shows the R^2 calculated for the data from this work and from available in literature, except for the Ohgaki et al. (1993) and Mooijer-Van Den Heuvel et al. (2001). In addition, the term A from the Clausius-Clapeyron relation, which is related to its slope, is calculated and compared with the one obtained from data of this work.

As it is shown in Table 4.2, the data from this work agrees well with data available in literature that is consistent with relation to the linearity of the Clausius-Clapeyron equation, showing that the experimental procedure used in this work was able to reliably obtain experimental equilibrium points of hydrates of carbon dioxide.

Table 4.2. Clausius-Clapeyron consistency check of data available in literature and compared with this work.

	R^2	Linearity Verdict	A	Deviation of A From This Work
This Work	1.95%	**Pass**	-56732	-
Takenouchi et al. (1965)	1.14%	**Pass**	-53987	-4.84%
Shin et al. (2014)	1.85%	**Pass**	-57406	1.19%
Fan et al. (1999)	2.49%	**Acceptable**	-54855	-3.31%
Chapoy et al. (2011)	2.93%	**Acceptable**	-44483	-21.59%
Ng et al. (1985)	9.04%	**Fail**	-72223	27.31%

Furthermore, when analyzing and comparing this data, it is important to note that the temperature scale, in the region above Q_2, is very small in comparison with pressure, causing a high inclination of the equilibrium curve.

4.3 CO_2 HYDRATES WITH THERMODYNAMIC INHIBITORS

MEG and NaCl were used to evaluate their influence as thermodynamic inhibitors in the formation of CO_2 hydrates. As discussed in the second chapter, they act by interacting with water molecules, making them less available to form hydrates, thus it is expected that their presence will cause a decrease in the equilibrium temperature for the same pressure. In section 4.5, the plot of the results is presented alongside predictions of software products and models.

4.3.1 CO_2 Hydrates With MEG

To evaluate the inhibition effect of MEG, mass concentrations of 10%, 20% and 30% were used. Each experiment was performed once due to time restrictions. In general, the slow heating rate was chosen as one that allowed the system to be in equilibrium. To guarantee that the system was kept in equilibrium, this rate varied between 0.02 K/h and 0.06 K/h, which was adjusted accordingly. This procedure took on average 95 hours to complete for each data point, as shown with the example of Table 3.2.

Figure 4.8 shows the data obtained for the equilibrium point of carbon dioxide hydrates inhibited with MEG. It is plotted as pressure versus temperature at the equilibrium for the pressures of 8.5, 13, 18 and 25 MPa. The concentrations are in mass percentage of the aqueous phase. As expected, MEG acted as a thermodynamic inhibitor, decreasing the equilibrium temperature for the formation of hydrates. In addition, a higher concentration caused a higher inhibition effect. Table 4.3 shows the results that were plotted in the aforementioned figure.

Figure 4.8. CO_2 hydrate equilibrium results for MEG inhibited systems.

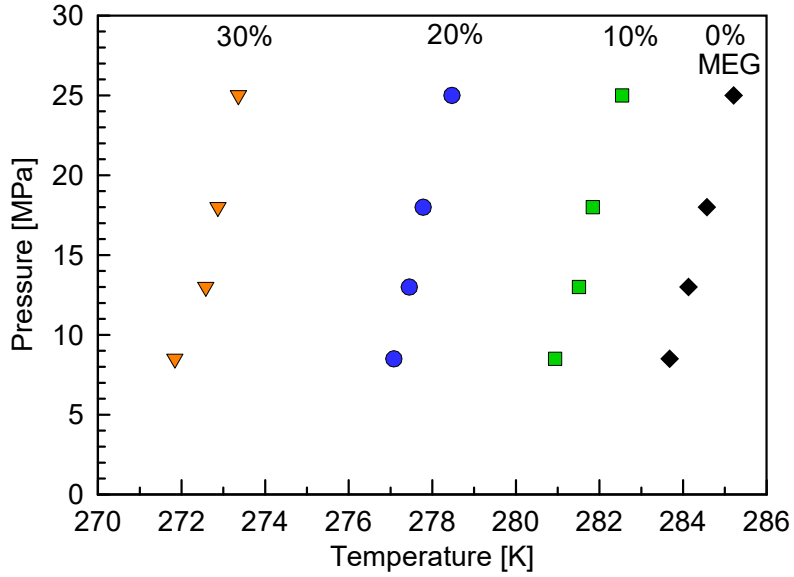

◆ **Pure Water;** ● **20 mass% MEG;**

■ **10 mass% MEG;** ▼ **30 mass% MEG.**

Table 4.3. Hydrate equilibrium data for CO_2-MEG-Water system collected.

x% MEG	8.5 MPa	13 MPa	18 MPa	25 MPa
0%	283.68 K	284.14 K	284.57 K	285.21 K
10%	280.94 K	281.51 K	281.84 K	282.54 K
20%	277.08 K	277.45 K	277.78 K	278.47 K
30%	271.84 K	272.58 K	272.87 K	273.36 K

4.3.2 CO_2 Hydrates With NaCl

Figure 4.9 shows the results obtained for hydrates of CO_2 inhibited with sodium chloride. Concentrations are in mass percentages in the aqueous phase. Similarly to MEG, NaCl acts as a thermodynamic inhibitor, lowering the equilibrium conditions for the formations of hydrates. Additionally, a higher concentration of salt resulted in a higher inhibition effect, acting as a thermodynamic inhibitor. Table 4.4 shows the data obtained for this system.

Figure 4.9. CO_2 hydrate equilibrium results for NaCl inhibited systems.

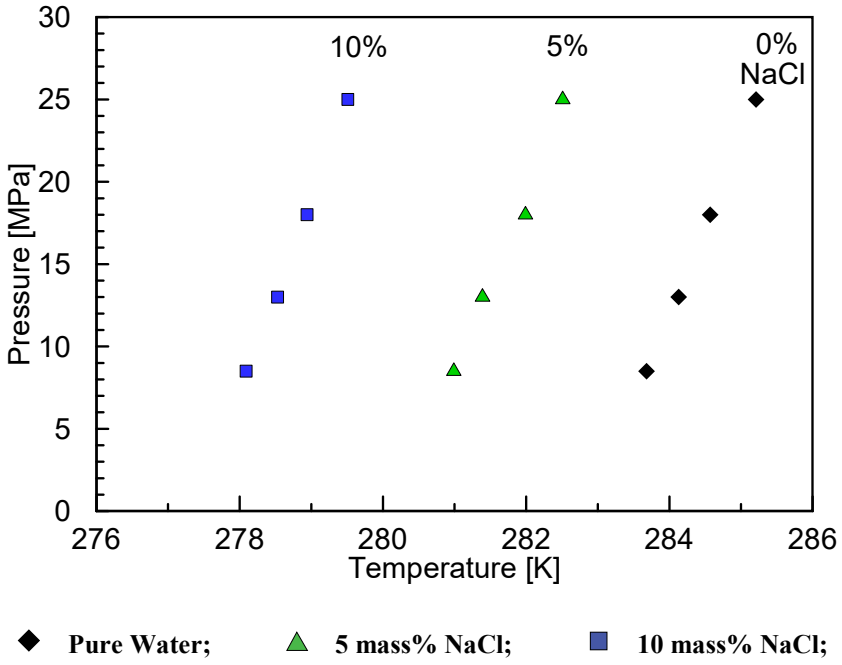

Table 4.4. Hydrate equilibrium data for CO_2-NaCl-Water system collected.

x% NaCl	8.5 MPa	13 MPa	18 MPa	25 MPa
5%	280.99 K	281.39 K	281.99 K	282.51 K
10%	278.09 K	278.53 K	278.94 K	279.51 K

4.3.3 CO_2 Hydrates With NaCl And MEG Mixtures

As mentioned in previous chapters, the water produced in offshore oil extraction is naturally inhibited due to the presence of salts. In order to evaluate the influence of the water salinity, a fixed amount of 5 mass% of NaCl was used with different concentrations of MEG. This way, it is expected that a lower concentration of MEG would be necessary for achieving the same inhibition effect when compared with a pure water system.

Figure 4.10 shows the results from this work for the system with 5% of NaCl and different concentrations of MEG. Table 4.5 shows the equilibrium temperatures obtained and shown in the aforementioned figure for the pressures of 8.5, 13, 18 and 25 MPa. The concentrations are in mass% in the aqueous phase, as shown in Equation (12).

Figure 4.10. CO_2 hydrate equilibrium results inhibited with 5% of NaCl and different concentrations of MEG.

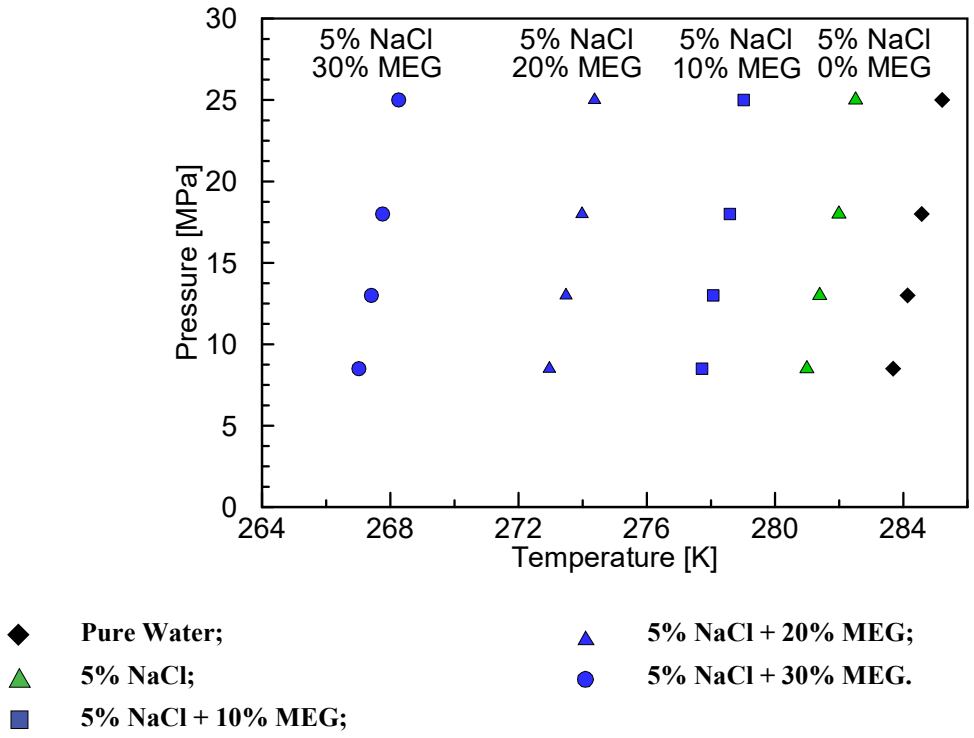

Table 4.5. Hydrate equilibrium data for CO_2-NaCl-MEG-Water system obtained.

5% NaCl + x% MEG	8.5 MPa	13 MPa	18 MPa	25 MPa
10%	277.72 K	278.07 K	278.59 K	279.02 K
20%	272.96 K	273.48 K	273.98 K	274.37 K
30%	267.02 K	267.41 K	267.76 K	268.26 K

Using the concept freezing temperature depression, Equation (13) describes the difference in equilibrium temperature caused by the presence of a thermodynamic inhibitor.

$$\Delta T = T_W - T_{INH} \tag{13}$$

Table 4.6 shows the use of Equation (13) in order to compare the inhibition effect between different inhibitor concentrations, particularly to see how the temperature suppression from the mixture of NaCl and MEG stack.

Table 4.6. Temperature suppression of inhibited systems.

Pressure [MPa]	**8.5**	**13**	**18**	**25**
Teq [K] - Pure Water				
	283.68	284.13	284.57	285.21
Teq [K] - MEG				
10 mass%	280.94	281.51	281.85	282.54
ΔT [K]	2.74	2.62	2.72	2.67
20 mass%	277.08	277.45	277.78	278.47
ΔT [K]	6.60	6.68	6.79	6.74
30 mass%	271.58	271.99	272.54	273.41
ΔT [K]	12.1	12.14	12.03	11.8
Teq [K] - NaCl				
5 mass%	280.99	281.39	281.99	282.51
ΔT [K]	2.69	2.74	2.58	2.7
Teq [K] - 5% NaCl + x% MEG				
10 mass%	277.72	278.07	278.59	279.02
ΔT [K]	**5.96**	**6.06**	**5.98**	**6.19**
20 mass%	272.96	273.48	273.98	274.37
ΔT [K]	**10.72**	**10.65**	**10.59**	**10.84**
30 mass%	267.02	267.41	267.76	268.26
ΔT [K]	**16.66**	**16.72**	**16.81**	**16.95**
ΔT [K] 5% NaCl + ΔT [K] 10% MEG	**5.43**	**5.36**	**5.3**	**5.37**
ΔT [K] 5% NaCl + ΔT [K] 20% MEG	**9.29**	**9.42**	**9.37**	**9.44**
ΔT [K] 5% NaCl + ΔT [K] 30% MEG	**14.79**	**14.88**	**14.61**	**14.5**

When MEG and NaCl are mixed, the inhibition effect (ΔT) is higher than the simple sum of the corresponding inhibition suppression temperatures. For example, the addition of the ΔT of 30% of MEG and the 5% of NaCl will result in $\Delta T = 14.88\ K$, while the inhibition effect of the mixture 30% MEG + 5% NaCl is $\Delta T = 16.72\ K$ for the pressure of 13 MPa.

4.4 CONSISTENCY OF THE DATA

As discussed in section 2.6, the consistency of the data obtained is evaluated. The criteria used was proposed by Sa et al. (2018) and consists of three types: 1. Linearity of the Clausius-Clapeyron equation; 2. Consistency of the heat of dissociation; and 3. Consistency of the water activity. In following sections, the results for the consistency check are presented.

4.4.1 Linearity Of The Clausius-Clapeyron Relation

The most commonly used consistency check is the linearity of the Clausius-Clapeyron equation. The relation utilized for this consistency check is the Equation (14).

$$ln(P) = \frac{A}{T} + B \tag{14}$$

Following the criteria set by Sa et al. (2018), Table 4.7, 4.8 and Table 4.9 shows the numerical results obtained by the linearization of the data points for the Equation (14). The data collected was consistent concerning the linearity of the Clausius-Clapeyron equation. Concentrations are in mass% and the verdict indicates the quality of each set of data.

Table 4.7. Clausius-Clapeyron linearity consistency check for the CO_2-MEG-Water system.

x% MEG	R^2	$(1-R^2)x100\%$	Verdict
0%	0.981	1.9%	**Pass**
10%	0.980	2.0%	**Pass**
20%	0.951	4.9%	**Acceptable**
30%	0.986	1.4%	**Pass**

Table 4.8. Clausius-Clapeyron linearity consistency check for the CO_2-NaCl-Water system.

x% NaCl	R^2	$(1-R^2)x100\%$	Verdict
5%	0.981	1.9%	**Pass**
10%	0.985	1.5%	**Pass**

Table 4.9. Clausius-Clapeyron linearity consistency check for the CO_2-NaCl-MEG-Water system.

5% NaCl + x% MEG	R^2	$(1-R^2)x100\%$	Verdict
10%	0.983	1.7%	**Pass**
20%	0.998	0.2%	**Pass**
30%	0.986	1.4%	**Pass**

Figure 4.11 shows a bar graph with the percentages of the linearity of Clausius-Clapeyron relation criteria. Most of the data obtained felled within the pass region, being less than 2%, while one felled within the acceptable region, being less than 5%.

Figure 4.11. Linearity of the Clausius-Clapeyron relation consistency check comparison. (1) Pure water, (2) 10% MEG, (3) 20% MEG, (4) 30% MEG, (5) 5% NaCl, (6) 10% NaCl, (7) 5% NaCl + 10% MEG, (8) 5% NaCl + 20% MEG, (9) 5% NaCl + 30% MEG.

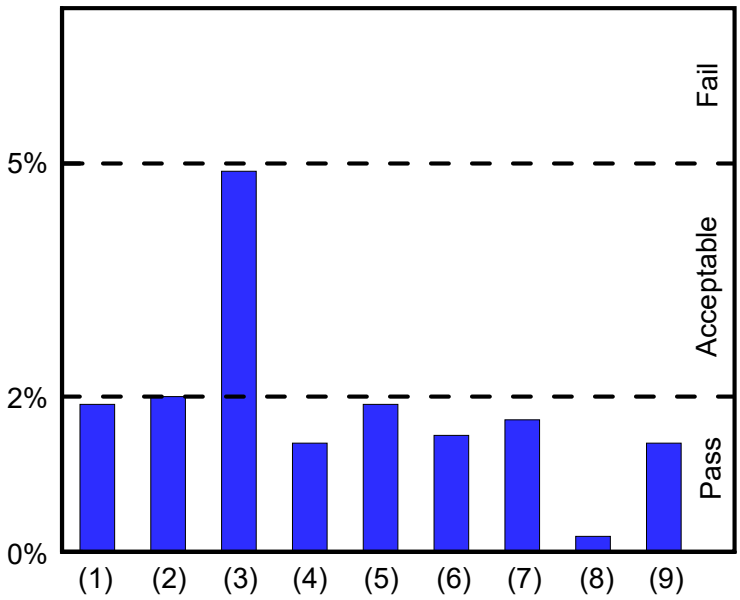

4.4.2 Consistency Of The Heat Of Dissociation

Table 4.10, 4.11 and 4.12 shows the results obtained for the consistency check regarding the heat of dissociation, which is calculated as the term *A* of Equation (14). The data obtained as thermodynamically consistent regarding this criterion. Concentration of inhibitor are indicated as mass% of aqueous phase. *A* is the inclination resulting from the linearization of the Clausius-Clapeyron equation. The deviation is the result of the comparison with the pure water system, which is the most reliable system.

Table 4.10. Consistency of the heat of dissociation for the CO_2-MEG-Water system.

x% MEG	*A*	Deviation	Verdict
0%	56.731	-	-
10%	54,190	-4.5%	**Pass**
20%	58,724	-3.5%	**Pass**
30%	53,478	5.7%	**Acceptable**

Table 4.11. Consistency of the heat of dissociation for the CO_2-NaCl-Water system.

x% NaCl	*A*	Deviation	Verdict
5%	-54,241	-4.4%	**Pass**
10%	-58,821	3.7%	**Pass**

Table 4.12. Consistency of the heat of dissociation for the CO_2-NaCl-MEG-Water system.

5% NaCl + x% MEG	*A*	Deviation	Verdict
10%	-61,879	9.1%	**Acceptable**
20%	-56,340	-0.7%	**Pass**
30%	-62,194	9.6%	**Acceptable**

Figure 4.12 shows a bar chart with the heat of dissociation consistency check for all the systems evaluated in this work. On the vertical axis, it is plotted the percentage deviation calculated with Equation (7). The criteria is then evaluated according to Table 2.3.

Figure 4.12. Heat of dissociation consistency check comparison. (1) 10% MEG, (2) 20% MEG, (3) 30% MEG, (4) 5% NaCl, (5) 10% NaCl, (6) 5% NaCl + 10% MEG, (7) 5% NaCl + 20% MEG, (8) 5% NaCl + 30% MEG.

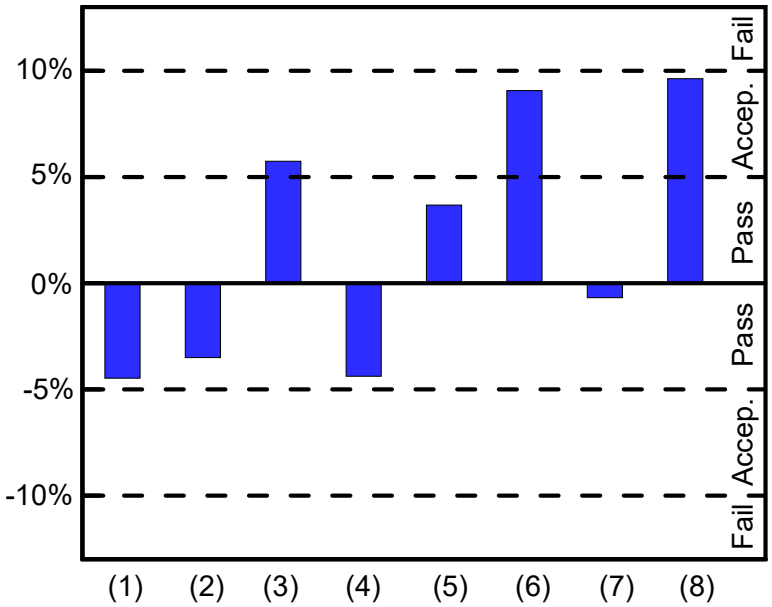

Figure 4.13 shows the results for the linearity of the Clausius-Clapeyron equation for all the data collected. The data is plotted as *ln(P)* versus *1/T*, and it is expected that this linearization will give a good linearity and similar inclination for data with good quality. The data collected showed very similar inclination between the analyzed systems with very good linearity, indicating a good quality.

Figure 4.13. Linearity of the Clausius-Clapeyron equation for all data collected. Dashed lines represents the line resulting from the linearization of each system.

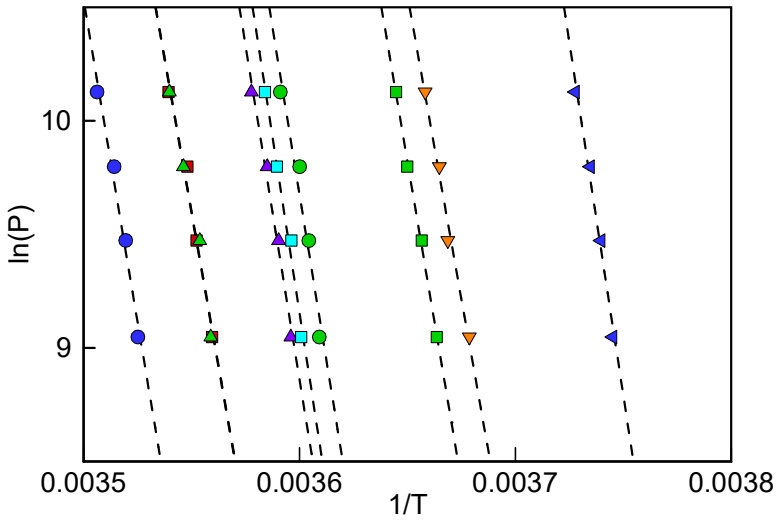

Pure Water;
10 mass% MEG;
20 mass% MEG;
30 mass% MEG;
5 mass% NaCl;
10 mass% NaCl;
5 mass% NaCl + 10 mass% MEG;
5 mass% NaCl + 20 mass% MEG;
5 mass% NaCl + 30 mass% MEG.

4.4.3 Consistency Of The Water Activity

The last consistency check is the water activity evaluation, performed according to the criteria and equations described in section 2.6.3. Tables Table 4.13, Table 4.14 and Table 4.15 shows the results from this consistency check evaluation for the data collected in this work. The concentrations are in mass percentage of inhibitors in the aqueous phase. All the data collected passed this consistency check.

Table 4.13. Consistency of the water activity for the CO_2-MEG-Water system.

x% MEG	RSD	Verdict
0%	-	-
10%	2.1%	**Pass**
20%	1.3%	**Pass**
30%	1.2%	**Pass**

Table 4.14. Consistency of the water activity for the CO_2-NaCl-Water system.

x% NaCl	RSD	Verdict
5%	2.8%	**Pass**
10%	0.5%	**Pass**

Table 4.15. Consistency of the water activity for the CO_2-NaCl-MEG-Water system.

5% NaCl + x% MEG	RSD	Verdict
10%	1.4%	**Pass**
20%	0.9%	**Pass**
30%	0.3%	**Pass**

Figure 4.14 shows the bar chart for the comparison between the consistencies of each data set collected concerning water activity. All the data felled within the pass region, indicating that the data has good quality concerning the consistency of the water activity. The calculations for this criteria are detailed in the Appendix D of this work.

Figure 4.14. Water activity consistency check comparison. (1) 10% MEG, (2) 20% MEG, (3) 30% MEG, (4) 5% NaCl, (5) 10% NaCl, (6) 5% NaCl + 10% MEG, (7) 5% NaCl + 20% MEG, (8) 5% NaCl + 30% MEG.

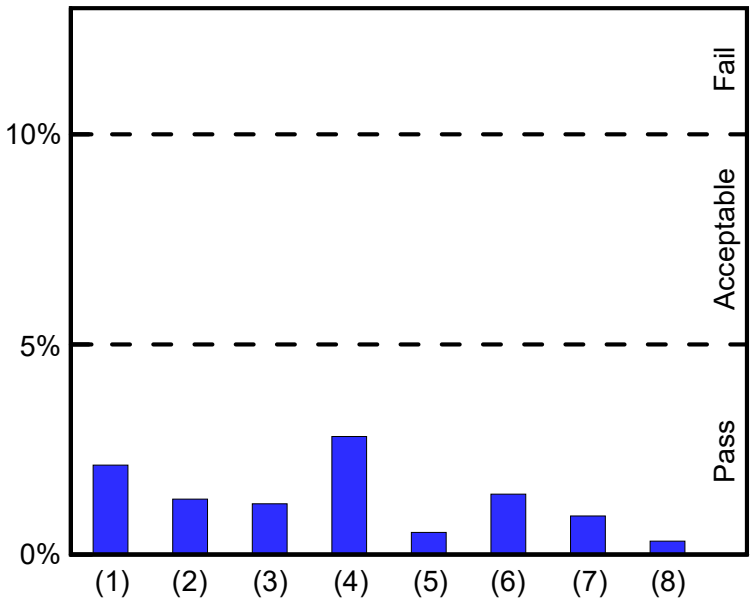

The experimental data obtained in this work was evaluated according to the three consistency check proposed by Sa et al. (2018). This method was used in order to guarantee the quality of the data collected. For all data sets, the three consistency check had good results, indicating that the data is indeed reliable.

4.5 COMPARISON WITH SOFTWARE AND MODEL PREDICTIONS

To evaluate the precision of selected software products available, its predictions were compared to the experimental data obtained. The software products used were CSMGem (indicated as dash-dot lines), Multiflash (indicated as black continuous lines) and PVTSim (indicated as blue continuous lines). Furthermore, the results of this work is then compared with the model for inhibited systems from the Hu-Lee-Sum correlation developed by Hu et al. (2017 a) (indicated as dashes lines) and from Sirino et. al. (2018) model (indicated as red continuous lines). The characteristics of each one is discussed in the Appendix E of this work.

The absolute average deviation (AAD) was calculated for each data set of different inhibitor concentrations. This allows for a general analysis of the precision of each model for each concentration rather than just for each data point. The calculations are presented in detail in the Appendix F of this work.

Figure 4.15 shows a plot of pressure versus temperature for CO_2 hydrate equilibrium data points obtained in this compared with software products and model for pure water system. The black diamond symbols indicate the data collected in this work and the lines are the predictions from software products and the models. Overall, all predictions were very satisfactory, with the highest error being from Multiflash (AAD = 0.27 K) and the lowest error from CSMGem (AAD = 0.12 K). Carbon dioxide hydrates with pure water is more studied in literature and is simpler than inhibited systems, thus low errors are expected.

Furthermore, it is important to note that due to the high inclination of the equilibrium curve in the region above Q_2, a small change in temperature causes a high change in pressure. For instance, for the pure water system the equilibrium temperature for 8.5 MPa is 283.68 K,

while for 13 MPa is 284.13 K. This results in a difference in temperature of 0.45 K, while the difference in pressure relative to this small temperature change is 4.5 MPa.

Figure 4.15. Comparison between models and experimental data from this work for CO_2-Water hydrate system.

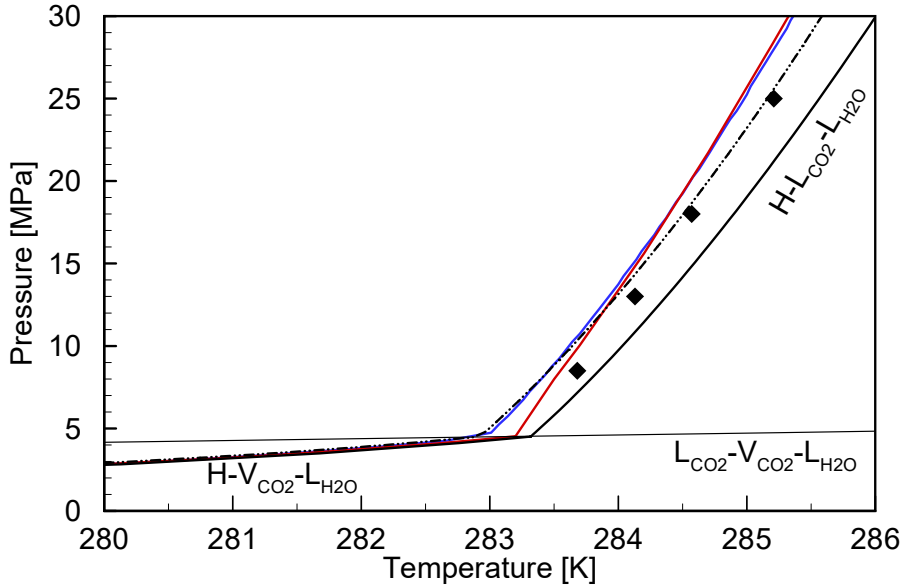

◆ **This Work;**
CSMGem;
Multiflash;
PVTSim;
Sirino et al. (2018).

Figure 4.16 shows pressure versus temperature equilibrium points for CO_2 hydrates inhibited with MEG. The V_{CO2}-L_{CO2}-L_{H2O} was plotted according to Multiflash's prediction in order to facilitate the observation of the upper quadruple point amongst all the concentrations of MEG used. Concentrations are in mass percentage in the aqueous phase.

In general, the discrepancies between the predictions increases with concentration of MEG. For the 10% and 20% of MEG systems, Multiflash gave the best predictions, with AAD equal to 0.08 K and 0.10 K respectively. For 10% of MEG, PVTSim and Hu-Lee-Sum correlation have the highest error, with AADs of 0.52 K and 0.49 K respectively.

For 20% and 30% of MEG, the Hu-Lee-Sum (2017) correlation significantly increases its error, with AADs of 1.30 K and 2.40 K respectively. At 30% of MEG, PVTSim gave the best prediction, of with an AAD of 0.13 K. For this same system, Multiflash was very similar, with an AAD of 0.20 K, and Sirino et al. (2018) model had an increase in error to an AAD of

1.39 K. Overall, Multiflash gave the best results for MEG inhibited system, except with higher concentrations of MEG, where PVTSim proved to have a similar reliability.

Figure 4.16. Experimental results of this work (symbols) compared with software products and models predictions (lines) for MEG inhibited systems.

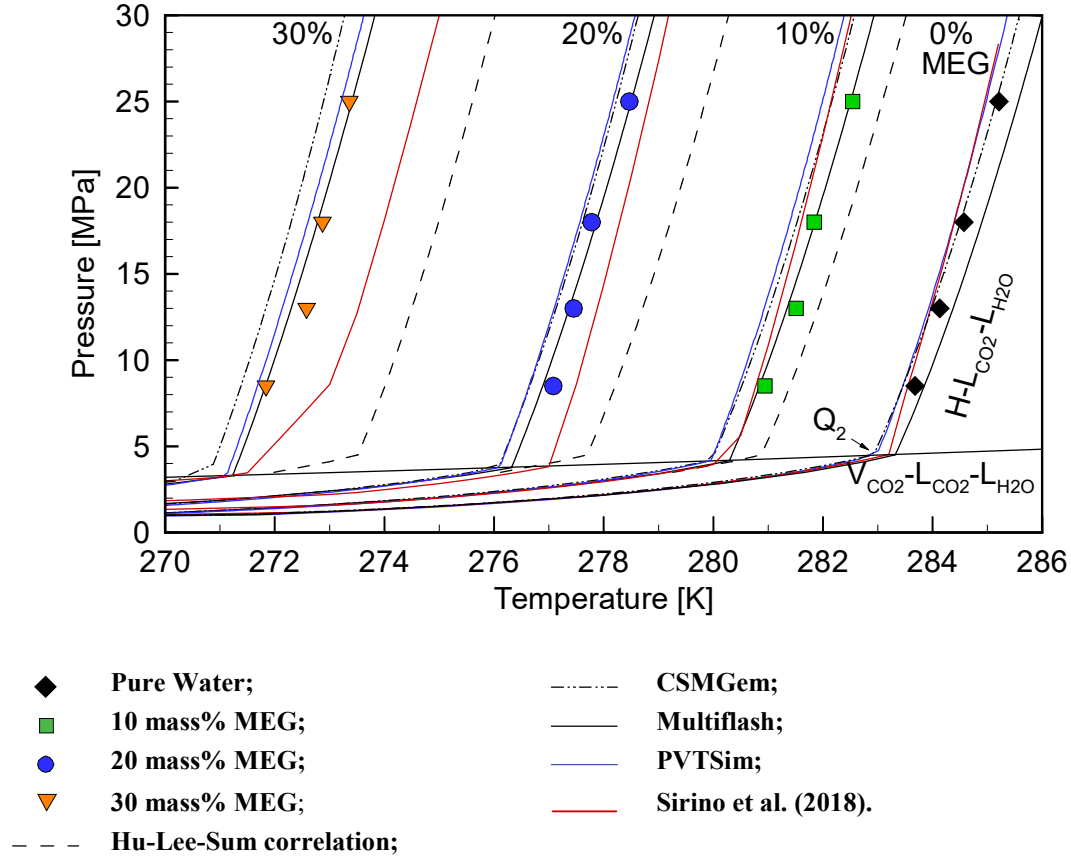

Figure 4.17 shows the equilibrium pressure and temperatures for the NaCl inhibited systems. Concentrations are in mass percentages in the aqueous phase. For the 5% of NaCl system, PVTSim gave the best predictions, with an AAD of 0.15 K, with CSMGem being very similar, with an AAD of 0.17 K. For this system, the highest error was from Hu-Lee-Sum correlation, with an AAD of 0.64 K.

With 10% of NaCl, the discrepancies between predictions rose. In this case, Multiflash gave the lowest error, with an AAD of 0.13 K, closely followed by PVTSim, with an AAD of 0.18 K. Hu-Lee-Sum correlation increased its error to an AAD 1.18 K, being the highest one for this system.

Multiflash error decreased with NaCl concentration, while the error from the other predictions increased. However, as PVTSim gave low errors in both cases, it proves to be the most reliable for NaCl inhibited systems with the analyzed concentrations.

Figure 4.17. Results for CO_2 hydrates with water and NaCl. Symbols are this work results and lines are software products and models predictions.

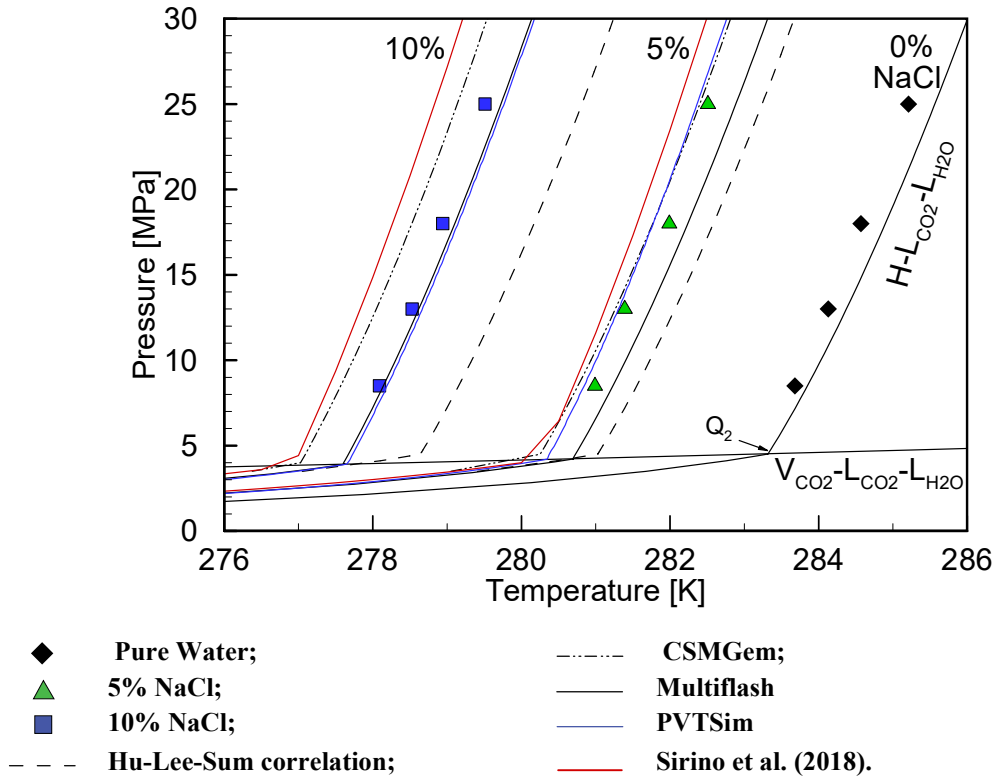

In Figure 4.18, data for the system with mixture of 5% of NaCl and different MEG concentrations is displayed in a pressure versus temperature plot. The concentrations are in mass percentages in the aqueous phase. For the system with 5% of NaCl + 10% of MEG, CSMGem showed the lowest error, with an AAD of 0.29 K, followed by Multiflash, with an AAD of 0.34 K. The Hu-Lee-Sum correlation gave the highest error, with an AAD of 1.24 K, followed by PVTSim, with an AAD of 0.77 K.

At 5% of NaCl + 20% of MEG, CSMGem gave the best results with an AAD of 0.27 K, followed by the model from Sirino et al. (2018), which resulted with an AAD of 0.56 K.

For the system with 5% of NaCl + 30% of MEG, the discrepancies and errors were significantly higher than any other systems studied here, which is expected as it is the most

complex system. PVTSim showed to be the most reliable one, with an AAD of 0.28 K. The second best was Multiflash, with an AAD of 1.27 K, which is a much higher difference when compared to the other systems.

For this system, the other models struggle to give good predictions. The worst one by a significant margin was CSMGem, with an AAD of 10.31 K, the highest one from all the comparisons. The Hu-Lee-Sum correlation resulted in an AAD of 3.58 K and the Sirino et al. (2018) model was not able to converge.

Figure 4.18. Results for the system with 5 mass% NaCl and MEG compared with software products and models.

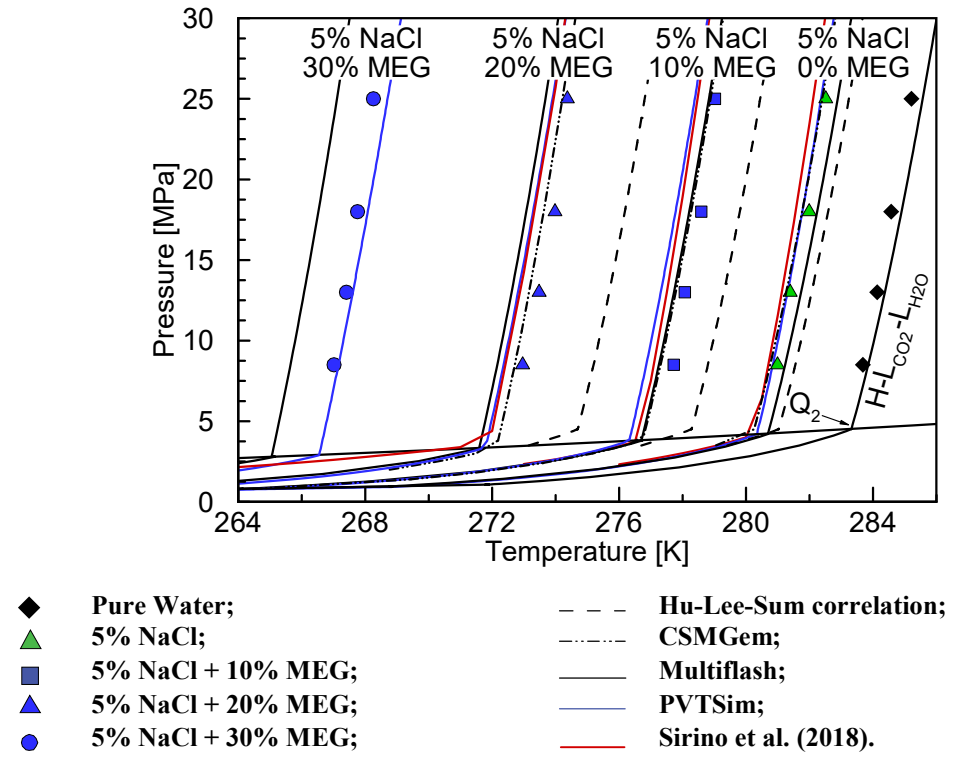

The average absolute deviation can be calculated for each concentration in order to evaluate the error from each model and software. The calculations and equations used are explained in detail in the Appendix F of this work. Figure 4.19 shows a bar comparison between the AAD of each system analyzed in this work.

The red bars corresponds to the Sirino et al. (2018) model, the dark grey bars are from Multiflash, the blue bars are from the PVTSim program, the green bars are from CSMGem and

the light grey bars corresponds to the Hu-Lee-Sum correlation. The error is calculated in the equilibrium temperature obtained for each pressure.

Figure 4.19. Root mean square error from model and software in comparison with experimental data from this work. (1) Pure water, (2) 10% MEG, (3) 20% MEG, (4) 30% MEG, (5) 5% NaCl, (6) 10% NaCl, (7) 5% NaCl + 10% MEG, (8) 5% NaCl + 20% MEG, (9) 5% NaCl + 30% MEG.

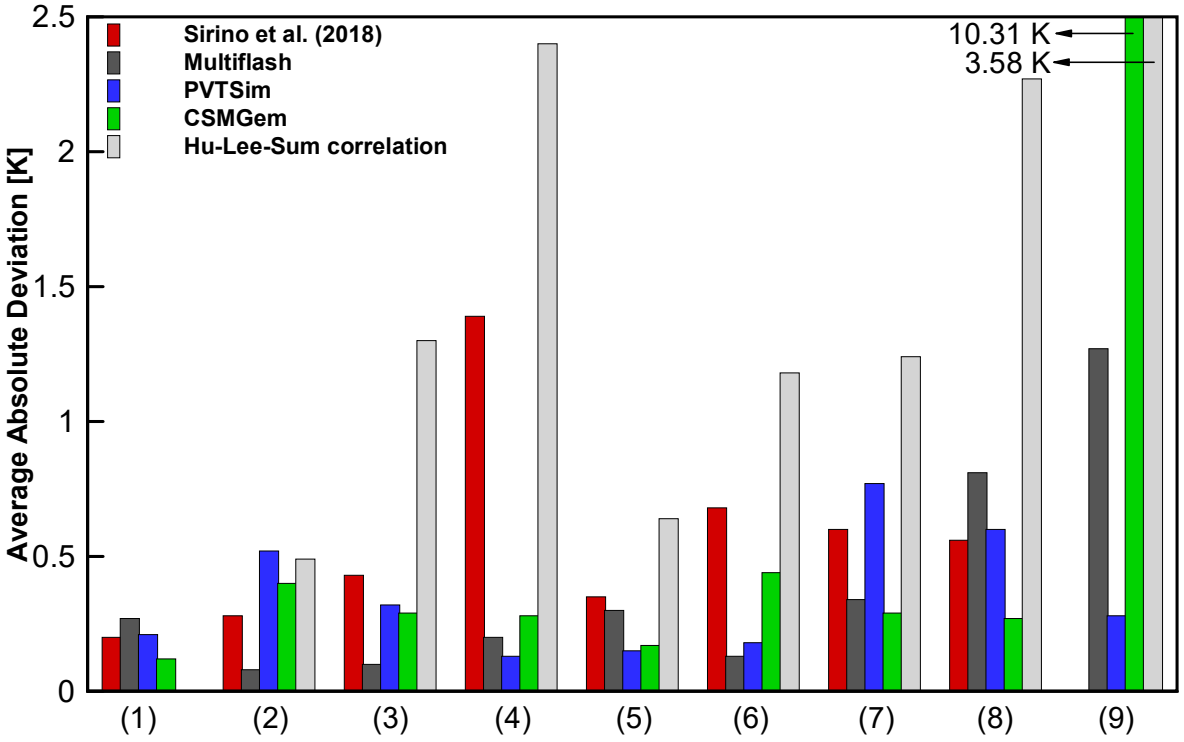

For systems with low concentrations of MEG, the software products and models showed very good agreement, with errors less than 0.5% in the equilibrium temperature. The system with 30% of MEG, the Hu-Lee-Sum correlation and the model from Sirino et al. (2018) showed the worst results, with errors above 0.5%, with Multiflash being the one with less error.

For the 5% NaCl inhibited system, Sirino et al. (2018) model showed good agreement with data, so did the other software products. At 10% of NaCl however, both Sirino et al. (2018) and the Hu-Lee-Sum correlation were the ones with the worst predictions, but still with less than 0.5% error.

The Hu-Lee-Sum correlation was the one with the highest errors when predicting equilibrium data for carbon dioxide hydrates in inhibited systems. As the systems tested by

them were mostly gaseous, the presence of the condensate CO_2 phase proves to be a challenge for the correlation. Although it does show good predictions for gaseous systems (HU et al., 2017 a), it may be necessary to account for the condensation of the gas phase in order to increase the reliability of the correlation.

For the more complex systems, which have a mixture of inhibitors, the discrepancies between the predictions were more apparent. The system with 5% NaCl + 30% MEG showed very poor predictions by the software products CSMGem and Multiflash, and from the Hu-Lee-Sum (2017) correlation. In addition, the model from Sirino et al. (2018) was not able to converge. In this case, PVTSim gave very good results, with an AAD of 0.28 K. In order to determine which software is best, more results should be evaluated, especially with complex systems, such as the ones with mixture of inhibitors.

Overall, Multiflash was able to predict equilibrium temperatures for carbon dioxide hydrates with good reliability for almost all systems. For complex systems, PVTSim showed very good results, particularly with the mixture of inhibitors in high concentrations.

PVTSim and Multiflash are commercial software products and there is limited information on the models that they use. PVTSim uses a modified version of the SRK EoS, while Multiflash uses the CPA EoS. CSMGem is an academic open source product with more information available, although there are still some difficulties to make conclusions about why it may give better results. Sirino et al. (2018) model also uses CPA EoS but still gives different results when compared Multiflash. The main reason between the discrepancies between those predictions, when it comes to EoS, are due to the binary interaction parameters used in each one.

All of the software products and the model by Sirino et al. (2018) use the van der Waals and Platteeuw hydrate prediction model. This model relies on the experimental regression of Kihara parameters in order to reliably predict hydrate formation. This is also a big contribution on the differences between the predictions. By not having access to all binary parameters and Kihara parameters used in each model, it is very difficult to take conclusions on the reasons for better prediction results. The van der Waals and Platteeuw hydrate model is better explained in the Appendix E and in the publication Sirino et al. (2018).

The Hu-Lee-Sum correlation does not make flash calculations and neither uses a model for hydrate formation, instead it calculates the activity of water and makes an estimation on the

temperature suppression due to the presence of the inhibitor. This causes it to increases its prediction error, underestimating the inhibition effect of the inhibitors used. Although it has the highest error of them all, for the region bellow Q_2 the errors are less impactful, as noted in (HU et al., 2017 a). In addition, its ease of use can prove to be useful since the equations used are significantly simpler than those used by software products and from the CSMGem model.

5 CONCLUSIONS

An isobaric experimental procedure was performed in order to achieve high enough pressures to allow for the condensation of the gas phase. Experimental data for the equilibrium conditions of CO_2 hydrates were obtained. The pure water system data was used to validate the experimental procedure by comparing the results with available data in literature, while the inhibited systems was not previously reported in literature.

The pressured evaluated were of 8.5, 13, 18 and 25 MPa, which were chosen in order to achieve the condensation of the gas phase and due to limitations of the experimental apparatus. To evaluate the inhibition effect of thermodynamic inhibitors, MEG and NaCl were used at different concentrations. The isobaric method has proved to be very reliable for determining experimental equilibrium temperatures for the chosen pressures, allowing for hydrates to form and dissociate with no pressure variation.

As the water produced with oil in the industry is naturally inhibited by the presence of salts, the amount of thermodynamic inhibitor can be optimized. This way, the equilibrium conditions for CO_2 hydrates inhibited with mixtures of NaCl and MEG was determined.

The consistency was evaluated for all the data collected in this work. This way, the quality of the data obtained was assured. Furthermore, a comparison with software products Multiflash, PVTSim and CSMGem and the model by Sirino et al. (2018) and the Hu-Lee-Sum correlation was done. Overall, Multiflash gave good results for most systems, while PVTSim was able to better predict equilibrium conditions for more complex systems, such as in high concentrations of inhibitors.

5.1 SUGESTIONS FOR FUTURE WORK

For future work, the following topics are presented as suggestions.

- Higher concentrations of inhibitors: this evaluation can help to provide a better understanding of the reliability of the consistency analysis, which may have limitations at high

concentrations of inhibitors. In addition, the predictions done by software products and models may show to be less reliable in these more complex systems.

- Different mixtures of inhibitors: as in high concentrations, particularly in the mixed systems, the predictions were not as reliable, it is interesting to determine the equilibrium conditions for system with high concentrations of NaCl and MEG. This data can be used to help optimize the amount of inhibitor to be added in systems with high concentrations of salt.
- Different inhibitors: as the water produced in offshore oil industries is naturally inhibited by a variety of salts, the evaluation of the inhibition effect of these salts can also be important, as well as other types of inhibitors such as ethanol and isopropanol.

6 REFERENCES

ANGUS, S.; ARMSTRONG, B.; DE REUCK, K. M., (1976) International Thermodynamic Tables of the Fluid State - 3 Carbon Dioxide.

ATKINS, P. W. (Peter W.; JONES, L., (2008) *Chemical principles : the quest for insight*. W.H. Freeman.

AUSTVIK, T.; LI, X.; GJERTSEN, L. H., (2000) Hydrate Plug Properties: Formation and removal of plugs. *Ann. N.Y. Acad. Sci.*, 294–303.

AYA, I.; YAMANE, K.; NARIAI, H., (1997) Solubility of CO2 and density of CO2 hydrate at 30 MPa. *Energy*., **22**, 263–271.

BESNARD, G.; SONG, K. Y.; HIGHTOWER, J. W.; KOBAYASHI, R.; EL, D., (1991) New Method of Temperature-Ramping, Isobaric Experiments to Study the Hydrate Formation and Decomposition.

BI, Y.; YANG, T.; GUO, K., (2013) Determination of the upper-quadruple-phase equilibrium region for carbon dioxide and methane mixed gas hydrates. *Journal of Petroleum Science and Engineering*., **101**, 62–67.

CARROLL, J., (2014) *Natural Gas Hydrates - A Guide for Engineers (3rd Edition)*. *Elsevier*.

CHAPOY, A.; BURGASS, R.; TOHIDI, B.; AUSTELL, J. M.; EICKHOFF, C., (2011) Effect of Common Impurities on the Phase Behavior of Carbon-Dioxide-Rich Systems: Minimizing the Risk of Hydrate Formation and Two-Phase Flow. *SPE Journal*., **16**, 921–930.

COLEMAN, H. W.; STEELE, W. G., (2018) *Experimentation, validation, and uncertainty analysis for engineers*.

DAHM, K. D. (Kevin D.; VISCO, D. P., (2014) *Fundamentals of Chemical Engineering Thermodynamics*.

DEATON, W. M.; FROST, E. M., (1937) No Title. *Oil and Gas Journal*., **36**, 75.

FAN, S. S.; GUO, T. M., (1999) Hydrate Formation of CO 2 -Rich Binary and Quaternary Gas Mixtures in Aqueous Sodium Chloride Solutions. *Journal of Chemical & Engineering Data*., **44**, 829–832.

FERRARI, P. F.; GUEMBAROSKI, A. Z.; MARCELINO NETO, M. A.; MORALES, R. E. M.; SUM, A. K., (2016) Experimental measurements and modelling of carbon dioxide hydrate phase equilibrium with and without ethanol. *Fluid Phase Equilibria*., **413**, 176–183.

GUEMBAROSKI, A. Z., (2016) *An experimental study on the phase equilibrium of carbon dioxide hydrates in the presence of thermodynamical inhibitors*. Federal University of Technology - Curitiba/PR - Brazil.

GUEMBAROSKI, A. Z.; MARCELINO NETO, M. A.; MORALES, R. E. M., (2016) Equilíbrio de Fases de Hidratos na Presença de Inibidores Termodinâmicos. *Congresso Nacional de Engenharia Mecânica*.

HAMMERSCHMIDT, E. G., (1934) Formation of Gas Hydrates in Natural Gas Transmition Lines. *Industrial & Engineering Chemistry*., **26**, 851–855.

HEADRICK, J. M.; DIKEN, E. G.; WALTERS, R. S.; HAMMER, N. I.; CHRISTIE, R. A.; CUI, J.; MYSHAKIN, E. M.; DUNCAN, M. A.; JOHNSON, M. A.; JORDAN, K. D., (2005) Chemistry: Spectral signatures of hydrated proton vibrations in water clusters. *Science*., **308**, 1765–1769.

HU, Y.; LEE, B. R.; SUM, A. K., (2017a) Universal correlation for gas hydrates suppression temperature of inhibited systems: I. Single salts. *AIChE Journal*., **63**, 5111–5124.

HU, Y.; MAKOGON, T. Y.; KARANJKAR, P.; LEE, K. H.; LEE, B. R.; SUM, A. K., (2017b) Gas hydrates phase equilibria for structure I and II hydrates with chloride salts at high salt concentrations and up to 200MPa. *Journal of Chemical Thermodynamics*.

KAKITANI, C., (2014) *Study of Phase Equilibrium of Methane Hydrate and Mixture of Methane and Carbon Dioxide Hydrate*. Federal University of Technology of Parana - Curitiba/PR - Brazil.

KELLAND, M. A., (2006) History of the development of low dosage hydrate inhibitors. *Energy and Fuels*., **20**, 825–847.

KIM, S. H.; SEO, M. Do; KANG, J. W.; LEE, C. S., (2011) Hydrate-containing phase equilibria for mixed guests of carbon dioxide and nitrogen. *Fluid Phase Equilibria*., **306**, 229–233.

KIYONO, F.; TAJIMA, H.; OGASAWARA, K.; YAMASAKI, A., (2005) Method to determine quadruple points of a two-component system containing a simple hydrate phase and behavior of the system near these points. *Fluid Phase Equilibria*., **230**, 90–98.

KOH, C. A.; SLOAN, E. D.; SUM, A. K.; WU, D. T., (2011) Fundamentals and Applications of Gas Hydrates. *Annual Review of Chemical and Biomolecular Engineering*., **2**, 237–257.

MELO, C. L.; THEDY, E. A.; ROCHA, P. S.; ALMEIDA, A. S. De; PAULA, A., (2011) The challenges on the CCGS monitoring in the development of Santos Basin Pre-salt Cluster. *Energy Procedia*., **4**, 3394–3398.

MOOIJER-VAN DEN HEUVEL, M. M., C. J.; DE SWAAN ARONS, J., (2002) Gas hydrate phase equilibria for propane in the presence of additive components. *Fluid Phase Equilibria*., **193**, 245–259.

MOOIJER-VAN DEN HEUVEL, M. M.; WITTEMAN, R.; PETERS, C. J., (2001) Phase behaviour of gas hydrates of carbon dioxide in the presence of tetrahydropyran, cyclobutanone, cyclohexane and methylcyclohexane. *Fluid Phase Equilibria*., **182**, 97–110.

MORAN, M. J.; SHAPIRO, H. N.; BOETTNER, D. D.; BAILEY, M. B. (Margaret B., (2014) *Fundamentals of engineering thermodynamics* 8th edn. Wiley.

MULTIFLASH, (2017) Multiflash 6.1.

NAGASHIMA, H. D.; FUKUSHIMA, N.; OHMURA, R., (2016) Phase equilibrium condition measurements in carbon dioxide clathrate hydrate forming system from 199.1 K to 247.1 K. *Fluid Phase Equilibria*., **413**, 53–56.

NG, H. J.; ROBINSON, D. B., (1985) Hydrate formation in systems containing methane, ethane, propane, carbon dioxide or hydrogen sulfide in the presence of methanol. *Fluid Phase Equilibria*., **21**, 145–155.

NG, H. J.; CHEN, C. J.; ROBINSON, D. B., (1985) Effect of Ethylene Glycol or Methanol on

Hydrate Formation in Systems Containing Ethane, Propane, Carbon Dioxide, Hydrogen Sulfide or a Typical Gas Condensate. *DB Robinson Associates Ltd. Research Report, @92 Edmonton, Alberta, Canada*.

OBANIJESU, E. O.; PAREEK, V.; TADE, M. O., (2010) Hydrate Formation and its Influence on Natural Gas Pipeline Internal Corrosion Rate. *Environment*., **62**, 164–173.

OHGAKI, K.; MAKIHARA, Y.; TAKANO, K., (1993) Formation Of CO2 Hydrate In Pure And Sea Waters. *J. Chem. Eng. Jpn.*, **5**, 558–564.

PARK, K. nam; LEE, J. D.; CHOI, S. J.; KANG, K. C.; LINGA, P., (2014) Seawater desalination by gas hydrate process and removal characteristics of dissolved ions (Na+, K+, Mg2+, Ca2+, B3+, Cl−, SO42−). *Desalination*., **353**, 84–90.

PETERS, D.; SELIM, S.; SLOAN, E. D., (2000) Hydrate dissociation in pipelines by two-sided depressurization: experiment and model. *Ann. N.Y. Acad. Sci.*, 304–313.

PIEROEN, A. P., (1955) Gas hydrates - approximate relations between heat of formation, composition and equilibrium temperature lowering by “inhibitors”, **74**, 995–1002.

RUFFINE, L.; TRUSLER, J. P. M., (2010) Phase behaviour of mixed-gas hydrate systems containing carbon dioxide. *Journal of Chemical Thermodynamics*., **42**, 605–611.

SA, J. H.; HU, Y.; SUM, A. K., (2018) Assessing thermodynamic consistency of gas hydrates phase equilibrium data for inhibited systems. *Fluid Phase Equilibria*., **473**, 294–299.

SCHROETER, J. P.; KOBAYASHI, R.; HILDEBRAND, M. A., (1983) Hydrate decomposition conditions in the system hydrogen sulfide-methane-propane. *Industrial & Engineering Chemistry Fundamentals*., **22**, 361–364.

SEO, Y. T.; LEE, H., (2001) Hydrate Phase Equilibria of the Carbon Dioxide, Methane, and Water System, 381–384.

SHIN, B. S.; KIM, E. S.; KWAK, S. K.; LIM, J. S.; KIM, K. S.; KANG, J. W., (2014) Thermodynamic inhibition effects of ionic liquids on the formation of condensed carbon dioxide hydrate. *Fluid Phase Equilibria*., **382**, 270–278.

SIRINO, T. H.; MARCELINO NETO, M. A.; BERTOLDI, D.; MORALES, R. E. M.; SUM, A. K., (2018) Multiphase flash calculations for gas hydrates systems. *Fluid Phase Equilibria*., **475**, 45–63.

SLOAN, E. D., (1991) Natural Gas Hydrates. *Journal of Petroleum Technology*., **43**, 1414–1417.

SLOAN, E. D., (2003) Fundamental principles and applications of natural gas hydrates. *Nature*., **426**, 353–359.

SLOAN, E. D.; KOH, C. A. (Carolyn A., (2008) *Clathrate hydrates of natural gases.* CRC Press.

SLOAN, E. D.; KOH, C.; SUM, A. K., (2011) *Natural gas hydrates in flow assurance*. Gulf Professional Pub./Elsevier.

STRAUME, E. O.; KAKITANI, C.; MERINO-GARCIA, D.; MORALES, R. E. M.; SUM, A. K., (2016) Experimental study of the formation and deposition of gas hydrates in non-emulsifying oil and condensate systems. *Chemical Engineering Science*., **155**, 111–126.

TAKENOUCHI, S.; KENNEDY, G. C., (1965) J. Geology, **73**, 383.

UNRUH, C. H.; KATZ, D. L., (1949) -. *Trans. AIME*., **183**, 83.

VAN DER WALLS, J. H.; PLATTEEUW, J. C., (1959) Validity of Clapeyron's Equation for Phase Equilibria involving Clathrates. *Nature*., **183**, 462.

WEBER, E. (Ed.), (1987) *Molecular Inclusion and Molecular Recognition — Clathrates I*. Topics in Current Chemistry. Springer-Verlag, Berlin/Heidelberg, Vol. 140.

APPENDIX A - WATER ACTIVITY CONSISTENCY EQUATIONS

The third and last consistency check, as proposed by Sa et al. (2018), is not commonly used in the technical community. In this appendix, it is presented the deduction alongside all the hypothesis and considerations of this consistency check. We start from the suppression temperature expressed in Equation (15).

$$\Delta T = T_W - T_{THI} \tag{15}$$

Considering a system where hydrates are dissociating in equilibrium, the fugacity between the water phase and the hydrate phase are equal. Equation (16) indicates this relation, where *H* corresponds to the solid hydrate phase and *L*, to the liquid phase (Dahm and Visco, 2014).

$$f_w^{\,H}(T,P) = f_w^{\,L}(T,P) \tag{16}$$

From the definition of activity coefficient ($\gamma_i = a_i/x_i$), which is function of temperature, pressure and composition, and from Equation (16), the following equality is obtained, shown as Equation (17).

$$f_w^{\,H}(T,P) = f_w^{\,L}(T,P) = x_w \gamma_w(T,P,x) f_w^{\,L_0}(T,P) \tag{17}$$

The assumptions made are that the pressure is constant, hydrate forms a pure phase (inhibitors do not form hydrates), the composition of the hydrate phase is constant and the composition of the hydrocarbon rich phase is constant (HU et al., 2017 a).

From the definition of Gibbs energy of fusion, the ratio between the fugacity of the liquid pure phase (L_0) and the solid pure phase (*S*) can be related as shown in Equation (18).

$$\frac{\Delta_{fus} G(T,P)}{RT} = \ln\left(\frac{f_w^{\,L_0}(T,P)}{f_w^{\,S}(T,P)}\right) \tag{18}$$

The definition of enthalpy and entropy of fusion is given by Equation (19) (Dahm and Visco, 2014) and can be expressed as Equations (20) and (21), where ΔC_p is the heat capacity difference between that of the pure water and from the solid hydrate.

$$\Delta G = \Delta H - T\Delta S \tag{19}$$

$$\Delta_{fus}H(T,P) = \Delta_{fus}H(T_0) + \int_{T_0}^{T} \Delta C_p dT \tag{20}$$

$$\Delta_{fus}S(T,P) = \Delta_{fus}S(T_0) + \int_{T_0}^{T} \Delta C_p dT \tag{21}$$

These equations make a relation between the system at temperature T and at temperature T_0, which is the solidification temperature associated with hydrate formation. When those temperatures are the same ($T = T_0$), the following simplifications can be made with Equation (22).

$$\begin{aligned} \Delta G_{fus}(T_0) &= \Delta H_{fus}(T_0) - T_0 \Delta S_{fus}(T_0) = 0 \\ \Delta S_{fus}(T_0) &= \frac{\Delta H_{fus}(T_0)}{T_0} \end{aligned} \tag{22}$$

Substituting Equation (22) into Equation (21), the entropy change associate with hydrate fusion is obtained.

$$\Delta_{fus}S(T,P) = \frac{\Delta_{fus}H(T_0)}{T_0} + \int_{T_0}^{T} \Delta C_p dT \tag{23}$$

By combining Equations(19), (20) and (23) into Equation(18), the following relation can be obtained.

$$\frac{\Delta_{fus}G(T,P)}{RT} = \ln\underbrace{\left(\frac{f_w^{L_0}(T,P)}{f_w^{S}(T,P)}\right)}_{x_w\gamma_w} = \frac{\Delta H_{fus}(T,P) - T\Delta S_{fus}(T,P)}{RT}$$

$$\ln(x_w\gamma_w) = \ln(a_w) = \frac{1}{RT}\left[\Delta H_{fus}(T,P) - T\Delta S_{fus}(T,P)\right]$$

$$= \frac{1}{RT}\left[\Delta_{fus}H(T_0) + \int_{T_0}^{T}\Delta C_p dT - T\frac{\Delta_{fus}H(T_0)}{T_0} - T\int_{T_0}^{T}\Delta C_p dT\right]$$

$$= \frac{1}{RT}\left[\Delta_{fus}H(T_0) - T\frac{\Delta_{fus}H(T_0)}{T_0} + \underbrace{\int_{T_0}^{T}\Delta C_p dT - T\int_{T_0}^{T}\Delta C_p dT}_{(1)}\right]$$

The term (1) is usually very small, thus it can be neglected, resulting in Equation (24)

.

$$\ln(a_w) = \frac{1}{RT}\left[\Delta_{fus}H(T_0)\left(1-\frac{T}{T_0}\right)\right] \tag{24}$$

In hydrate formation, water molecules (indicated as *W*) combine with a guest molecule of a second type (indicated as *A*) in order to form a solid phase. This process can be expressed as an equilibrium, shown in Equation (25).

$$A + n \cdot W \rightleftharpoons A \cdot n \cdot W \tag{25}$$

Considering a system where a thermodynamic inhibitor is present, which causes the equilibrium temperature to shift from T_0 to T, but does not participate in hydrate formation, the equilibrium condition in terms of chemical potential (μ) can be described as shown in Equation (26).

$$\mu_A + n \cdot \mu_W = \mu_{A \cdot n \cdot W}$$

$$\mu_W = \frac{\mu_{A \cdot n \cdot W} - \mu_A}{n} \tag{26}$$

From the definition of chemical potential, Equation (27) is introduced for the chemical potential of water (μ_w), where the water activity (a_w) is used to describe its deviation from ideality and μ_w^0 is the chemical potential of pure water.

$$\mu_W = \mu_W^0 + RT\ln(a_W) \tag{27}$$

Rearranging Equation (27) and inserting Equation (26).

$$RT\ln(a_W) = \mu_W - \mu_W^0$$

$$RT\ln(a_W) = \frac{\mu_{A \cdot n \cdot W} - \mu_A}{n} - \mu_W^0$$

$$nR\ln(a_W) = \frac{1}{T}\left[\mu_{A \cdot n \cdot W} - \mu_A - n\mu_W^0\right]_T \tag{28}$$

Applying the same process but considering the absence of thermodynamic inhibitor, i.e. a pure water system, which will have a hydrate equilibrium temperature of T_0, Equation (29) is obtained.

$$nR\ln(a_W\,') = \frac{1}{T_0}\left[\mu_{A\cdot n\cdot W} - \mu_A - n\mu_W^0\right]_{T_0} \tag{29}$$

Subtracting Equation (29) from (28).

$$nR\ln(a_W) - nR\ln(a_W\,') = \frac{1}{T}\left[\mu_{A\cdot n\cdot W} - \mu_A - n\mu_W^0\right]_T - \frac{1}{T_0}\left[\mu_{A\cdot n\cdot W} - \mu_A - n\mu_W^0\right]_{T_0} \tag{30}$$

From the fundamental relation of Gibbs free energy (Equation (31)) and the definition of entropy with respect to G (Equation (32)), the following relation can be obtained.

$$G = H - TS = n\mu \tag{31}$$

$$S = -\left(\frac{\partial G}{\partial T}\right)_{P,n} \tag{32}$$

$$G = H - T\left(-\left(\frac{\partial G}{\partial T}\right)_{P,n}\right)$$

$$\left(-\frac{1}{T^2}\right)G = \left(-\frac{1}{T^2}\right)H + \left(-\frac{1}{T^2}\right)T\left(\frac{\partial G}{\partial T}\right)_{P,n}$$

$$\frac{1}{T}\left(\frac{\partial G}{\partial T}\right)_{P,n} - \frac{G}{T^2} = -\frac{H}{T^2}$$

$$\left(\frac{\partial G/T}{\partial T}\right)_{P,n} = -\frac{H}{T^2} \tag{33}$$

Equation (33) is the Gibbs-Helmholtz relation, which gives the Gibbs free energy (G) in terms of enthalpy (H). By inserting the relation between G and the chemical potential μ from Equation (31) into Equation (33), the following relation is obtained.

$$\left(\frac{\partial n\mu/T}{\partial T}\right)_{P,n} = -\frac{H}{T^2} \quad \rightarrow \quad n\left(\frac{\partial \mu/T}{\partial T}\right)_{P,n} = -\frac{H}{T^2}$$

$$\left(\frac{\partial \mu / T}{\partial T}\right)_{P,n} = -\frac{1}{T^2} \underbrace{\frac{H}{n}}_{\text{Molar Enthalpy}}$$

$$\left(\frac{\partial \mu / T}{\partial T}\right) = -\frac{\bar{H}}{T^2} \tag{34}$$

Integrating the Equation (34) from a condition of pure water system (T_0) to a condition of an inhibited system (T). The variation of enthalpy

$$\int_{T}^{T_0} d(\mu / T) = -\int_{T}^{T_0} \frac{\bar{H}}{T^2} dT$$

$$\frac{\mu_T}{T} - \frac{\mu_{T_0}}{T} = \left[\bar{H}\right]_T^{T_0} \left(\frac{1}{T} - \frac{1}{T_0}\right) \tag{35}$$

The left side of Equation (35) can then be equated to the right side of Equation (30) leading to the following relation.

$$nR\ln(a_W) - nR\ln(a_W\,') = \left[\bar{H}\right]_T^{T_0} \left(\frac{1}{T} - \frac{1}{T_0}\right)$$

$$nR\ln\left(\frac{a_w}{a_w\,'}\right) = \left[\bar{H}\right]_T^{T_0} \left(\frac{1}{T} - \frac{1}{T_0}\right) \tag{36}$$

The term $\bar{H}$ is assumed independent from the temperature. The hydrate dissociation enthalpy will be the change in enthalpy associated with the process described in reaction Equation (25).

$$H_A + nH_W \xrightarrow[\Delta H_{diss}]{} H_{AnW}$$

$$\Delta H_{diss} = H_A + nH_W - H_{AnW} \tag{37}$$

Then, the term $\bar{H}$ in Equation (37) can be described as the following (Pieroen, 1955).

$$\left[\bar{H}\right]_T^{T_0} = H_{A\cdot n\cdot W} - \bar{H}_A - n \cdot H_W \tag{38}$$

Now, it is assumed that the enthalpy change associated with the process is not dependent on the presence of the inhibitor and the temperature. This way, Equation (38) can be simplified as being equal to Equation (39).

$$\left[\bar{H}\right]_{T}^{T_0} = \Delta H = \left(H_{A\cdot n\cdot W} - \bar{H}_A - n\cdot\bar{H}_W\right)_{T_0} \tag{39}$$

Substituting Equation (39) into Equation (36). This substitution is mainly justified due to the low solubility of the hydrate former in the water phase. This enthalpy change (ΔH) is the difference due to hydrate formation, which is the same one that can be obtained with the Clausius-Clapeyron relation (Equation (3)).

$$nR\ln\left(\frac{a_w}{a_w'}\right) = \Delta H\left(\frac{1}{T} - \frac{1}{T_0}\right) \tag{40}$$

Next assumption is that the activity of water ($a_w = \gamma_w\, x_w$) will mostly depend on its molar fraction. This can be affirmed mainly due to the low solubility that most hydrate formers have in water, even if the inhibitor concentration is high. In addition, as A will have very low solubility in water, the term a_w', which corresponds to the pure water system, can be assumed as one. This way, Equation (40) can be further simplified (PIEROEN, 1955).

$$a_w' = x_w'\gamma_w' = 1 \qquad \frac{a_w}{a_w'} = \frac{x_w\gamma_w}{x_w'\gamma_w'} = x_w$$

$$nR\ln\left(x_w\right) = \Delta H\left(\frac{1}{T} - \frac{1}{T_0}\right) \tag{41}$$

By rearranging Equation (41) and using the concept of temperature depression seen in Equation (8), the following relation is obtained.

$$\frac{\Delta T}{T_0 T} = -\frac{nR}{\Delta H_d} ln\, a_W \tag{42}$$

Finally, the constant terms can be arranged into a single constant (β).

$$\beta = \frac{nR}{\Delta H_d} \tag{43}$$

$$\frac{\Delta T}{T_0 T} = \beta\, ln\, a_W(x_i, T) \cong \beta\, ln\, a_W(x_i) \tag{44}$$

APPENDIX B - EVALUATION OF THE EXPERIMENTAL UNCERTAINTIES

From the concept, a measurement must accompanied by its uncertainty, which reflects the lack of knowledge of the referred measurand (actual value of the property measured), shown in Equation (45) for a generic property x with an uncertainty u_c (COLEMAN and STEELE, 2018).

$$x_{measured} = x_{true} + u_c \tag{45}$$

A standard uncertainty is defined as the deviation from the original population from which the error originates. Equation (46) shows the standard deviation, where x is a measured property, N is the number of measurements of x.

$$s_x = \left[\frac{1}{N-1} \sum_{i=1}^{N} \left(x_i - \bar{x} \right)^2 \right]^{1/2} \tag{46}$$

The mean value from the measurements are indicated as $\bar{x}$ and can be calculated with Equation (47).

$$\bar{x} = \frac{1}{N} \sum_{i=1}^{N} x_i \tag{47}$$

B.1 TEMPERATURE UNCERTAINTIES

The temperature was measured using a PT-100 ($T_{\text{PT-100}}$) with a temperature transmitter (YTA-710 from Yokogawa) connected to a USB interface from National Instruments and (NI-6009) a computer for data acquisition and recording. Calibration of the PT-100 probe was done with a chiller and a certified reference mercury thermometer (T_{ref}). Using the method of least squares, the uncertainty of the calibration curve is calculated with Equation (48), where N is the number of measurements and C is the degree of the adjusted curve fit.

$$u_{cal} = \left[\frac{\sum (T_{\text{ref}} - T_{\text{PT-100}})^2}{N - (1 + C)} \right]^{1/2} \tag{48}$$

Next, the is defined as Equation (49), where the uncertainty from the reference thermometer is 0.09 °C, given by the certification company.

$$
\begin{aligned}
u_c{}^2 &= u_{cal}{}^2 + u_{ref}{}^2 \\
u_c{}^2 &= 0.063^2 + 0.09^2 \\
u_c &= 0.11
\end{aligned}
\tag{49}
$$

The expanded uncertainty is given by Equation (50), with $k = 1.96$ for a 95% confidence level, resulting in measurements of temperature with uncertainty of ±0.21 K.

$$
\begin{aligned}
U_{95\%}(T) &= 1.96 \times u_c \\
U_{95\%}(T) &= 1.96 \times 0.11 \\
U_{95\%}(T) &= \pm 0.21\,\mathrm{K}
\end{aligned}
\tag{50}
$$

B.2 MANUFACTURE PROVIDED UNCERTAINTIES

For measures of pressure and volume, the syringe pump model 260HP from TELEDYNE ISCO was used. The uncertainties are provided by the manufacture and are displayed in Table B.1.

Table B.1 - Manufacture provided uncertainties.

Property	Uncertainty
Pressure	±2.85 bar (0.285 MPa)
Volume	±0.0001 ml

APPENDIX C - EXTERNAL INFLUENCE OF ROOM TEMPERATURE

Although the syringe pump and the equilibrium cell have their temperature controlled, the valves that connect them do not. This causes an effect on the measured volume due to changes in ambient temperature. Depending on the temperature of the room, the heating curve may go over or under the cooling line. With that in mind, the equilibrium points were taken always as being the temperature at which hydrates were no longer present, which can be identified by the change in inclination of a volume versus pressure plot.

To reduce the effect of room temperature, a couple of precautions were taken. The syringe pump was isolated with thermal resistant material, lowering its heat transfer to the ambient. In addition, to lower the influence in the piping that connects the cell to the syringe pump, it was inserted inside a silicone tube, which had water circulating at a constant temperature. This proved to be very effective to lower the influence of room temperature changes.

Figure C.1 shows the before and after thermal isolations graphs. On the first graph, (a) and (b) clearly shows a change in volume for the same temperature, which should not occur. It can be inferred that this change is due to the influence of room temperature changes. The second graph is after the thermal isolations were installed and it can be seen that the behavior of temperature with volume is much more consistent, giving results that are more reliable.

Figure C.1. Experiment done before and after the room temperature changes precautions.

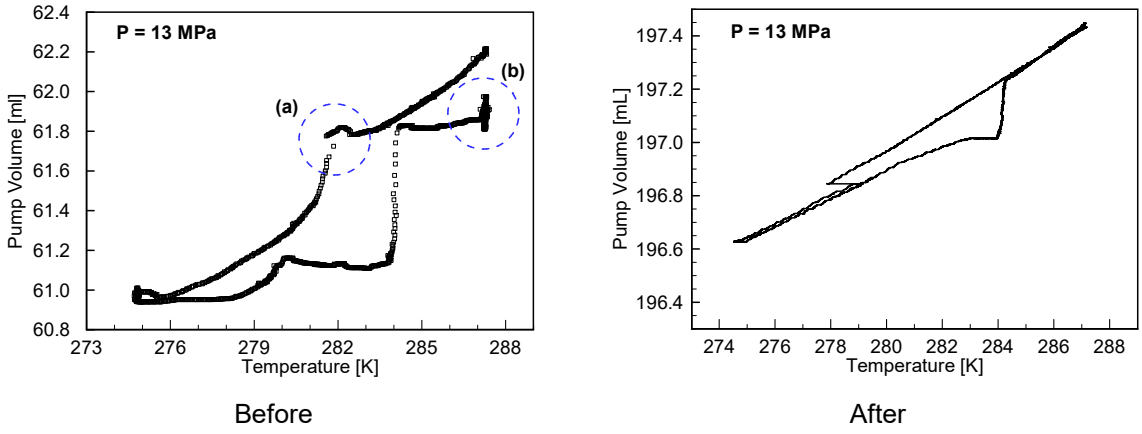

APPENDIX D - WATER ACTIVITY CONSISTENCY CHECK

The water activity consistency check criteria is calculated from Equation (51). T_0 is the equilibrium temperature for the pure water system and T, for the inhibited system. ΔT is the hydrate suppression temperature, calculated with Equation (52).

$$\frac{\Delta T}{T_0 T} = \beta \ln a_W(x_i, T) \cong \beta \ln a_W(x_i) \tag{51}$$

$$\Delta T = T_0 - T \tag{52}$$

For each pressure, $\Delta T/T_0T$ is calculated. Next, the average for each result obtained is calculated, i.e. the average of $(\Delta T/T_0T)_i$. Following that, the standard deviation (σ) is calculated with Equation (53), where i is reference to each pressure and N is the total number of pressures calculate, i.e. $N = 4$.

$$\sigma = \sqrt{\frac{\sum_{i=1}^{n}\left(\left[\frac{\Delta T}{T_0 T}\right]_i - \overline{\left[\frac{\Delta T}{T_0 T}\right]}\right)^2}{N}} \tag{53}$$

Lastly, the relative standard deviation (RSD) is calculated, which is defined as the ratio between the standard deviation and the average, shown in Equation (54). The results from this calculations are displayed in tables from D.1 to D.8.

$$RSD = \frac{\sigma}{\overline{\left[\frac{\Delta T}{T_0 T}\right]}} \times 100\% \tag{54}$$

Table D.1 - 10 mass% of MEG water activity calculations.

P [MPa]	T_0 [K]	T [K]	ΔT	$\Delta T/T_0T$	Average	RSD
8.5	283.68	280.94	2.74	3.44E-05	3.36E-05	**2.13%**
13	284.14	281.51	2.63	3.29E-05	**Std. Deviation**	**Verdict**
18	284.57	281.84	2.73	3.40E-05	7.16E-07	**Pass**
25	285.21	282.54	2.67	3.31E-05		

Table D.2 - 20 mass% of MEG water activity calculations.

P [MPa]	T_0 [K]	T [K]	ΔT	$\Delta T/T_0T$	Average	RSD
8.5	283.68	276.82	6.86	8.74E-05	8.56E-05	**1.32%**
13	284.14	277.43	6.71	8.51E-05	**Std. Deviation**	**Verdict**
18	284.57	277.77	6.80	8.60E-05	1.13E-06	**Pass**
25	285.21	278.47	6.74	8.49E-05		

Table D.3 - 30 mass% of MEG water activity calculations.

P [MPa]	T_0 [K]	T [K]	ΔT	$\Delta T/T_0T$	Average	RSD
8.5	283.68	271.84	11.84	1.54E-04	1.51E-04	**1.21%**
13	284.14	272.58	11.56	1.49E-04	**Std. Deviation**	**Verdict**
18	284.57	272.87	11.70	1.51E-04	1.83E-06	**Pass**
25	285.21	273.36	11.85	1.52E-04		

Table D.4 - 5 mass% of NaCl water activity calculations.

P [MPa]	T_0 [K]	T [K]	ΔT	$\Delta T/T_0T$	Average	RSD
8.5	283.68	280.99	2.69	3.37E-05	3.36E-05	**2.81%**
13	284.14	281.39	2.75	3.44E-05	**Std. Deviation**	**Verdict**
18	284.57	281.99	2.58	3.22E-05	9.44E-07	**Pass**
25	285.21	282.51	2.70	3.35E-05		

Table D.5 - 10 mass% of NaCl water activity calculations.

P [MPa]	T_0 [K]	T [K]	ΔT	$\Delta T/T_0T$	Average	RSD
8.5	283.68	278.11	5.57	7.06E-05	7.09E-05	**0.53%**
13	284.14	278.53	5.61	7.09E-05	**Std. Deviation**	**Verdict**
18	284.57	278.94	5.63	7.09E-05	3.77E-07	**Pass**
25	285.21	279.51	5.70	7.15E-05		

Table D.6 - 5 mass% NaCl + 10 mass% MEG water activity calculations.

P [MPa]	T_0 [K]	T [K]	ΔT	$\Delta T/T_0T$	Average	RSD
8.5	283.68	277.72	5.96	7.57E-05	7.62E-05	**1.44%**
13	284.14	278.07	6.07	7.68E-05	**Std. Deviation**	**Verdict**
18	284.57	278.59	5.98	7.54E-05	1.09E-06	**Pass**
25	285.21	279.02	6.19	7.78E-05		

Table D.7 - 5 mass% NaCl + 20 mass% MEG water activity calculations.

P [MPa]	T_0 [K]	T [K]	ΔT	$\Delta T/T_0T$	Average	RSD
8.5	283.68	272.96	10.72	1.38E-04	1.38E-04	**0.92%**
13	284.14	273.48	10.66	1.37E-04	**Std. Deviation**	**Verdict**
18	284.57	273.98	10.59	1.36E-04	1.27E-06	**Pass**
25	285.21	274.37	10.84	1.39E-04		

Table D.8 - 5 mass% NaCl + 30 mass% MEG water activity calculations.

P [MPa]	T_0 [K]	T [K]	ΔT	$\Delta T/T_0T$	Average	RSD
8.5	283.68	267.02	16.66	2.20E-04	2.20E-04	**0.32%**
13	284.14	267.41	16.73	2.20E-04	**Std. Deviation**	**Verdict**
18	284.57	267.76	16.81	2.21E-04	7.04E-07	**Pass**
25	285.21	268.26	16.95	2.22E-04		

APPENDIX E - DESCRIPTION OF PREDICTION SOFTWARE PRODUCTS AND MODELS

The experimental data obtained will be compared with prediction software and models in order to assess their accuracy. Table E.1 shows the characteristics of each software and model that will be used for comparison in this work. Flash corresponds to the calculation of the distribution of the components between the phases prior to hydrate equilibrium determination.

Table E.1 - Models characteristics.

Model	Eq. Of State	Flash
Multiflash	CPA	Yes
CSMGem	SRK	Yes
PVTSim	CPA	Yes
Sirino et al. (2018)	CPA	Yes
Hu-Lee-Sum correlation	Correlation	No

E.1 SIRINO ET AL. (2018) MULTIPHASE FLASH MODEL

The model uses the CPA equation of state (EoS), which is derived from the Soave-Redlich-Kwong EoS. Relative to pressure (P), the CPA EoS is expressed as Equation (55) . The model first do a calculation of flash using the concept of equality of fugacities as a convergence criterion.

$$P = \frac{RT}{v_m - b} - \frac{a}{v_m(v_m + b)} - \frac{1}{2}\frac{RT}{v_m}\left(1 + \frac{1}{v_m}\frac{\partial \ln(g)}{\partial(1/v_m)}\right)\sum_i x_i \sum_{A_i}(1 - X_{A_i}) \qquad (55)$$

In this model, the traditional van der Waals mixing rules (Equation (56)) are used to calculate the binary interaction parameters of que EoS. The classical combining rules are used aswell, shown in Equation (57). Where i and j are in reference to the corresponding componentes.

$$a = \sum_i \sum_j x_i x_j a_{ij} \qquad \mathrm{b} = \sum_i x_i b_i \tag{56}$$

$$a_{ij} = \sqrt{a_i a_j}\,(1 - k_{ij}) \qquad b_{ij} = \frac{b_i + b_j}{2} \tag{57}$$

Next, using the van der Waals-Platteeuw (vdW-P) hydrate prediction model, it calculates *f(P)* (Equation (58)) with the initial pressure guess from Equation (55). This continues until the criteria of convergence is satisfied, i.e. *f(P)=0*.

$$f(P) = \frac{\Delta\mu_0}{RT_0} - \int_{T_0}^{T} \frac{\Delta H_W^{L-\beta}(T,P)}{RT^2}\,dT + \int_{P_0}^{P} \frac{\Delta V_W^{L-\beta}(T,P)}{RT}\,dP - \frac{\Delta\mu_W^{H-\beta}(T,P)}{RT} + ln(a_W^{\alpha}) - \frac{\Delta\mu_W^{H-\beta}}{RT} \tag{58}$$

E.2 HU-LEE-SUM CORRELATION

Developed by the Hydrate Innovation Research Center in Colorado School of Mines (USA), the Hu-Lee-Sum correlation is based on the concept of freezing point depression, as shown with Equation (59), where ΔT is the hydrate suppression temperature, T_0 is the hydrate equilibrium temperature for pure water and T for the inhibited system, n is the hydration number, R is the gas constant, ΔH_{diss} is the hydrate dissociation enthalpy and a_w is the water activity. The details of the correlation are available at the publications Hu et al. (2017 a) and Hu et al. (2017 b).

$$\frac{\Delta T}{T_0 T} = -\frac{nR}{\Delta H_{diss}} \ln(a_w) = -\beta_{gas} \ln(a_w) \tag{59}$$

The correlation considers that the water activity has contributions from electrolytes (salt) and from organic inhibitors (oi), as shown in Equation (60).

$$\ln(a_w) = \ln(a_w^{salt}) + \ln(a_w^{oi}) \quad (60)$$

To calculate the water activity, the universal correlation shown in Equation (61) is used, where B_1, B_2 and B_3 are the coefficients that are fitted according to the inhibitor and X is the effective mole fraction, which is calculated with Equation (62), where z is the charge of the ion z in salt j and x is the mole fraction in solution of ion i in salt j. The effective mole fraction for organic inhibitors is calculated based in the salt solution.

$$\ln(a_w) = B_1 X + B_2 X^2 + B_3 X^3 \quad (61)$$

$$X = \sum_{j=salt} \sum_{i=ions} |z_{j,i}| x_{j,i} \quad (62)$$

Above Q_2, data for the influence of thermodynamic inhibitors is scarce in literature, so that it becomes very important to study the formation of hydrates with the presence of MEG and NaCl. By using a salt mixed with MEG, we can better understand the hydrate formation in offshore oil extraction, where the water from the well is naturally inhibited with salts.

The checking of the consistency of the experimental data is a good way to evaluate its reliability. The comparison reliable data with prediction software and models can be done in order to determine which of them gives better predictions.

APPENDIX F - CALCULATION OF THE SOFTWARE PRODUCTS AND MODELS COMPARISONS

For comparing the data collected from this work with the software products CSMGem, Multiflash and PVTSim and the models from Hu-Lee-Sum correlation (shown as Hu-Lee-Sum in the tables) and Sirino et al. (2018) (shown as Sirino (2018) in the tables), the average absolute deviation (AAD) was calculated for each system, as shown in Equation (63).

$$\mathrm{AAD} = \frac{\sum_{i=1}^{N} \left| T_{\mathrm{Prediction}} - T_{\mathrm{Experimental}} \right|}{N} \tag{63}$$

The results obtained are summarized in Table F.1 for all systems and predictions used. The predictions with the lowest AAD for each system is highlighted as bold text.

Table F.1 - Results for the average absolute deviation between predictions and experimental results. Units are temperatures in Kelvin.

System	CSMGem	PVTSim	Multiflash	Sirino (2018)	Hu-Lee-Sum (2018)
Pure Water	**0.12**	0.21	0.27	0.20	-
10% MEG	0.40	0.52	**0.08**	0.28	0.49
20% MEG	0.29	0.32	**0.10**	0.43	1.30
30% MEG	0.28	**0.13**	0.20	1.39	2.40
5% NaCl	0.17	**0.15**	0.30	0.35	0.64
10% NaCl	0.44	0.18	**0.13**	0.68	1.18
5% NaCl+10% MEG	**0.29**	0.77	0.34	0.60	1.24
5% NaCl+20% MEG	**0.27**	0.60	0.81	0.56	2.27
5% NaCl+30% MEG	10.31	**0.28**	1.27	-	3.58